Global and Regional Sea Level Rise Scenarios for the United States: Updated Mean Projections and Extreme Water Level Probabilities Along U.S. Coastlines

Executive Summary

This report and accompanying datasets from the U.S. Sea Level Rise and Coastal Flood Hazard Scenarios and Tools Interagency Task Force provide 1) an update of future sea level rise scenarios to 2150 and 2) a new set of extreme water level (tide gauge) probabilities to assess flood risk out to 2050 applicable for most US coastlines. This effort builds on the 2017 Task Force report (Sweet et al., 2017) and leverages methods and insights from both the United Nations Intergovernmental Panel on Climate Change (IPCC) 6th Assessment Report (AR6) and supporting research for the U.S. DoD Defense Regional Sea Level (DRSL) database. The information contained in this report is intended to inform Federal agencies, state and local governments, and other stakeholders in coastal communities about current and future sea level rise to help contextualize its effects for decision making purposes. This report is also a key technical input for the 5th U.S. National Climate Assessment (NCA5).

Key message #1:

The modeled scenarios and extrapolations of the observed trends of relative sea level (RSLs: combination of land and ocean height changes) project a rise of 0.3-0.5 meters by 2050 (relative to sea level in 2000) along U.S. coastlines.

- On global and national scales, both sea level observations and scenario pathways agree on a narrower range in possible near-term sea-level change than provided in Sweet et al. (2017)
- Extrapolations of sea level trends from NOAA and NASA observations point to a U.S. (global) rise of about 0.35 m (0.25 m) by 2050 or about a 0.25-m (0.15-m) rise measured since 2020.
- This projected U.S. RSL rise over the next 30 years equals estimates for 1920 to 2020.
- Considering the modeled scenario providing an upper bound to the observed trend extrapolations, RSL projections range from 0.40-0.45 m along the NE and SE East Coasts, 0.55-0.65 m along the E and W Gulf Coasts, 0.20-0.30 m along the SW and NW West Coast, 0.20-0.35 m along the Caribbean and Hawaii Islands, 0.30 m along the northern coast of Alaska, and an RSL decrease along the southern coast of Alaska.

Key message #2:

Higher global temperatures increase the chances of higher sea level by the end of the century and beyond. The scenario projections of RSL along U.S. coastlines are about 0.6-2.2 m in 2100 and 0.8-3.9 m in 2150 with this range driven by uncertainty in both the underlying physical processes and future emissions pathway.

- Not considering the potential contributions from ice sheet processes in which there is limited agreement (low confidence) among modeling approaches, with 2 degrees C warming, the probability of >0.5 m rise globally (0.7 m along the U.S.) by 2100 is about 50%. At 3 to 5 degrees C, this probability rises from >80 to >99%. Exceeding 1 m globally (1.2 m U.S.) by 2100 rises from <5% with 3 degrees and almost <25% with 5 degrees C rise; exceeding 1.5 m globally (about 1.7 m along the U.S.) by 2100 remains <2% with up to 5 degrees C warming.
- Considering low-confidence ice sheet processes, with warming approaching 5 degrees C, there could be probabilities as high as about 50%, 20% and 10% of exceeding 1, 1.5 or 2.0 meters of global rise by 2100, respectively.
- Regionally, the projections are near or higher than the global average in 2100 and 2150 for almost all U.S. coastlines due to effects from vertical land motion (VLM), gravitational, rotational

and deformational changes from melting of land ice, and circulation changes. Largely due to VLM, RSL projections are less than the global amounts along southern Alaskan coasts and are highest along the Gulf Coast.

Key Message #3

By 2050, a shift in coastal flood regimes is projected with potentially significant consequences if U.S. flood defenses do not improve, with major and moderate flood frequencies becoming those of moderate and minor by today's standards.

- By 2050, minor/mostly disruptive flooding (≥0.5 m above high tide) is projected to occur >10 events/year (3 events/year in 2020) for the average location along the U.S. coastlines.
- Moderate/often damaging flooding (≥0.8 m) is projected to occur about 4 events/year (a 30% annual chance event in 2020)
- Major/often destructive flooding (≥1.2 m) would become a 20% annual chance event (4% annual chance in 2020)
- There is regional variability in the assessment of future high tide flooding, and the national estimates will be exceeded in many locations; East and Gulf Coast locations, in particular, are slated to be well above these amounts.

Key Message #4

Monitoring the sources of ongoing sea level rise and the global-scale drivers of these changes is important to assess scenario divergence and track the trajectory of observed sea level rise, particularly during the time period when emissions scenarios become important and leads to increased ranges in projected sea level rise.

- Efforts are underway to narrow the uncertainties in ice sheet dynamics and future sea level rise amounts in response to increasing greenhouse gas forcing and associated global warming
- Continuous monitoring and assessments of global to local RSL levels and their key source contributions affecting U.S. coastlines, such as ocean heat content, ice mass loss from Greenland and Antarctica, VLM, and Gulf Stream system changes, can establish 'gates' to alert for potential scenario boundary crossing and to trigger adaptive management plans.

These data and information are being incorporated into current and planned agency tools and services like NOAA's Sea Level Rise Viewer and Inundation Dashboard, NASA's Sea Level Change Portal and others to help decision makers and engineers confront the uncertainties that the future holds...

Section 1: Introduction

Sea level rise driven by global climate change is a clear and present risk to the United States today, and will continue over the coming decades and centuries (USGCRP, 2018; Hall et al., 2019). Millions of people in the United States already live in areas at risk of coastal flooding, with more moving to the coasts every year. Rising sea levels, along with sinking lands, will combine with other coastal flood factors (e.g., storm surge, wave effects, heavy rains, as shown in Figure 1.1) to dramatically increase the vulnerability of this growing population, along with critical infrastructure related to transportation, energy, trade, military readiness, and coastal ecosystems and the supporting services they provide.

Figure 1.1: Schematic showing physical processes affecting coastal flood risk. Due to the clear and strong relative sea level (RSL) rise signal (e.g., combination of sea level rise and land sinking), flood risk is increasing along most U.S. coastlines.

Global mean sea level (GMSL) rise is a certain consequence of climate change, resulting from a combination of thermal expansion of warming ocean waters and the addition of water mass into the ocean, largely associated with melting land ice. These processes are well understood for the recent past, and their contributions have been estimated over the 20th century (Fig. 1.2A). With regard to increasing sea levels associated with climate change, the questions are *when*, and *how much*, rather than *if* (USGCRP, 2017; Hall et al., 2019). Increases in GMSL provide an important indicator of the changing climate, but it is the sea level rise on local and regional scales that is most relevant for coastal communities around the world. Sea level rise has not been and will not be uniform. Rather, sea levels change at the local level due to many factors that affect relative sea levels (RSL), and which are measured by NOAA with their tide gauge network. For example, vertical land motion (VLM) can exacerbate the effects of the rising ocean. For context, whereas GMSL has risen by about 17 cm over the last 100 years (i.e., 1920 to 2020), with noted acceleration since about 1970, RSL averaged along the contiguous U.S. has risen about 25 cm over the same period with similar onset of acceleration (Figure 1.2B).

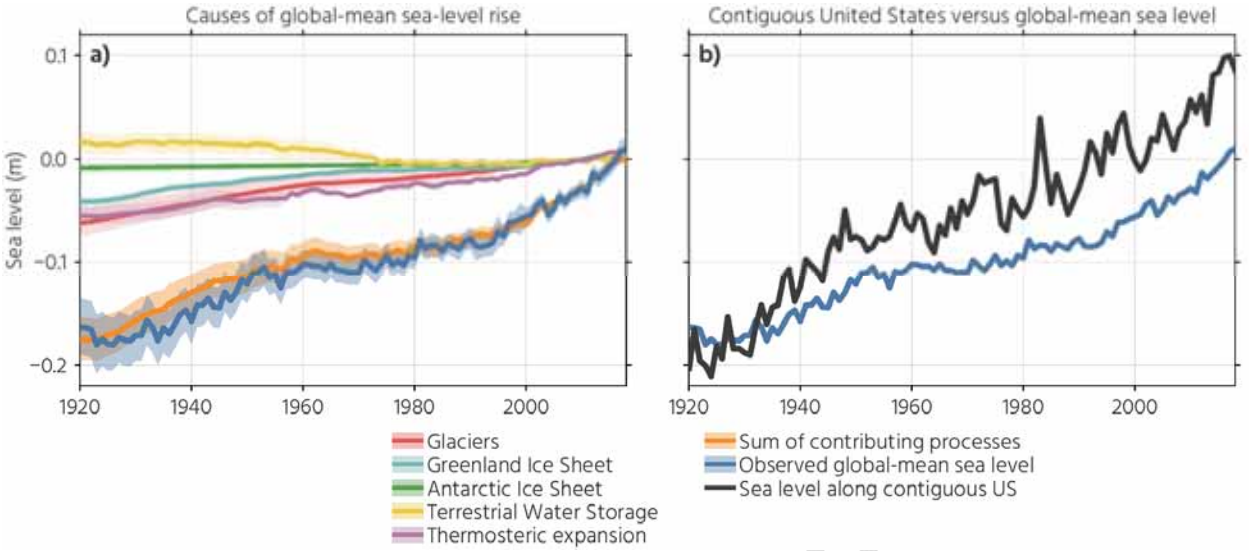

Figure 1.2: a) Observed GMSL change from global tide gauges along with the contributions from thermal expansion (thermosteric) and water mass-driven increases in GMSL. b) Observed GMSL change from global tide gauges along with average mean sea level from tide gauges around the Contiguous United States. Note: 0.3 m = 1 foot. (Adaptation of Frederikse et al., 2020).

While this long-term and upward shift in mean RSL is the underlying driver of changes to the nation's coasts, extreme water levels (EWLs) occurring against the background of this shifting sea level baseline are responsible for most of the impacts, chronic and acute, at a particular place and time. Higher sea levels worsen the impacts of storm surge, high tides, and wave action, even absent any changes in storm frequency and intensity (Figure 1.1). Because of threshold effects (Figure 1.3a), even the relatively small increases in sea level over the last several decades have led to greatly increased frequency of flooding at many places along the U.S. coast (Figure 1.3b). Much of the coastline is already close to a tipping point with respect to flood frequency (and presumably damages), as only 0.3-0.7 m currently separates infrequent, damaging-to-destructive flooding, from minor 'nuisance' high tide flooding (HTF) within U.S. coastal cities (Sweet et al., 2018). Decades ago, powerful storms were what typically caused coastal inundation but today, due to RSL rise, even common wind events and seasonal high tides regularly flood coastal communities, affecting homes and businesses, overloading stormwater and wastewater systems, infiltrating coastal groundwater aquifers with saltwater, and stressing coastal wetlands and estuarine ecosystems. At some locations along the U.S. coast, the frequency of tidal flooding has increased by an order of magnitude over the past several decades, turning it from a rare event into a recurrent and disruptive problem (Sweet and Park, 2014; Sweet et al., 2018; USGCRP, 2018). This increase is expected to continue and accelerate in the next couple of decades (Sweet et al., 2021; Thompson et al., 2021). Accurate projections of the background sea level rise and assessments that integrate across processes and temporal and spatial scales are key inputs to planning efforts.

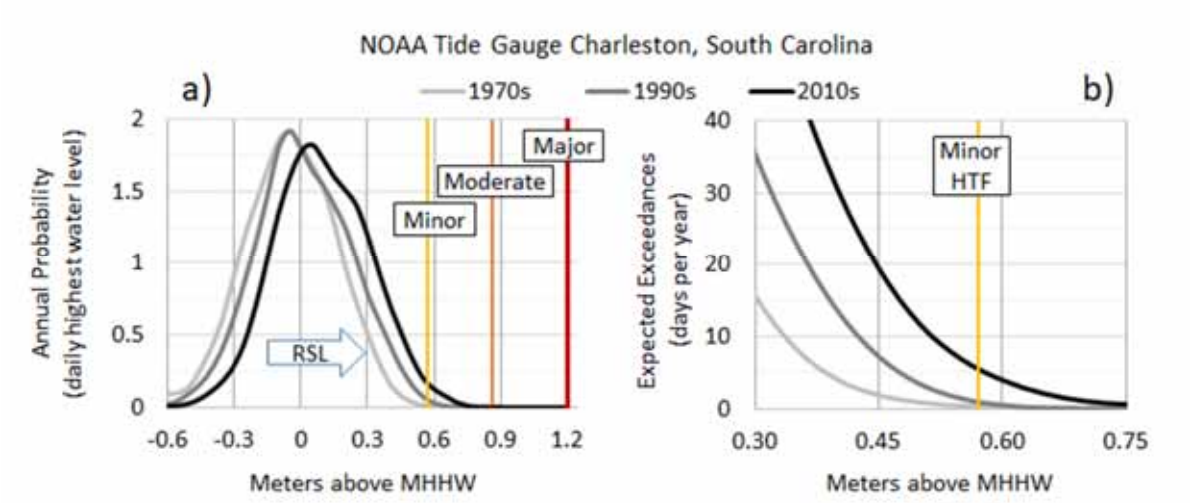

Figure 1.3: a) annual probability density and b) annual expected exceedances for daily highest water levels relative to current MHHW tidal datum with NOAA minor, moderate and major flood heights for the NOAA tide gauge at Charleston, SC. Extreme water levels (EWLs) are considered those occurring 10 or fewer times per year on average, which generally equates to the range of contemporary NOAA coastal flood stages and their probabilities (Sweet et al., 2018).

The Sea Level Rise and Coastal Flood Hazard Scenarios and Tools Interagency Task Force (hereafter "Task Force") was jointly convened at the direction of the White House Resilience Council, in 2015, under the U.S. Global Change Research Program (USGCRP), the Subcommittee on Ocean Sciences and Technology (SOST), and the National Ocean Council (NOC). This was in recognition of the strong need and demand for authoritative, consistent, accessible sea level rise and associated coastal hazard information for the entire U.S. coastline, coordinated across the relevant Federal agencies, to serve as a starting point for on-the-ground coastal preparedness planning and risk management activities. The goal of the Task Force, since its inception, has been to develop the necessary products through sustained and coordinated participation of key agencies, based on the best available science, including regional science and expertise when possible and appropriate. The goal has also been to incorporate those products into user-friendly mapping, visualization, and analysis tools made easily accessible through existing agency portals serving specific partners and stakeholders, as well as interagency venues such as the National Climate Assessment (NCA), the U.S. Climate Resilience Toolkit, and others.

The Task Force focused its initial efforts on the development of an interagency report (Sweet et al., 2017) providing updated GMSL rise focused primarily on 2100, integrating these GMSL rise scenarios with regional factors contributing to sea level change to produce, for the first time, a set of RSL scenarios for the entire U.S. coastline. These scenarios were also a major technical input to Volumes I and II of the 4th NCA (NCA4) and have been widely used in the development of state (e.g., Florida, Virginia and New Hampshire) and local adaptation plans (e.g., Pensacola, FL; Biloxi, MS; Dauphin Island, AL; Tybee Island, GA) and processes for anticipating and managing future coastal risks.

Building on recent, previous scenario development and sea-level projection efforts (e.g., Parris et al., 2012; Miller et al., 2013; Kopp et al., 2014; Hall et al., 2016), the 2017 report estimated the full, possible range for GMSL rise by 2100 as being bounded by 0.3 m on the low end, representing a simple linear extrapolation of the GMSL trend since the early 1990s, and by 2.5 m on the high end, representing an extreme ice sheet melt/discharge scenario. This 0.3-2.5 m range was discretized and aligned with

emissions-based, conditional probabilistic storylines and global model projections into six GMSL rise scenarios: *Low*, *Intermediate-Low*, *Intermediate*, *Intermediate-High*, *High*, and *Extreme*, corresponding to GMSL rise by 2100 of 0.3 m, 0.5 m, 1.0 m, 1.5 m, 2.0 m and 2.5 m, respectively. These GMSL rise scenarios were then used to derive regional RSL responses on a 1-degree grid covering the coastlines of the U.S. mainland, Alaska, Hawaii, the Caribbean, and the Pacific island territories, as well as at the precise locations of tide gauges along these coastlines.

This report takes the 2017 report as its starting point, updating the GMSL scenarios and the associated RSL projections to reflect recent advances in sea level rise science, as well as expanding the types of scenario information provided to better serve stakeholder needs for coastal risk management and adaptation planning. As with the 2017 report, this iteration will also serve as a key technical input to the NCA, in this case NCA5. Specific updates in this report include the following:

- While this report still references and uses the same nomenclature as the NOAA 2017 GMSL rise scenarios, along with associated RSL projections for the U.S. coastline (gridded and at individual tide gauge locations), it draws upon new science since that time to provide updated temporal trajectories and exceedance probabilities based upon different levels of global warming. In particular, it builds off of the sea-level projections associated with the Intergovernmental Panel on Climate Change (IPCC) Sixth Assessment Report (Fox-Kemper et al 2021, Garner et al 2021).
- In addition, in leveraging this updated science, including a longer observational record, improved understanding of ice sheet dynamical processes, and better-constrained models, this report provides a more comprehensive and detailed assessment of the distinct types and range of uncertainties associated with the GMSL rise scenarios, particularly at the high end.
- By utilizing 50-year regional sets of tide gauge data and satellite altimetry data, observational data extrapolated to year 2050 are used to identify the projections aligning with current RSL trajectories.
- Lastly, gridded EWL probabilities are provided with methods to localize them along most U.S. coastlines to contextualize each of the regionalized sea level scenarios, across a range of flood frequencies/severities under current conditions/flood defenses from recurrent tidal flooding to storm surge, out to 2050.

At this point and to frame the remainder of this report, it is important to emphasize the distinction between describing scientific progress, in terms of current understanding and key uncertainties, and the translation of such advances in the scientific knowledge base into actionable science, which requires sustained engagement with users around their specific planning and decision contexts. Our development of scenarios in this report is grounded in the principles of risk-based framing for climate assessment (King et al., 2015; Weaver et al., 2017; Sutton et al., 2019; Kopp et al., 2019) and is consistent with adaptation pathways approaches for long-term planning. What we thus aim to provide are screening-level products suitable for framing and bounding important problems in coastal risk assessment and management, along with contextualization of the underlying science and illustrative case studies. For example, consistent with this purpose, this report aims to provide both "planning" and "bounding" type scenarios, across the full spectrum of coastal risk: i.e., (1) scenarios intended to frame near-to-mid-term decision contexts and/or longer-term decisions with high risk tolerance or ability to adjust plans, which address the question: “what is most likely to happen?” and (2) scenarios designed to set the envelope of possible future outcomes and which can be used to stress-test long-term plans,

"when, and not if" a given level of sea level rise is reached, and which address the question: “how bad could things get?” *What this report does NOT provide is authoritative guidance, nor design specifications for a specific project.*

Section 2 describes the advances in sea level rise science since the 2017 report, discusses the use of observations for a near-term assessment and provides the updated GMSL rise scenarios and their associated RSL projections. Section 3 focuses on EWLs, including historical frequency analysis and projections (to 2050) across a range of flood levels. Section 4 applies these scenarios and projections in illustrative use-case examples. Section 5 provides a summary of the report findings and conclusions and next steps.

Section 2: Future Mean Sea Level: Scenarios and Observation-Based Assessments

Since Sweet et al. (2017), the sea-level observation network has been enhanced and existing platforms have generally been maintained. The available data records of both sea-level change and the associated processes have increased in number and length. In part due to these observations, our understanding of the drivers of sea-level change has advanced. There have also been significant advances in modeling how these processes will cause sea level to change in the future. This has led to a better understanding of the possible trajectory of future sea-level rise. In this report, these advances are reflected both in an update to the scenarios and a change in approach from Sweet et al. (2017). The primary change in approach is in separating this section into two different time periods: 1) near-term (2020-2050) and 2) long-term (2050-2150). There is also an additional section discussing scenario divergence and tracking that is particularly relevant during the transition between the near- and long-term time period. In the remainder of this section, a brief overview of the drivers of global and regional sea-level rise is provided. Next, updates to Sweet et al. (2017) are discussed and the motivation and scientific justification for these changes is given. Finally, the updated information for the two time periods, along with the transition between these periods, is provided.

Section 2.1. Overview of Regional and Global Sea Level Rise

Over long timescales, the primary drivers of global mean sea level (GMSL) are thermal expansion due to heating of the ocean and the addition of water mass associated with melting ice from the ice sheets and mountain glaciers. Other changes in the movement of water between ocean and land, including from groundwater depletion and water impoundment, have a secondary impact on GMSL, although they can increase in importance for certain time periods (see Frederikse et al., 2020). During the 20th century, GMSL estimated from tide gauge records has been explained by the individual processes contributing to it (Figure 1.1A; Frederikse et al., 2020). More recently, observed GMSL from satellite altimetry during the past 15 years has been explained using the in-situ measurements of the Argo profiling floats and the observations of water mass change from the GRACE and GRACE-FO satellites (WCRP, 2018). On shorter timescales, there is considerable interannual variability in GMSL change linked primarily to variations in terrestrial water storage and driven heavily by the El Niño-Southern Oscillation (ENSO).

At the regional level, rates of sea-level rise can vary significantly from the globally averaged rate. Sea-level rise has not been and will not be uniform; rather it manifests as relative sea level (RSL) rise that also responds to several key factors important at regional and local scales (Kopp et al, 2014; Sweet et al., 2017; Hamlington et al., 2020; Fox-Kemper et al., 2021). On short timescales and in short records, natural variations on interannual to decadal timescales can impact estimates of trends. On long timescales, however, there are three primary causes of regional variations: 1) sterodynamic sea level change; 2) gravitational, rotational, and deformational (GRD) changes due to melting land-ice and the movement of water between land and ocean; and 3) vertical land movement (VLM; subsidence or uplift) due to glacial isostatic adjustment (GIA), tectonics, sediment compaction, groundwater and fossil fuel withdrawals, and other non-climatic factors. These factors are discussed briefly below.

Sterodynamic sea level changes are those that arise from changes in the ocean's circulation (currents) and its density (temperature and saltiness). Sea-level rise associated with sterodynamic sea-level change is the combination of global mean thermosteric rise associated with global ocean warming and long-term changes in ocean dynamics. It is these changes in ocean dynamics that lead to regional differences. For the U.S. coastlines, future changes in the Atlantic Meridional Overturning Circulation (AMOC) are particularly relevant. The IPCC 6th Assessment Report determined that it is very likely that

the AMOC will decline in the future, although there is still disagreement as to the extent of this decline. A weakening AMOC will lead to an increase in sea level along the U.S. East Coast. For the U.S. West Coast, ENSO plays a substantial role in interannual sea-level change, although there is no clear evidence for a sustained shift in ENSO that will result in a long-term increase or decrease in sea level. Some models project the future changes associated with ocean dynamics to be large in magnitude, but these projections remain uncertain.

The ice mass loss from ice sheets and mountain glaciers to the ocean has a strong influence on regional sea level. Changes in Earth's GRD responses dictate the spatial distribution of water across the global ocean (Farrell and Clark, 1976; Milne and Mitrovica, 1998; Mitrovica et al., 2001). These so-called 'sea level fingerprints' are important to determining regional sea-level rise. Mass loss causes a sea level fall in the near-field, a reduced sea-level rise at intermediate distances, and a greater-than-global-average sea-level rise at larger distances. For the coastlines of the U.S., this then means that a similar amount of ice mass loss in Antarctica will have a larger impact than ice mass loss in Greenland. Similarly, ice mass loss in Greenland leads to bigger increases in sea level on the West Coast than along the Northeast Coast. At any time horizon, the regional sea level rise associated with GRD will be driven both by the amount of ice that is being lost and the source of that ice. These regional fingerprints are tied to projected trajectories of mass loss from the associated source. Changes in terrestrial water storage (groundwater withdrawal, dam building) also have an associated fingerprint but the regional contribution is generally smaller.

Lastly, the VLM considered in this report refers to either subsidence or uplift that occurs in coastal regions and can lead to the change in the height of sea level relative to land. VLM is not a singular phenomenon but instead results from various processes that display different patterns in space and time. These patterns have different impacts from place to place, especially in coastal settings where many of them operate at the same time. For much of the coastal U.S., subsidence is driven on local scales by groundwater and fossil fuel withdrawal and on larger scales by GIA. On the other hand, in some regions like southern Alaska, GIA leads to high rates of uplift in coastal regions. Accurate future projections of VLM require an understanding of the underlying processes and the time and space scales on which they vary. Currently and in this report, VLM projections are based in part on analysis of past observations. If activities change in a particular location (e.g. reduction in groundwater pumping), an associated change in the rate of VLM will not necessarily be captured. Modeling of future VLM under a range of possible scenarios is not currently available over large scales.

Beyond these processes that impact long-term changes in sea level, there is also considerable natural variability that can lead to significant, albeit temporary, changes to sea level on the order of years or even decades. In many of the available observational records, it can be a challenge to distinguish between these natural signals and those processes discussed above. As an example, in Fig. 2.1, the regional rates of sea level rise around the coastlines of the U.S. are shown for the first half (A: 1993-2006), second half (B: 2007-2020) and full (C: 1993-2020) satellite altimeter record along with overlaid tide gauge rates measured over the same time period. A significant shift occurs between the first half of the record to the second half, with high sea level rise rates found along all coastlines of the contiguous U.S. from 2007-2020. For the west coast, in particular, the rate was near 0 for the first half of the record before shifting to almost 10 mm/year over the second half, driven by decadal variability linked to the Pacific Decadal Oscillation (e.g. Bromirski et al., 2011; Hamlington et al., 2021). For the full record, there is considerably less spatial variability with most regions approaching the globally averaged rate of 3.1 mm/year. In this section of the report, the contribution of natural variability is not assessed directly, but its importance and contribution should be considered when looking at observed rates and assessing

possible sea level at a specific time in the future. In other words, there is an "envelope" of natural variability on top of the sea level rise discussed here that needs to be included to estimate sea level at a particular location at a specific time in the future.

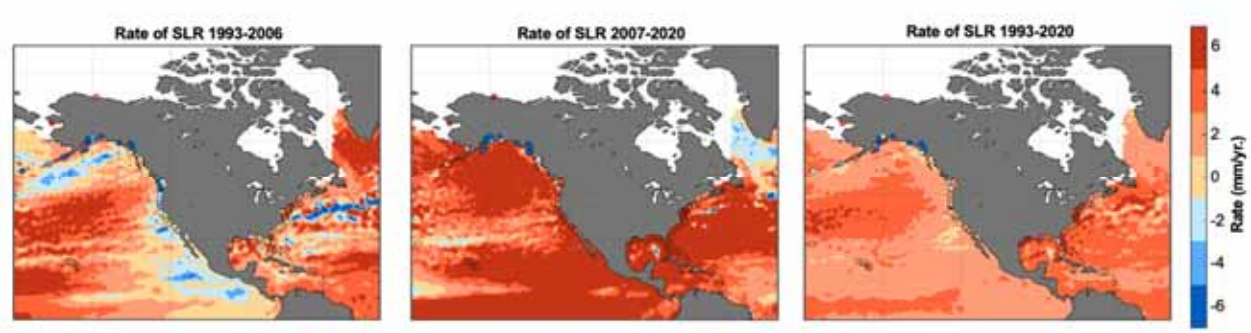

Fig. 2.1. Regional sea level trends from satellite altimetry over three different time periods. Relative sea level trends from tide gauges over the same time period are also shown (circles).

Section 2.2 : Updates from Sweet et al. (2017)

One of the main structural changes from the Sweet et al. (2017) report to this one is a specific emphasis on the near-term time period from 2020-2050. There is also a detailed discussion of scenario divergence and tracking that becomes particularly important in the transition from the near-term to the long-term. The motivation for the focus on these two topics is given below. Following this explanation, the primary advances in the sea-level scenarios and assessments of future sea level are discussed in two subsections below. The first provides an overview of the science and framework advancements that have led to an update of the scenarios first presented in Sweet et al. (2017). The second covers the inclusion of observation-based assessments of near-term sea-level change for the first time.

Section 2.2.1 Inclusion of Near-Term Time Period (2020-2050)

The dedicated focus on the near-term time period represents a new element in this report. Motivation for this change is provided briefly here. With increasing record lengths, the impact of natural sea-level variability on estimated rates and accelerations diminishes. Tide gauges surrounding the U.S. coastlines provide records exceeding 100 years in some locations, and the satellite altimeter record is nearing three decades in length. Recent studies have assessed the degree to which rates and accelerations estimated from these records are reflective of the long-term increase in RSL (e.g. Fasullo and Nerem, 2018; Richter et al., 2020). These studies suggest, with appropriate consideration of uncertainty, that observation-based extrapolated projections can be informative in the near-term. In this report, an assessment based solely on extrapolation of observed trends out to 2050 allows for trajectory tracking and a comparison to model-based scenarios. Beyond this renewed observational focus, the inclusion of this near-term time-period is motivated by the fact that for certain decision types, short time horizons are most relevant. For real estate investment and the typical lifetime of buildings and infrastructure in coastal areas, for example, a thirty-year planning horizon has particular relevance (e.g. Fu et al., 2020; Hinkel et al., 2018). Additionally, flexible adaptation pathways and solutions typically require significant lead-times on upgrades or replacements of coastal structures that lead to an emphasis on these shorter-planning horizons (Haasnoot et al., 2013; 2019; Bloeman et al., 2018; Werner et al., 2021; Hall et al., 2019).

354
355 **Section 2.2.2 Scenario Divergence and Tracking**
356 After the next three decades, the observation-based assessments become less informative. This
357 is both because uncertainty in the contemporary estimates of rates and accelerations increases, leading
358 to large projected ranges, and also because current estimates may not be reflective of shifts or process
359 changes that may occur in the future with additional emissions and global warming. Additionally, beyond
360 this near-term time-period, divergence between the future GMSL scenarios increases. During the
361 transition from near- to long-term assessments, an understanding of when the GMSL scenarios will
362 diverge and what drives this divergence becomes increasingly important. There are two types of
363 uncertainty that are important to consider in this context: uncertainty in physical processes and
364 uncertainty in future emissions and ensuing warming. Process-based uncertainty is associated with how
365 well we currently understand why sea level has changed in the past and how it will change in the future.
366 Stated another way, how well do we understand the processes that will combine to impact sea level at a
367 specific time and location in the future? This uncertainty is reflected in the likely range of future sea level
368 rise for a given scenario. The difference between scenarios is associated with the range of potential future
369 emissions pathways and associated warming levels.
370 At some point in the future, the separation between scenarios will overtake the physical process-
371 based uncertainty. In other words, scenario dependence will emerge, and it will be possible to distinguish
372 between the trajectories associated with two neighboring GMSL scenarios. In general, these time periods
373 are important for connecting the near-term similarities between scenarios to the time period where
374 scenarios diverge rapidly. An effort is made here to understand when divergence of the GMSL scenarios
375 might occur and to link them to possible future warming and emissions pathways. This analysis then serves
376 as the foundation for process-based monitoring that could be useful in determining the trajectory of
377 ongoing sea-level rise and by extension, the possible future sea-level rise out to 2150.
378
379 **Section 2.2.3 Updates to the 2017 Sea Level Scenarios**
380 In order to support decision-making efforts related to future sea-level risks, past Interagency
381 efforts (Parris et al., 2012; Hall et al., 2016; Sweet et al., 2017) have defined a set of sea-level scenarios
382 spanning a range from a 'Low' scenario consistent with no additional GMSL acceleration to a 'worst case'
383 or a high-end 'Extreme' scenario judged to be at the limits of the physically plausible. In Sweet et al. (2017),
384 these scenarios were developed to span a range of 21st century GMSL rise from 0.3 m to 2.5 m. Sweet et
385 al. (2017) built these scenarios upon the probabilistic, emissions-scenario driven projections of Kopp et al.
386 (2014). Kopp et al. (2014) combined a variety of different lines of evidence – including global climate
387 model projections, the IPCC AR5 assessment of ice-sheet changes, and structured expert judgement ice-
388 sheet projections, among other sources of information – to generate distributions of future global and
389 associated regional sea-level changes consistent with low, medium, and high emissions scenarios. Sweet
390 et al. (2017) filtered the ensemble of different future projections generated by Kopp et al. (2014) to
391 identify those subsets consistent with 0.3 m, 0.5 m, 1.0 m, 1.5 m, 2.0 m, and 2.5 m of 21st century GMSL
392 rise. These subsets constituted the six Sweet et al. (2017) sea-level scenarios. For most purposes, Sweet
393 et al. (2017) focused on the median of each subset, though 17th and 83rd percentile levels were also
394 reported.
395 This report retains the Sweet et al. (2017) scenarios (except the 2.5 m, discussed below), with the
396 principal difference being updated temporal trajectories and exceedance probabilities now based upon
397 global warming levels rather than emissions scenarios. Specifically, the updates reflect the underlying

ensemble of future projections based upon methods used in the IPCC AR6 (Fox-Kemper et al., 2021; Garner et al., 2021) and listed in Table A1. As in Sweet et al. (2017), these projections are filtered based on 21st century GMSL rise. In addition to being updated based on the latest generation of global climate models and the AR6 assessment, this set of projections incorporates multiple different methods of projecting future ice sheet changes, which are the major sources of future sea level rise and pose the biggest source of uncertainty in projecting the onset and magnitude of future possible rise amounts. For Antarctica, this includes emulators derived from two different ice-sheet model intercomparison exercises (Edwards et al., 2021; Levermann et al., 2020), as well as both a single-model study focused on the potentially high-impact but uncertain likelihood Marine Ice Cliff Instability mechanism (DeConto et al. 2021) and a structured expert judgement study (Bamber et al, 2019). For Greenland, this includes a single intercomparison-derived emulator (Edwards et al., 2021) and a structured expert judgement study (Bamber et al., 2019). The end result is that there is now a broader range of both Antarctic, and more importantly, Greenland distributions (potential contributions) as compared to Sweet et al. (2017). Whereas the high-end scenarios of Sweet et al. (2017) were all dominated by Antarctic contributions, the potential for high Greenland contributions tends to lessen the overall RSL rise in the regional projections.

The use of multiple methods, including methods that consider mechanisms that could substantially increase ice-sheet sensitivity under high-emissions scenarios, means that the time-path of the higher sea-level scenarios is more realistic than in Sweet et al. (2017), which assumed (based on the underlying Kopp et al,. 2014 projections) that ice sheet loss would accelerate at a constant rate over the remainder of the century. A result is that there is less acceleration in the higher scenarios until about 2050 and greater acceleration toward the end of this century. This has two primary implications. First, despite maintaining the same target values and having the same range between scenarios in 2100, the range covered by the scenarios is smaller in the near-term than in Sweet et al. (2017). Second, it also means that the likely (17-83rd percentile) ranges of projections consistent with each scenario before and after the 2100 time point used to define the scenarios tend to be broader than in Sweet et al. (2017).

An important change from the Sweet et al. (2017) report is the exclusion of the Extreme (2.5 m) scenario in this report. Based on the most recent scientific understanding and as discussed in the AR6, the uncertain physical processes that could lead to much higher increases in sea level are now viewed as less plausible in the coming decades before potentially becoming a factor towards the end of the 21st century. A GMSL increase of 2.5m is thus viewed as less plausible and the associated scenario has been removed from this report. Nevertheless, the increased acceleration in the late 21st century and beyond means that the other high-end scenarios provide pathways that potentially reach this threshold in the decades immediately following 2100 (and continue rising).

Section 2.2.4 Observation-Based Extrapolated Projections

As discussed above, the pathways of the updated scenarios differ from those presented in Sweet et al., (2017), including in the coming decades. In particular, the range between the scenarios in the near term is now reduced. To serve as a near-term comparison for the scenarios, this report for the first time includes observation-based extrapolations. Such extrapolations can be potentially misleading if not appropriately constrained. As a starting point, no assessment of whether the long-term rate and acceleration have emerged from the influence of natural variability in the observational record is made in this report, although recent studies suggest this could be the case in some regions (Lyu et al. 2014; Richter et al., 2020; Fasullo and Nerem, 2018). Instead, several methodological choices are made to generate comparable projections to the scenarios. First, the rates and accelerations are estimated from the tide

gauge records starting in 1970. Recent studies have shown a consistent acceleration in GMSL since 1970 (Dangendorf et al., 2019; Frederikse et al., 2020). The impact of varying this start date was assessed and found to be negligible if shortening by only a few years but a larger factor when extending before 1970 or shortening the record length by a decade or more. Second, the extrapolations are made only to 2050. Beyond that date, it is assumed processes not fully represented in the observations could become important or even dominant. Next, the uncertainty in the rate and acceleration associated with the influence of natural variability is accounted for as fully as possible and included in the extrapolation. Finally, the extrapolations are made for GMSL, the coastlines of the contiguous U.S., and eight separate coastal regions around the U.S. and outlying islands. By grouping tide gauges regionally, the influence of localized variability is reduced, yielding more useful extrapolated ranges. For each individual region, the extrapolation is performed as follows:

1. The tide gauges in the region are grouped and combined following the virtual station method (see Frederikse et al., 2020) to generate a monthly time series of relative sea level from 1920 to present.
2. Natural variability is partially removed through regression analysis using climate indices representing El Niño-Southern Oscillation, Pacific Decadal Oscillation and North Atlantic Oscillation (see Calafat et al., 2012; Hamlington et al., 2021).
3. The rate and acceleration from 1970 to present is computed and the uncertainty on each term is assessed accounting for the influence of remaining natural variability (see Hamlington et al., 2021) and serially-correlated variability in the tide-gauge record (Bos et al., 2014).
4. The rates, accelerations and uncertainties are used to generate an ensemble of 5000 extrapolations with a baseline year of 2000 and extending to 2050. Median projections and a likely (17th-83rd) range are computed from this ensemble.

Following this procedure, extrapolated projections are obtained for GMSL, the coastlines of the contiguous U.S, Northeast (ME to VA), Southeast (NC to east coast of FL), Eastern Gulf Coast (west coast of FL to MS), Western Gulf Coast (LA to TX), Southwest Coast (CA), Northwest Coast (OR to WA), Hawaiian Islands, and the Caribbean. Elsewhere in the report, projections are discussed for the Pacific Islands. Due to the availability of tide gauge data and the geographic range covered by the region, the extrapolations are only conducted using those gauges on the Hawaiian Islands. An observation-based assessment is also made separately for the southern and northern coastlines of Alaska and mentioned in the text, but not included in the tables below. Differential vertical land motion heavily impacts the tide gauge records along the southern coastline of Alaska and makes the creation of a regionally representative time series challenging.

Section 2.3 Near-Term Sea Level Change (2020-2050)

In Sweet et al. (2017), the range between the median values of the Low and High scenarios in 2020, 2030, 2040 and 2050 was 0.05 m, 0.12 m, 0.23 m and 0.38 m, respectively. As a result of improved science and the updated framework and procedure for generating the scenarios, the time-path (or trajectory) of the scenarios – particularly the higher scenarios – is now more realistic and consistent with current process-based understanding. In this report, the range between the Low and High scenarios in 2020, 2030, 2040 and 2050 is now 0.02 m, 0.06 m, 0.18 m and 0.28 m, respectively (see Table 2.1). In other words, there is less divergence between the scenarios in this near-term time-period. The Low scenario remains largely the same between this report and Sweet et al. (2017); this range reduction

reflects a downward shift in the higher scenarios in 2050 and times prior, as discussed above. As an example, the projected value in 2050 for the High scenario in this report is the same as that for the Intermediate-High projected value in 2050 in Sweet et al. (2017). In short, while the scenarios continue to be defined by values in 2100, it is important to note that the time-paths have changed in this report compared to the previous one.

Following the procedure outlined in section 2.2.4, an observation-based extrapolated projection of GMSL is computed using the global tide gauge reconstruction from Frederikse et al. (2020) (Figure 2.2A; see top row of Table 2.1). A similar extrapolation was made using GMSL measured by satellite altimeters with comparable results to the tide gauge extrapolation. The projected value of GMSL increase in 2050 relative to a baseline of 2000 is 0.24 m with a likely (17th-83rd percentile) range between 0.19 m and 0.29 m. Based on the updated scenarios, the median of the 2050 observation-based extrapolation is bounded by the Intermediate-Low and Intermediate scenarios. The likely ranges for the Low and High scenarios do not overlap with the likely range of observation-based extrapolation in 2050, though the very likely ranges (5th-95th percentiles) do overlap. The likely range of the Intermediate High scenario does overlap with the likely range of the observation-based extrapolation. The same extrapolation is completed for the contiguous United States (Figure 2.2B) resulting in a projected increase of 0.34 m in 2050 with a likely range of 0.27 m to 0.40 m. This observation-based assessment closely tracks the Intermediate-Low scenario from 2020 to 2050, with the same median and likely range in 2050.

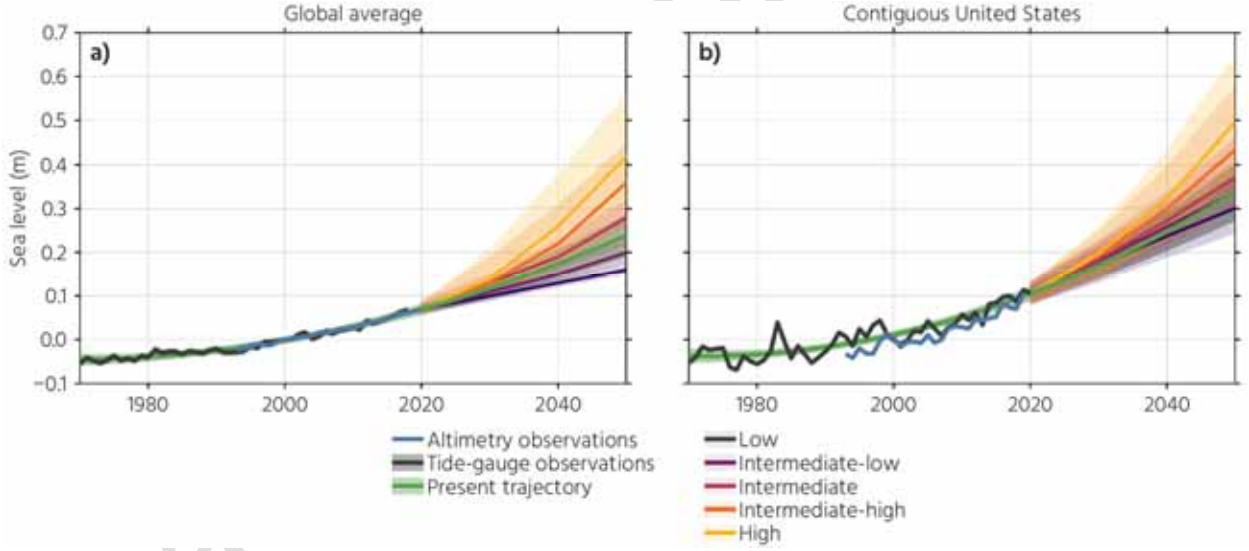

Figure 2.2. Observation-based extrapolations and 5 Scenarios, in meters, for Global Mean Sea level (a) and Contiguous United States (b) from 2020 to 2050 relative to a baseline of 2000. Median values are shown by the solid lines while the shaded regions represent the likely ranges for the observation-based extrapolations and each scenario. Altimetry data (1993 to 2020) and tide gauge data (1970 to 2020) are overlaid for reference.

As a result of the smaller region used and the increased influence of natural variability and VLM, the ranges in 2050 for the US CONUS in both the scenario projections and extrapolations are larger than those associated with GMSL scenarios themselves. The likely range from the observation-based extrapolation does narrowly overlap with the likely ranges from both the Low and High scenarios. This is both a reflection of the larger range in the extrapolation for the contiguous U.S. and the narrower range

between the High and Low scenarios in this report. A key takeaway from this assessment is that on global and national scales, two lines of evidence (observations and scenario pathways) support a narrower range in possible near-term sea-level change than provided in Sweet et al. (2017). As discussed previously, this is consistent with and a result of the improved process-based understanding and projection approach that has been incorporated in this report.

Table 2.1. Observation-based extrapolations and 5 Scenarios, in meters, for Global Mean Sea level and Contiguous United States from 2020 to 2050 relative to a baseline of 2000. Median [likely ranges] are shown.

Global Mean Sea Level				
	2020	**2030**	**2040**	**2050**
Obs. Extrapolation	0.07 [0.06,0.08]	0.12 [0.10, 0.14]	0.17 [0.14,0.21]	0.24 [0.19,0.29]
Low	0.07 [0.06,0.08]	0.10 [0.09,0.11]	0.13 [0.12,0.14]	0.16 [0.15,0.18]
Intermediate Low	0.08 [0.07,0.08]	0.12 [0.10,0.13]	0.16 [0.14,0.18]	0.21 [0.19, 0.24]
Intermediate	0.08 [0.08,0.10]	0.14 [0.12,0.16]	0.20 [0.17,0.24]	0.29 [0.23,0.33]
Intermediate High	0.09 [0.08,0.11]	0.15 [0.12,0.21]	0.24 [0.19,0.33]	0.38 [0.28,0.45]
High	0.09 [0.08,0.10]	0.16 [0.12,0.23]	0.28 [0.19,0.40]	0.44 [0.32,0.58]
Contiguous United States				
	2020	**2030**	**2040**	**2050**
Obs. Extrapolation	0.10 [0.09,0.12]	0.17 [0.14,0.20]	0.25 [0.20,0.29]	0.34 [0.27,0.40]
Low	0.10 [0.08,0.13]	0.17 [0.13,0.21]	0.24 [0.19,0.29]	0.30 [0.24,0.36]
Intermediate Low	0.10 [0.08,0.13]	0.18 [0.14,0.22]	0.26 [0.20,0.32]	0.34 [0.27,0.40]
Intermediate	0.10 [0.08,0.13]	0.18 [0.14,0.23]	0.27 [0.22,0.34]	0.37 [0.30,0.46]
Intermediate High	0.10 [0.08,0.13]	0.19 [0.14,0.25]	0.30 [0.23,0.40]	0.43 [0.33,0.58]
High	0.10 [0.08,0.13]	0.20 [0.14,0.26]	0.34 [0.23,0.43]	0.50 [0.38,0.65]

The observation-based assessment is also completed for eight coastal regions of the United States. At an individual tide gauge, the influence of local - including natural - variability can be large and result in large projected ranges for the near-term decades. To diminish the impact of this variability on rate and acceleration estimates, tide gauges are grouped into regions and combined. The selection of specific regions is driven by process-based similarities mostly associated with ocean dynamics and vertical land motion. As in the global and national cases, the observation-based extrapolations are extended out to 2050. The result is shown in Figure 2.3 for each of the eight regions and compared to the scenarios in each region. It is important to note that all regional scenarios are linked to a GMSL target in 2100 and thus are defined by the change occurring on global scales. In an ideal framework that perfectly represents this regionalization and the relevant regional processes, separate comparisons on a regional level would be unnecessary. Given the process-based uncertainty on a regional level and overlapping of neighboring scenarios in the near-term (discussed in sections 2.4 and 2.5), these comparisons provide an additional line of evidence for the possible trajectory of sea level in the near-term.

Regional differences in the extrapolations and scenarios are consistent with the current process-based understanding of sea-level rise. Processes like ocean dynamics, the gravitational, rotational, and deformational (GRD) response to ice melt (i.e. "fingerprints"), and coastal vertical land motion can lead to differences between the eight regions. Additionally, uncertainty ranges on the extrapolations can be bigger or smaller depending on the number of tide gauges in a particular region and the influence of natural variability on the rate and acceleration estimates. Despite the smaller regions, the projected likely ranges in 2050 are not significantly larger than those for the global and national cases. To demonstrate this regionalization, Figure 2.4 shows these regional variations of sea level in 2050 for the Intermediate Low and Intermediate High Scenarios. Higher values are found along the East and Gulf Coasts. This subsidence leads to the highest rates along the Gulf Coast, where subsidence is driven by regional and local factors, like river sediment compaction and withdrawal of subsurface fluids (Dokka 2011, NGS 2001, Rydlund & Densmore 2012), whereas along the East Coast subsidence is generally associated with the large-scale process of glacial isostatic adjustment, with fluid extraction an issue in some areas (Frederikse et al. 2017, Karegar et al. 2016). In 2050, the regional variation in future sea levels does not change significantly between scenarios. Although the values increase from the Intermediate Low Scenario to Intermediate High Scenario, the east-west difference in sea level rise is similar.

The 2050 values for the observation-based extrapolations and scenarios are shown in Table 2.2. For the observation-based extrapolations, the largest estimates of sea level rise in 2050 are found along the Gulf Coast. In both the scenarios and extrapolations, the Western Gulf Coast has the highest values in 2050, driven by high rates of coastal subsidence in the region. The two regions along the West Coast have the lowest observation-based extrapolations to 2050. For the purposes of offering a comparison to the scenarios, the scenarios that bound the median of the observation-based extrapolations are provided. The Intermediate-Low to Intermediate Scenarios bound three regions (Northeast, Northwest, Hawaiian Islands), the Intermediate to Intermediate High Scenarios bound four regions (Southeast, Western Gulf, Southwest, and Caribbean), and the Intermediate High to High Scenarios bound one region (Eastern Gulf). With only the exceptions of the Low Scenario in the Southwest and Caribbean, the likely ranges from the observation-based extrapolations have at least some overlap with the likely ranges of all the scenarios within a given region. This is again due to a combination of the larger uncertainty on the observation-based assessments at these regional levels for an individual scenario and the narrower ranges between scenarios found in this report compared to Sweet et al. (2017). Finally, while not shown in Table 2.2, the observation-based extrapolation for the northern coastlines of Alaska in 2050 (median value of 0.27 cm) is bracketed by the Intermediate and Intermediate High Scenarios. The extrapolation of the southern coast of Alaska leads to a large RSL decrease in 2050 and is inconsistent with the scenario median values. As mentioned above, this is a result of the large VLM and challenges in generating a representative tide gauge time series to use in the extrapolation. The same framework used for extrapolating forward can also be used to assess the increases - or offsets - observed over different recent time periods. These offsets are useful for adjusting baselines of projections and the scenarios and are provided for each region in Appendix Table A2.

The regional comparisons between the observation-based extrapolations and scenarios need to be considered in the context of the global comparison in Fig. 2.2. The regional scenarios are intrinsically linked to their associated GMSL target value in 2100. In other words, if the observed GMSL trajectory is near the Intermediate Low scenario as shown here, based on the current understanding of the processes driving regional relative sea-level rise, it is not expected that a particular region would track a much higher scenario. These regional comparisons during the near-term time period then serve two potential

purposes: 1) they provide an additional line of evidence along with the GMSL comparisons for the near-term trajectory of sea-level rise; 2) they can serve to identify cases when the contributions of regional processes may be tracking differently than represented by the regionalization of the global scenarios. With respect to the first point, the likely ranges of all but one of the regions is bounded on one side by the Intermediate scenario, showing consistency with the GMSL and contiguous U.S. comparisons. Regarding the second point, the Eastern Gulf is the only region bounded by the High scenario. The process most likely to lead to regional scenario differences from the associated GMSL scenario is VLM, which potentially plays a role here. As a general statement, the link between the regional and global scenarios needs to be considered when drawing conclusions at the regional level based on the observation-based extrapolations.

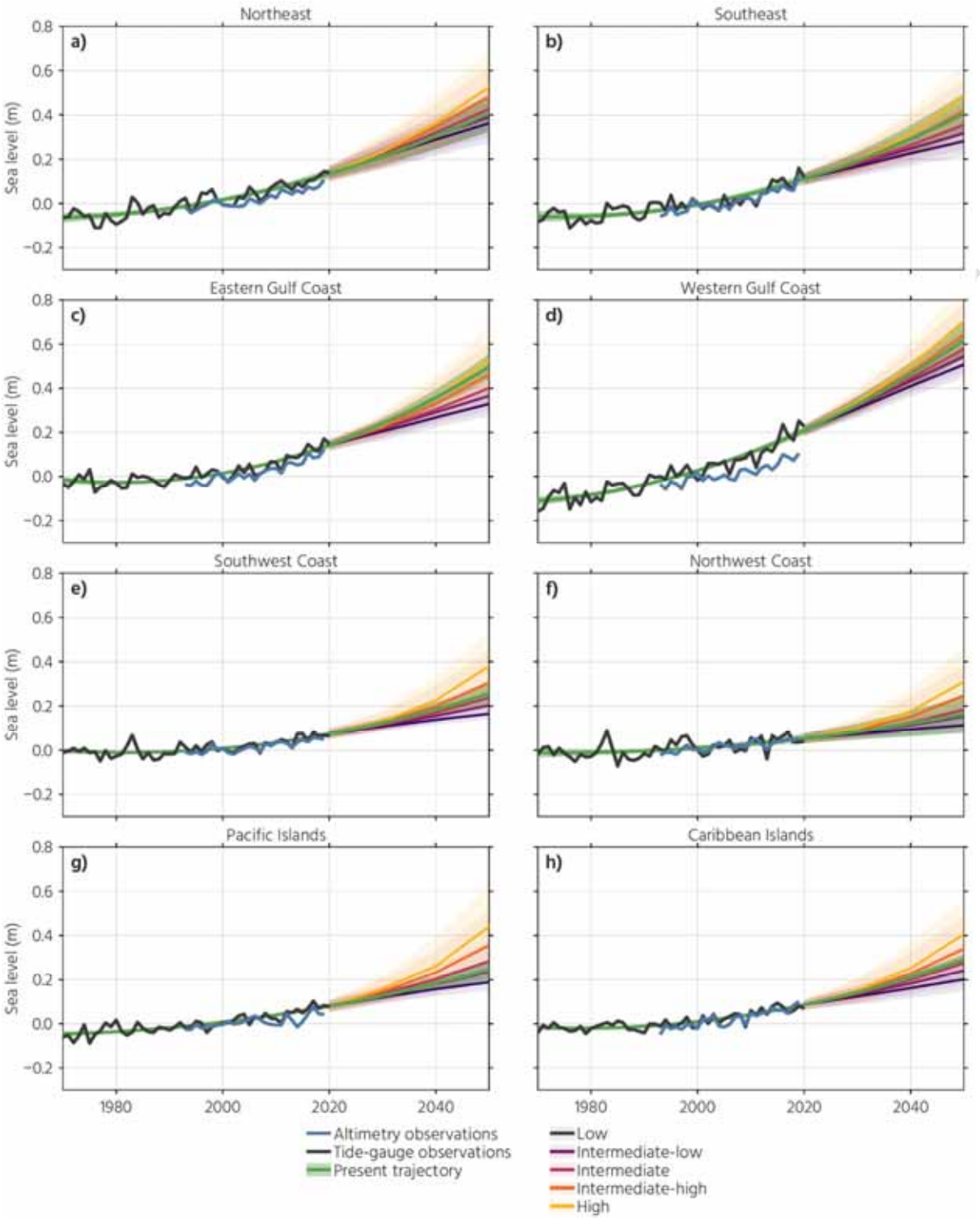

Figure 2.3. Observation-based extrapolations and 5 scenario projections, in meters, for eight coastal regions around the United States from 2020 to 2050 relative to a baseline of 2000. Median values are shown by the solid lines while the shaded regions represent the likely ranges for the observation-based extrapolations and each scenario. Tide gauge data (1970 to 2020) are overlaid for reference, along with satellite altimetry, which does not include contributions from VLM.

Table 2.2. Observation-based extrapolated and scenario-based estimates, in meters, of sea level in 2050 relative to a baseline of 2000 for eight coastal regions of the United States. Median [likely ranges] are shown. The two Scenarios that bound the median observation-based extrapolation are also provided for each region.

Observation Extrapolations	Low	Intermediate Low	Intermediate	Intermediate High	High	Median Bounding Scenarios
Northeast						
0.41 [0.32,0.49]	0.36 [0.28,0.45]	0.39 [0.30,0.49]	0.43 [0.33,0.53]	0.48 [0.37,0.62]	0.53 [0.40,0.69]	Int Low-Int
Southeast						
0.41 [0.32,0.50]	0.28 [0.21,0.35]	0.32 [0.25,0.39]	0.36 [0.28,0.45]	0.42 [0.31,0.56]	0.48 [0.35,0.63]	Int-Int High
Eastern Gulf						
0.5 [0.44,0.55]	0.33 [0.27,0.39]	0.37 [0.30,0.43]	0.4 [0.33,0.49]	0.46 [0.36,0.61]	0.53 [0.41,0.68]	Int High-High
Western Gulf						
0.62 [0.54,0.70]	0.51 [0.45,0.57]	0.55 [0.48,0.61]	0.58 [0.51,0.66]	0.64 [0.54,0.79]	0.71 [0.58,0.87]	Int-Int High
Southwest						
0.25 [0.21,0.30]	0.16 [0.14,0.20]	0.2 [0.16,0.24]	0.24 [0.19,0.31]	0.31 [0.23,0.45]	0.38 [0.26,0.53]	Int-Int High
Northwest						
0.16 [0.08,0.25]	0.11 [0.09,0.15]	0.15 [0.12,0.20]	0.18 [0.14,0.25]	0.25 [0.17,0.39]	0.31 [0.21,0.46]	Int Low-Int
Hawaiian Islands						
0.24 [0.20,0.29]	0.19 [0.15,0.23]	0.24 [0.19,0.29]	0.28 [0.22,0.37]	0.36 [0.26,0.51]	0.44 [0.31,0.63]	Int Low-Int
Caribbean						
0.29 [0.27,0.31]	0.2 [0.15,0.26]	0.24 [0.18, 0.3]	0.27 [0.21,0.36]	0.34 [0.25,0.49]	0.41 [0.29,0.57]	Int-Int High

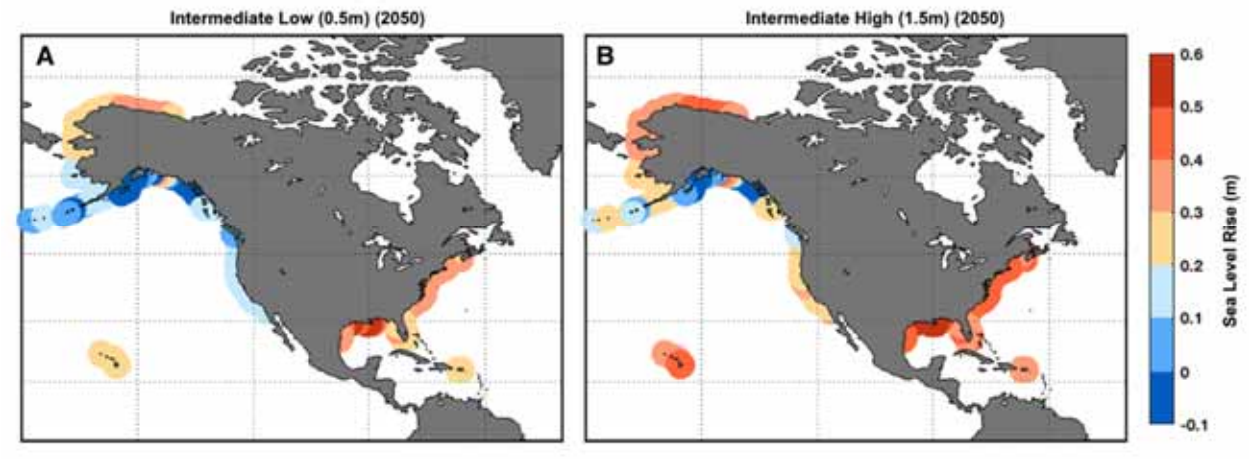

Figure 2.4. Relative sea level (RSL) rise (meters) in 2050 for the a) Intermediate Low and b) Intermediate High Scenarios relative to the year 2000.

2.4 Long-Term Sea-Level Change (2050-2150)

The updated GMSL values in 2050, 2100 and 2150 relative to a 2000 baseline are shown for each of the five scenarios in Table 2.3. Beyond the middle of this century, the differences between sea-level scenarios becomes increasingly large, and the differences between sea-level scenarios becomes increasingly associated with differences in potential future greenhouse gas emissions pathways and associated global warming. Although the scenarios are the same at 2100 between this report and the previous one, there is a narrowing in the range covered by the scenarios in both 2050 and 2150 driven primarily by a reduction in the values associated with the Intermediate High and High scenarios. As previously discussed, in 2050 the updated median value for the High scenario is similar to the median value for the Intermediate High scenario from Sweet et al. (2017). This is not the case in 2150, however, where the separation of the scenarios remains similar to Sweet et al. (2017). Because of this, and since the scenarios are defined by the 2100 values, the same scenario naming is used in this report as in Sweet et al. (2017) with the notable exception of no longer including the Extreme (2.5m) scenario.

Table 2.3: Global mean sea-level (GMSL) and Contiguous United States scenarios, in meters, relative to 2000 baseline.

Global Mean Sea Level			
	2050	**2100**	**2150**
Low	0.16	0.3	0.4
Intermediate Low	0.21	0.5	0.8
Intermediate	0.28	1.0	1.9
Intermediate High	0.37	1.5	2.7
High	0.44	2.0	3.7
Contiguous United States			
	2050	**2100**	**2150**
Low	0.30	0.6	0.8
Intermediate Low	0.34	0.7	1.2
Intermediate	0.37	1.2	2.2
Intermediate High	0.43	1.7	2.8
High	0.50	2.2	3.9

Based on the IPCC AR6 (Fox-Kemper et al., 2021), it is possible to crosswalk the scenarios to future global mean surface air temperatures. The median GMSL projection for 2100 for a world with global mean surface air temperature in 2081-2100 of 2.0°C above 1850-1900 levels is about 0.5 m (*likely* range of 0.4-0.7 m) (Table 2.4), consistent with the Intermediate Low scenario. The median GMSL projection for a world with global mean surface air temperature of 4.0°C higher is about 0.7 m (*likely* range of 0.6-0.9 m), between the Intermediate-Low and Intermediate scenarios, with the upper end of the *likely* range

approaching the Intermediate scenario. These two scenarios are also consistent with the current observed acceleration, which, if extrapolated, would yield about 0.24 m of GMSL rise by 2050 and 0.69 m by 2100.

However, these projections only include physical processes in which there is at least *medium confidence* in the current scientific understanding. As described in IPCC AR6 (Fox-Kemper et al, 2021), the largest potential contributions to long-term GMSL rise come from ice sheets processes in which there is currently *low confidence.* Projections that include the magnitudes, rates, and thresholds associated with these ice sheet processes, particularly under higher emissions futures, could give rise to GMSL rise values well above the *likely* range. Pathways to such lower-likelihood, high-impact outcomes — "potential surprises" in the words of NCA4 (Kopp et al., 2017) — include:

- Earlier-than-projected ice shelf disintegration in Antarctica
- Abrupt, widespread onset of Marine Ice Sheet Instability and/or Marine Ice Cliff Instability in Antarctica
- Faster-than-projected changes in surface mass balance on Greenland, potentially associated with changes in atmospheric circulation, cloud processes, or albedo changes

These outcomes are represented in the IPCC projections through the inclusion of an illustrative very high-emissions (SSP5-8.5), *low confidence* projection range, the 83rd percentile of which for 2100 extends to 1.6 m (modestly above the Intermediate-High scenario) and the 95th percentile of which extends to 2.3 m (above the High Scenario). In 2150, the 83rd and 95th percentiles of this *low confidence* scenario are 4.8 and 5.4 m, respectively. Because these outcomes are based on processes poorly represented in climate and ice sheet models, the IPCC assessment of these processes incorporates information from a structured expert judgement study (Bamber et al., 2019) and a single Antarctic ice sheet modeling study that explicitly incorporates ice shelf hydrofracturing and ice-cliff collapse mechanisms (DeConto et al., 2021).

To connect this to the scenarios provided here, the Intermediate-High and High scenarios represent potential futures in which these deeply uncertain ice-sheet processes play important roles, in the late 21st century and beyond. After 2100, these processes may also play important roles in the Intermediate scenario. As emphasized above, these trajectories are highly emissions-dependent. For example, in an illustrative low emissions (SSP1-2.6) future, in which the world achieves net-zero carbon dioxide emissions by the 2070s and net-negative emissions thereafter, the corresponding AR6 *low confidence* ranges in 2100 extend to 0.8 m at the 83rd percentile (between the Intermediate-Low and Intermediate scenarios) and 1.1 m at the 95th percentile (modestly above the Intermediate scenario), reaching 1.3 m (between the Intermediate-Low and Intermediate scenarios) and 1.9 m (consistent with the Intermediate scenario) respectively in 2150. Thus, in a low-emissions future, there is little evidence to support the plausibility of GMSL projections substantially higher than the median Intermediate scenario.

These warming levels are further compared to the five scenarios in this report by assessing the probability that the given GMSL value in 2100 will be exceeded for a particular warming level (Table 2.4). At all warming levels, there is at least a 92% chance of exceeding the Low scenario in 2100. The probabilities at all warming levels begin to decrease for exceeding the Intermediate-Low (0.5 m) scenario before dropping off rapidly for the Intermediate, Intermediate-High and High Scenarios. This is consistent with the framing of the five scenarios in this report, as greater warming and higher emissions are generally needed to arrive at the Intermediate through High scenarios in 2100.

Table 2.4. IPCC Warming Level Based GMSL Projections, relative to a 2005 baseline (adapted from Fox-Kemper et al, 2021). The probabilities are *imprecise probabilities,* representing a consensus among all projection methods applied. For imprecise probabilities >50%, all methods agree that the probability of the outcome stated is *at least* that value; for imprecise probabilities <50%, all methods agree that the probability of the outcome stated is *less than or equal to* the value stated.

Global Mean Surface Air Temperature, 2081-2100	**1.5°C**	**2.0°C**	**3.0°C**	**4.0°C**	**5.0°C**	**Unknown Likelihood, High Impact – Low Emissions**	**Unknown Likelihood, High Impact – Very High Emissions**
Closest Emissions Scenario-Based GMSL Projection	Low (SSP1-2.6)	Low (SSP1-2.6) to Intermediate (SSP2-4.5)	Intermediate (SSP2-4.5) to High (SSP3-7.0)	High (SSP3-7.0)	Very High (SSP5-8.5)	Low (SSP1-2.6), *Low Confidence* processes	Very High (SSP5-8.5), *Low Confidence* processes
Total (2050)	0.18 (0.16–0.24)	0.20 (0.17–0.26)	0.21 (0.18–0.27)	0.22 (0.19–0.28)	0.25 (0.22–0.31)	0.20 (0.16–0.31)	0.24 (0.20–0.40)
Total (2100)	0.44 (0.34–0.59)	0.51 (0.40–0.69)	0.61 (0.50–0.81)	0.70 (0.58–0.92)	0.81 (0.69–1.05)	0.45 (0.32–0.79)	0.88 (0.63–1.60)
Bounding Median Scenarios in 2100	Low to Intermediate Low	Intermediate Low to Intermediate	Intermediate Low to Intermediate	Intermediate Low to Intermediate	Intermediate Low to Intermediate	Low to Intermediate Low	Intermediate Low to Intermediate
Probability > 0.3 m in 2100	92%	98%	> 99% (99.5%)	> 99% (99.9%)	> 99% (100%)	89%	> 99%
Probability > 0.5 m in 2100	37%	50%	82%	97%	> 99%	49%	96%
Probability > 1.0m in 2100	< 1%	2%	5%	10%	23%	7%	49%
Probability > 1.5 m in 2100	< 1%	< 1%	< 1%	1%	2%	1%	20%
Probability > 2.0 m in 2100	< 1%	< 1%	< 1%	< 1%	< 1%	< 1%	8%

The median regional values in 2100 and 2150 for the eight coastal regions discussed in section 2.3 are provided in Table 2.5. The values in 2100 for each region differ from the GMSL value used to define a given scenario due to the combination of regionally relevant factors that are discussed in section 2.1. The highest values across all scenarios are found in Western Gulf, with the Eastern Gulf the next highest. These high values are heavily driven by the high rates of subsidence in the region. For all but two regions (Southwest and Northwest), the projected values exceed the GMSL values associated

with a particular scenario. The values for each scenario in the Southwest region correspond closely to the GMSL values, which is consistent with the agreement seen between the observation-based extrapolations in 2050 for the global and regional case discussed in section 2.3. To further understand the regional variability for a given scenario, Fig. 2.5 shows the regional departure from the GMSL value for each scenario in 2100. In other words, the provided maps display the amount that needs to be added to the global value to get the associated regional value for a given scenario. The regional pattern is similar in each case. The Gulf Coast is consistently much higher than the global value and the southern coast of Alaska is much lower across all scenarios. In the highest scenarios, the East and West coasts are near the global values, although there is a larger east-west separation in the lower scenarios.

Table 2.5. Scenarios, in meters, for eight coastal regions of the United States in 2100 and 2150 relative to a baseline of 2000. Median values are shown.

Region	Low	Intermediate Low	Intermediate	Intermediate High	High
Northeast					
2100	0.6	0.8	1.3	1.6	2.1
2150	0.9	1.3	2.3	2.7	3.7
Southeast					
2100	0.5	0.7	1.1	1.6	2.1
2150	0.7	1.1	2.1	2.7	3.7
Eastern Gulf					
2100	0.6	0.8	1.2	1.7	2.2
2150	0.8	1.2	2.2	2.8	3.9
Western Gulf					
2100	0.9	1.1	1.6	2.1	2.6
2150	1.3	1.7	2.8	3.4	4.5
Southwest					
2100	0.3	0.5	1.0	1.5	2.0
2150	0.4	0.8	1.9	2.6	3.7
Northwest					
2100	0.2	0.4	0.8	1.3	1.8
2150	0.3	0.7	1.6	2.3	3.3
Pacific Islands					
2100	0.4	0.6	1.1	1.7	2.3
2150	0.6	1.0	2.2	2.9	4.2
Caribbean					
2100	0.4	0.6	1.0	1.5	2.1
2150	0.5	0.9	2.0	2.6	3.7

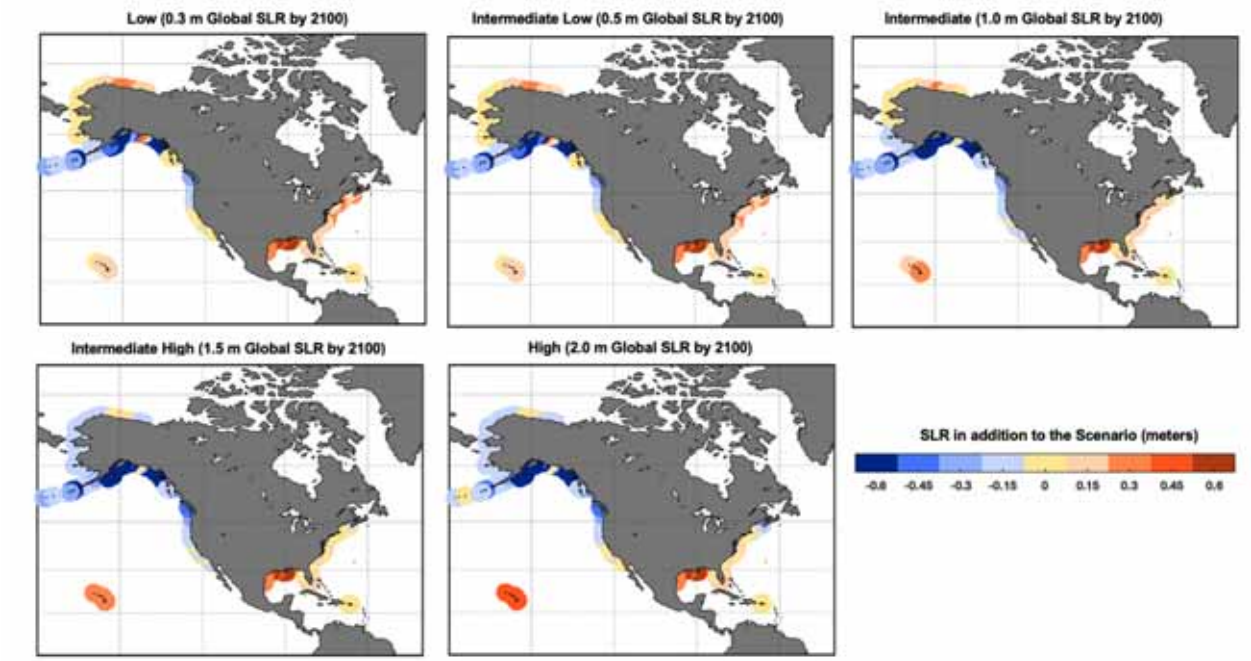

Figure 2.5. Regional deviations from the global mean sea level (GMSL; in meters) value for each scenario in 2100. To obtain the regional projection in 2100 for each scenario, the mapped values must be added to the GMSL value for the associated scenario.

2.5 Scenario Divergence and Tracking

In this report, a specific focus is given to the near-term time period (2020-2050) for the first time. During this window, observations can provide useful information on the trajectory of sea level rise on global and regional scales. Prior to 2050, there is relatively small process-based uncertainty and little sensitivity to different emissions trajectories, and there is reduced spread between the scenarios in this report compared to Sweet et al. (2017). Connected to this reduced spread, the likely ranges of the revised scenarios presented here remain overlapping after 2050 whereas the Sweet et al. (2017) scenarios do not overlap after about 2040. In other words, in this report the process-based uncertainty continues to exceed the scenario divergence past the near-term time period. Until the divergence exceeds the range for a given scenario, it will not be possible to determine when higher-end scenarios will unambiguously emerge from the potential range of the lower-end scenarios for decades to come. In this report, the time periods - or 'gates' - when the scenarios become separable are estimated. Different considerations for determining these gates must be made before and after the near-term time period when the observations are most useful. It should be noted that the gates presented here are based solely on the GMSL differences between scenarios. Regionally, the timing of these gates may be different due to uncertainty in the contributing regional processes. Additionally, other lines of evidence including monitoring of individual processes or emissions trajectories could allow for distinguishing between the scenarios earlier than the gates provided here.

In Figure 2.6, the trajectories of the five GMSL scenarios from 2020 to 2100 are shown and the times or "gates" at which the likely ranges diverge from a particular trajectory or scenario are determined. In Figure 2.6a, the divergence relative to the observation-based GMSL extrapolation is assessed. For the Low and High scenarios, the likely ranges separate prior to 2060 with the Intermediate High scenario

separating shortly after 2060. On the other hand, the Intermediate Low and Intermediate scenarios do not diverge from the extrapolated observation-based trajectory until after 2080. Consistent with the discussion in section 2.3, if the processes driving sea-level rise are assumed to remain similar for the next three decades, the intermediate-low and intermediate scenarios provide useful bounds on GMSL rise for the near-term time period.

In the decades beyond 2050, however, the more uncertain processes described in section 2.4 could become a factor and the extrapolated trajectory becomes less informative. Instead of assessing the divergence relative to this trajectory, the separation gates relative to the Intermediate scenario are shown in Fig. 2.6b. In this case, the Intermediate High and High scenarios will not diverge from the more moderate Intermediate scenario until 2062 and 2075. Only the Low scenario diverges from the Intermediate scenario prior to 2050. Although not depicted in Fig. 2.6, the higher scenarios also start to overlap again after 2100; e.g., GMSL rise consistent with the Intermediate scenario in 2100 (1.0 m) does not rule out GMSL rise consistent with the Intermediate-High scenario by 2150. To tie the two different gate assessments together, although the Intermediate scenario tracks near the current observation trajectory, it will not be possible to statistically distinguish between the Intermediate scenario and higher two scenarios for decades to come. This also provides important context and caution if attempting to use the observations directly to infer future sea-level rise beyond the near-term time period.

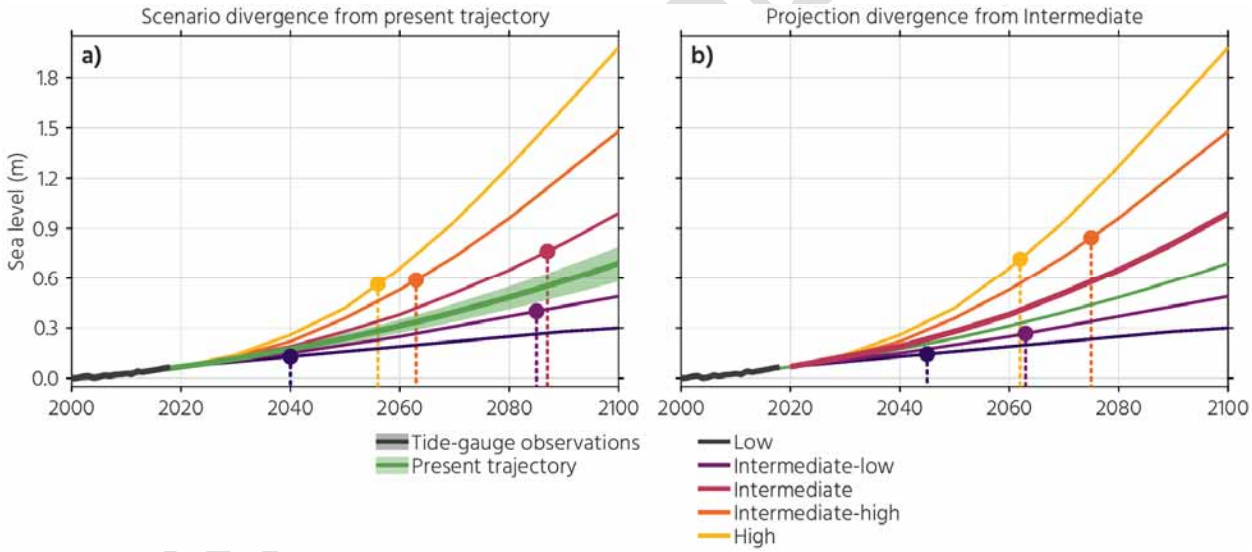

Figure 2.6. Divergence of GMSL trajectory and scenarios. The time series shows the observation-based GMSL trajectory and the five GMSL scenarios from 2000 to 2100. The dots denote where each scenario significantly (2 sigma) deviates from the observation-based trajectory (a) or from the Intermediate scenario (b).

To explore this further, the proportions of IPCC AR6 sea-level trajectories contributing to each GMSL rise scenario are shown in Fig. 2.7, with contributing emissions pathways specified. As an example interpretation of this figure, the Low scenario generally requires a low emissions pathway. Pathways consistent with the Intermediate scenario include both low emissions trajectories, which almost all lead to less than 2 m of GMSL rise through 2150, and high emissions trajectories, under which ice sheet processes could drive GMSL rise greater than 3 m by 2150. These high-end outcomes are also consistent

with the Intermediate High and High scenarios. The above estimates provide a link between the emissions trajectories in the near-term and the possible scenario for GMSL rise in the long-term. When coupled with the "gating" assessment in Fig. 2.6, these hold particular relevance for assessing the trajectory of sea level rise and determining which long-term scenarios are then possible or even likely.

As a way of connecting the elements of the report, this transition time-period can be put in the context of the analysis done in both the near-term and long-term sections. The likely ranges of the Low and Intermediate Low and Intermediate Low and Intermediate Scenarios separate around 2040 and 2055, respectively. The observation-based extrapolations of global GMSL rise have a relatively narrow range out to this time horizon and can therefore play a role in determining whether a particular low-end trajectory or scenario is more or less likely in the coming decades. As shown in Fig. 2.7, the Low scenario depends very heavily on a low emissions pathway on any time horizon. Monitoring using observations both of sea level and emissions can be useful for evaluating the likelihood of the Low Scenario both in the near-term and long-term. On the other hand, the separations of the likely ranges for the Intermediate to Intermediate High and Intermediate to High scenarios do not occur until around 2062 and 2075, respectively. Additionally, the values at the end of the 21st century and beyond for these scenarios can arise under a variety of different emissions pathways, although higher scenarios are predominantly linked to higher emissions, as expected. To state another way, the near-term trajectories discussed in Section 2.3 of this report do not currently inform the likelihood of a given scenario occurring in 2100 or 2150. However, the observations can provide useful monitoring as the windows of separation ("gates") for different scenarios approach in the future. On these global scales, process-based monitoring of the ice sheets, for example, can also play an important role as the higher scenarios are closely linked to the potential for ice sheet changes. Additionally, a link between the scenarios in 2100-2150, emissions pathways and warming levels has been established here. Ongoing and continuous monitoring of both global temperatures (https://climate.nasa.gov/vital-signs/global-temperature/) and emissions (https://gml.noaa.gov/ccgg/trends/) will aid in determining the possible trajectory of future global GMSL rise. It should be noted that while the windows provided in Fig. 2.6 would be different on the national or regional level, the scenarios for a given location are still closely linked to emissions and warming and the monitoring discussion above is still relevant.

FInally, regardless of future emissions pathways, GMSL rise will continue past 2150. The amount of "committed" rise can be assessed based on historical comparisons, modeling, and the current process-based understanding of GMSL rise. This committed rise is the amount of total sea level rise that will likely occur for a given warming level. Here, the committed sea level is shown for 100 year, 2000 year, and 10,000 year time periods. For higher warming levels, the ranges of committed sea level are wide but the possible values are large in magnitude. Even for a relatively low warming level of 1.5℃, the committed sea level over the next 2000 years still ranges between ~2-3 meters. For 2℃, the upper range increases to 6 meters (IPCC AR6). Although the focus of this report is on the time period between 2020 and 2150, this does reinforce the "when, not if" framing provided in Section 1.

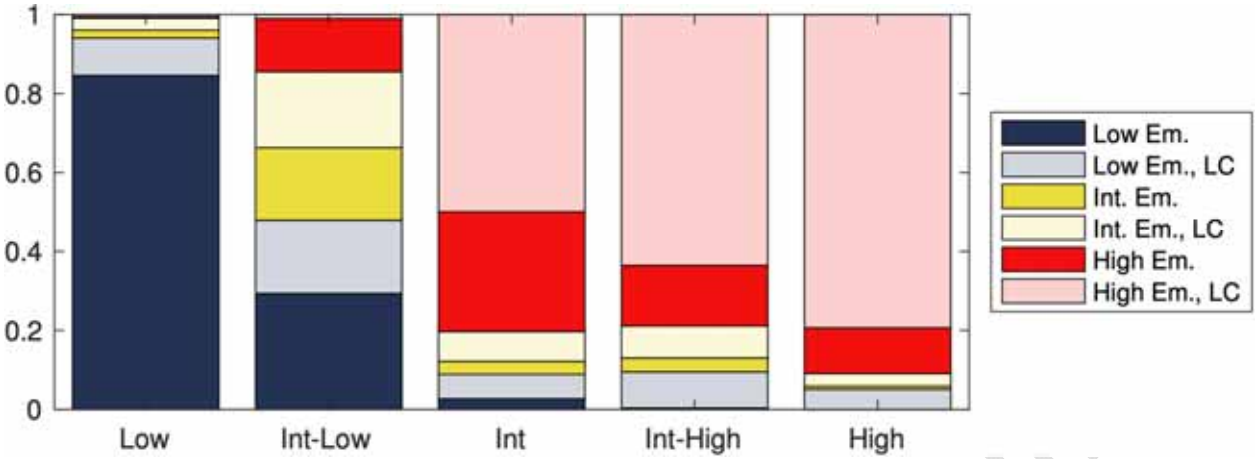

Figure 2.7. Proportions of IPCC AR6 sea-level trajectories contributing to each GMSL rise scenario, with contributing emissions pathways specified. (Low Emissions = SSP1-1.9 or SSP1-2.6; Intermediate Emissions = SSP 2-4.5; High Emissions = SSP3-7.0 or SSP5-8.5. LC indicates inclusion of low confidence ice-sheet processes.)

Section 3: Extreme Water Levels–Regionalization and Changing Coastal Flood Risk

As sea levels continue to rise, coastal water levels–from the mean to the extreme–are growing deeper along most US coastlines, with some limited exceptions like along Southeast Alaska where upward VLM is causing RSL to fall (https://tidesandcurrents.noaa.gov/sltrends/). In response, the wet-dry land delineation (mean higher high water [MHHW] tidal datum) is encroaching landward, causing more permanent inundation and land loss (e.g., in Louisiana), affecting groundwater levels (Befus et al., 2020) and water quality (McKenzie et al., 2021) and altering the intertidal zone and its ecosystems (Kirwan and Gedan, 2019). Especially problematic for the exposure of society's U.S. coastal footprint is that the entire spectrum of flood risk is also growing, from minor (aka "high tide", "nuisance" or "sunny day") flooding to more severe flooding during storms (Sweet and Park, 2014; Fox-Kemper et al., 2021). For example, the national rate of HTF is accelerating and is now (circa 2020) more than double what it was in 2000 due to RSL rise (Figure 3.1) with projections suggesting a doubling of its current rate by 2030 (Sweet et al., 2018; 2021: https://tidesandcurrents.noaa.gov/HighTideFlooding_AnnualOutlook.html; Thompson et al., 2021: https://sealevel.nasa.gov/data_tools/15).

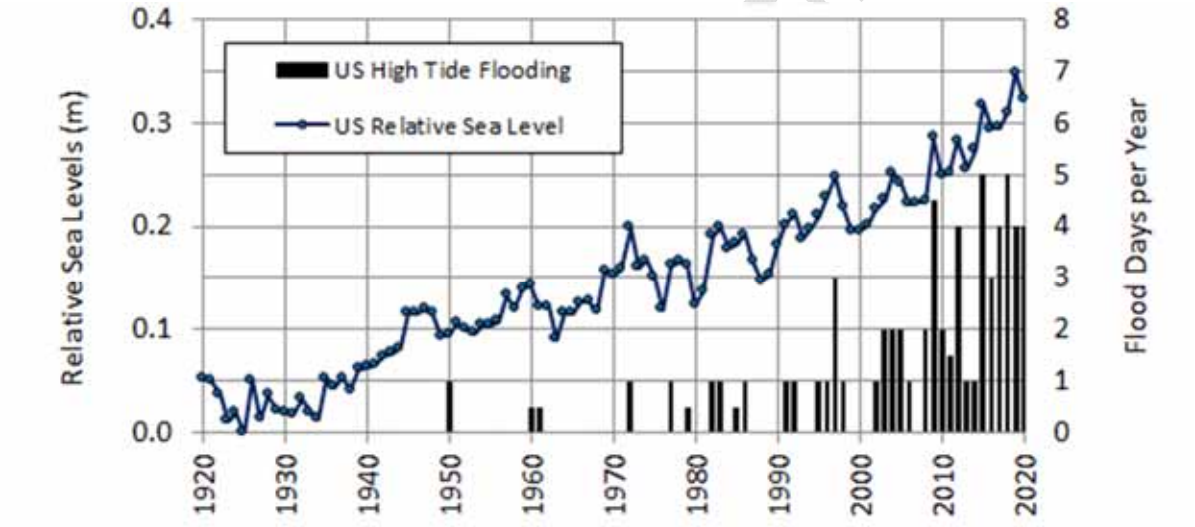

Figure 3.1: National median rate of HTF and relative sea level at 98 NOAA tide gauges along U.S. coastlines outside of Alaska used to monitor and track flood frequency changes (from Sweet et al., 2021). Note: 0.3 m = 1 foot.

Assessments of current and future changes in HTF or deeper, more severe flooding using RSL projections require–at a minimum–contemporary probabilistic information (magnitude and frequency of occurrence) about local water level variability. Specifically, the envelope of variability encapsulating extreme water levels (EWL) (Tebaldi et al., 2012; Church et al., 2013; Hall et al., 2016; Wuebbles et al., 2017; Oppenheimer et al., 2019; Fox-Kemper et al., 2021) capable of causing a range of impacts. The basis for quantifying EWLs along U.S. coastlines originates with NOAA's National Water Level Observation Network, which measures the response from multiple processes operating over a range of frequencies (Table 3.1). However, even this set of coastal tide gauges is relatively sparse compared to the density of coastal communities, and they have varying record lengths. From the perspective of a

particular coastal community, this often results in either 1) a data record that is missing regionally significant rare events like storm surges from land-falling tropical cyclones or 2) has no data at all and often data is simply extrapolated from the closest NOAA tide gauge. Probabilistic assessments using dynamical models can increase spatial coverage (Vousdoukas et al., 2018), but they often perform poorly in areas with high tropical storm activity or with complex bathymetries (Muis et al., 2016).

Table 3.1: Physical processes affecting coastal water levels and their temporal and spatial scale properties (modification of Sweet et al., 2017)

Physical Process	Spatial Scale			Temporal Scale	Potential Magnitude (yearly)
	Global	Regional	Local		
Wind Waves (e.g., dynamical effects, runup)			x	seconds to minutes	< 10 m
Tsunami		x	x	minutes to hours	< 10's of m
Storm Surge (e.g., tropical and extra-tropical storms)		x	x	minutes to days	< 10 m
Tides			x	hours	< 15 m
Seasonal Cycles		x	x	months	< 0.5 m
Ocean/Atmospheric Variability (e.g., ENSO response)		x	x	months to years	< 0.5 m
Ocean Eddies, Planetary Waves		x	x	months to years	< 0.5 m
Ocean Gyre and Over-turning Variability (e.g., PDO response)		x	x	years to decades	< 0.5 m
Land Ice Melt/Discharge	x	x	x	years to centuries	mm's to cm's
Thermal Expansion	x	x	x	years to centuries	mm's to cm's
Vertical Land Motion		x	x	minutes to centuries	mm's to m's

For the U.S. there are two primary sources of federally provided EWL probabilities. The first comes from FEMA (https://www.fema.gov/sites/default/files/documents/fema_coastal-statistical-simulation-methods_nov-2016.pdf) , which provides sets of regional solutions using a combination of NOAA storm-tide observations, historical high water marks (USGS Storm Tide Monitoring), synthetic storm simulations (e.g., Nadal-Caraballo et al., 2020; https://chs.erdc.dren.mil/) and wave effects to estimate the regulatory floodplain and its exposure to the rarest of events (aka 100-year and 500-year event). FEMA provides this information for national flood insurance purposes (https://www.fema.gov/flood-maps/national-flood-hazard-layer), but does not consider future sea levels. Another set of EWL probabilities is from NOAA's Center for Operational Products and Services (NOAA/Zervas, 2013) that currently uses a generalized extreme value (GEV) distribution fit to annual highest water levels for tide gauge records of >30 years https://tidesandcurrents.noaa.gov/est/). The USACE and their Sea Level Change Calculator (https://cwbi-app.sec.usace.army.mil/rccslc/slcc_calc.html) provide the NOAA (2013) EWL probabilities with several projections of future RSL to help in project planning, but for only for specific long-term tide gauge locations.

To further granulate and graduate the probabilistic EWL information currently available from FEMA and NOAA, EWL probabilities and their 95% confidence intervals are provided at a 1-degree spacing along nearly the entire U.S. coastline (Figure 3.2). The EWL information is based upon a regional frequency analysis (RFA; Hosking and Wallis, 1997) of NOAA tide gauges fit with a Generalized Pareto Distribution (GPD). The RFA process not only better assesses EWL exceedance probabilities from a regional perspective, but can supply information where no tide gauges exist. Furthermore, a GPD fit to exceedances above a high threshold as compared to a GEV fit to annual maxima uses more of the data record (e.g., two significant events within a particular year), not just those maxima within a certain (e.g., annual) time block. It also better resolves the high-frequency part of the flood frequency spectrum such as events occurring several times a year.

This work builds off of methods of Sweet et al. (2020) and by Hall et al. (2016), which supported exposure assessments for the U.S. Department of Defense coastal installations worldwide (https://drsl.serdp-estcp.org/). RFA-based studies are widely used to help provide spatial information where local observations are lacking, including rainfall intensity, duration and frequency curves used for stormwater management planning within the U.S. by NOAA (https://www.weather.gov/owp/hdsc; Perica et al., 2018).

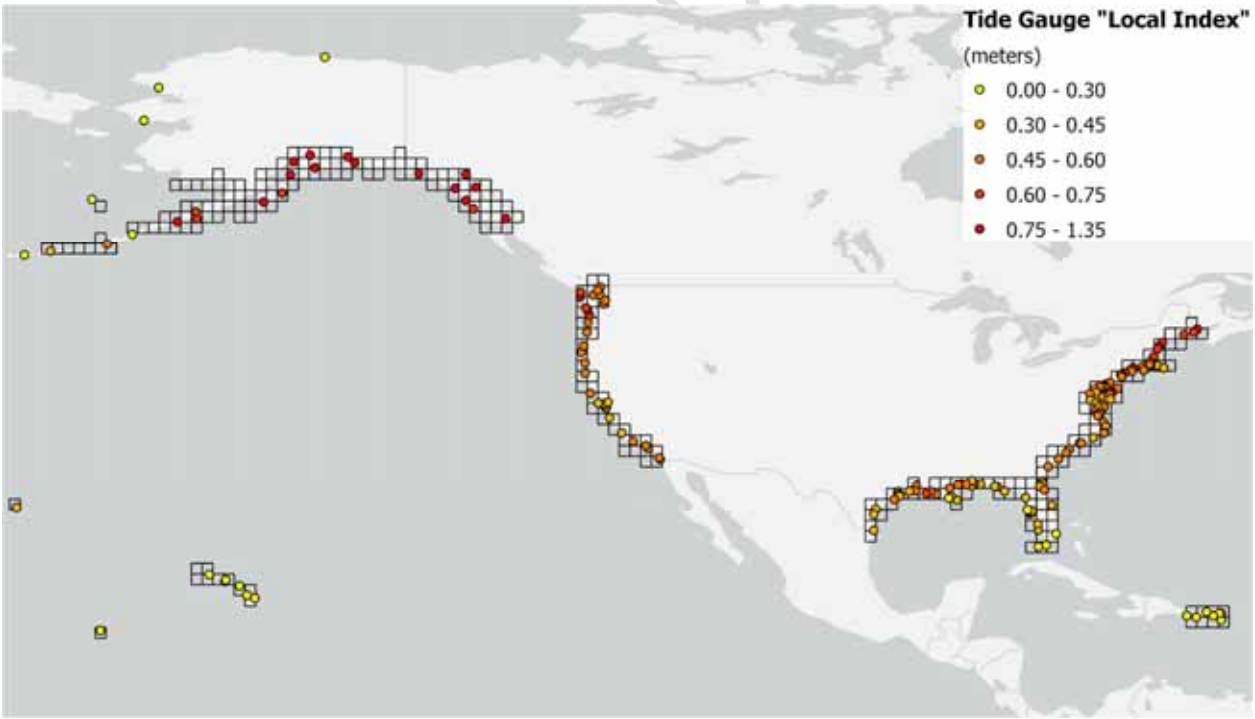

Figure 3.2. Regional Frequency Analysis (RFA) 1-degree grids and local indices (98th% of daily maximum water level) at the NOAA tide gauges used in this study.

To be useful for local decision making, the gridded EWLs ($EWL_{gridded}$) need to be further localized (EWL_{local}), which is achieved via a 'local index (u)' estimated at a particular tide gauge (u values are

shown in Figure 3.2) or for a particular location. The following equation is used to estimate EWL_{local} probabilities (median and 95% confidence intervals):

(1) $EWL_{local} = EWL_{gridded} * u_{local} + u_{local}$

where u_{local} referred below simply as 'u' are the same value and is the height of the 98th% of daily highest water levels with a 4-day event filter above the 1983-2001 (or 5-year modified epoch) MHHW tidal datum. Another way to understand Equation 1 is that because 'u' is both the threshold (height above MHHW) in the GPD fit and the local index (used to normalize the gauge-specific data before grouping) in the RFA process used to compute the $EWL_{gridded}$, to obtain a EWL_{local} estimate, a similar set of operations need to be applied. See the Method Appendix for more details.

Below, local indices for all NOAA tide gauges with >10 years of record are used to compute EWL_{local} probabilities and these results are compared to NOAA and FEMA datasets. Next, methods are discussed for how local indices can be 1) computed using other records, e.g., such as those of shorter duration (<10 years) from NOAA or other (user supplied) sources and 2) estimated approximately every 500 meters along the U.S. coastline based upon local tide range information from NOAA models (e.g., https://vdatum.noaa.gov/). Lastly, we will assess current and future flood risk within the coastal floodplain using NOAA's height/severity categories of minor, moderate and major coastal flooding (Sweet et al., 2018), which broadly define water levels where America's infrastructure becomes impacted and are used in weather forecasting to trigger emergency responses (NOAA, 2020). Estimates of how flood risk is projected to change by 2050 (assuming no additional adaptation) use the upper-bounding scenarios of the regional trend extrapolations along U.S. coastlines (Table 2.2).

For consistency, average annual event frequency terminology will be used to describe event probabilities that recur annually and more often (e.g., 1 per year, 10 per year) and less often such as 0.1 event per year, which has a 10% annual chance of occurring to describe an event with an average recurrence interval of 10 years.

3.1 Average Event Frequencies of Extreme Water Levels

The focus of this analysis is on EWL 'events' that occur between 10 times per year and those with about a 1% annual chance (Coles, 2001), which sufficiently spans the frequency space associated with coastal infrastructure flooding under contemporary sea levels (Sweet et al., 2018). Such events can last a couple days and span several tidal cycles. An example for The Battery in NYC (Figure 3.3a) shows NOAA flood heights and probability densities of total hours and daily highest water levels. Also shown is the local index (u=0.55 m above MHHW) computed at the NOAA tide gauge, which is used to estimate EWL_{local} from the $EWL_{gridded}$ probabilities for this location (Figure 3.3b). See Figure A2f in the Appendix for the gridded probability for the NYC region. At higher frequencies, the EWL_{local} exceedance probabilities for 'events' align with those for 'days' based upon those fit to highest daily water levels (Figure 3.3a), which NOAA uses when making HTF projections (Sweet et al., 2018). For reference, at the NYC tide gauge, a minor flood 'event' (≥ 0.56 m MHHW) has the EWL_{local} derived probability of occurring 4-5 times a year (Figure 3.3b) based upon contemporary (~2020) RSLs. For comparison, the NOAA HTF outlook for

2020 was 9-14 'days' for 2020, which is based upon historical trends fits of past annual HTF counts (Sweet et al., 2020).

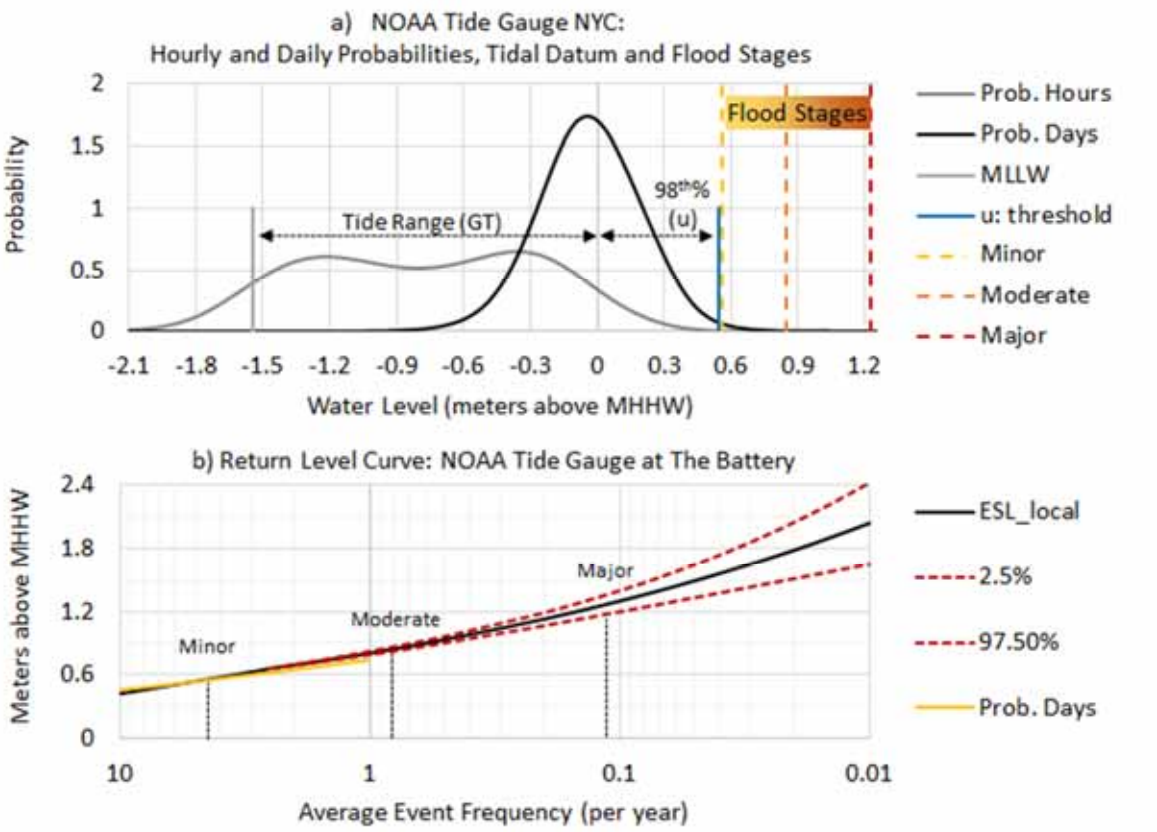

Figure 3.3: a) Probability densities of total hours and daily highest water levels at The Battery in NYC showing the tidal datums of MHHW, MLLW and GT (tide range), local flood heights and the local index (u) used to localize the RFA gridded EWL (see Appendix Figure A2f) shown in b) as a return interval curve with the 95% confidence interval (2.5 and 97.5% levels) normalized to year 2020 RSLs and an overlay showing close agreement with the daily highest water level probabilities shown in a).

Some general patterns emerge comparing $EWLs_{local}$ that occur once per year on average (Figure 3.4a) across the network of NOAA tide gauges and those having a 1% annual chance of occurring (Figure 3.4b). Locations with higher 1% annual chance EWL_{local} are found adjacent to wide, shallow continental coasts that are exposed to tropical or extratropical storm surges such as occurs along the Eastern and Western Gulf Coasts with (median ± 1 standard deviation) of 2.5±1.1 m and 2.8±0.8 m, respectively. In contrast, the U.S. Pacific Islands and the SW Pacific coasts have relatively smaller 1% annual chance $EWLs_{local}$ for the same reasons (0.8 ± 0.1 m and 1.0 ± 0.1 m, respectively). It should be stressed that the EWLs provided here are based upon tide gauge measurements, which do not typically report values that include higher frequency wave effects (Sweet et al., 2015), which tend to be the causes of flooding, overwash and erosion (Barnard et al., 2019; see 'waves' call out box below). In terms of the 1-yr event heights, larger tide ranges become increasingly influential (correlation of ~0.7 across all locations), such

as is the case along the NW Pacific and Alaskan coasts where highest 1-year EWLs occur (0.8±0.1 m and 1.0±0.3 m, respectively).

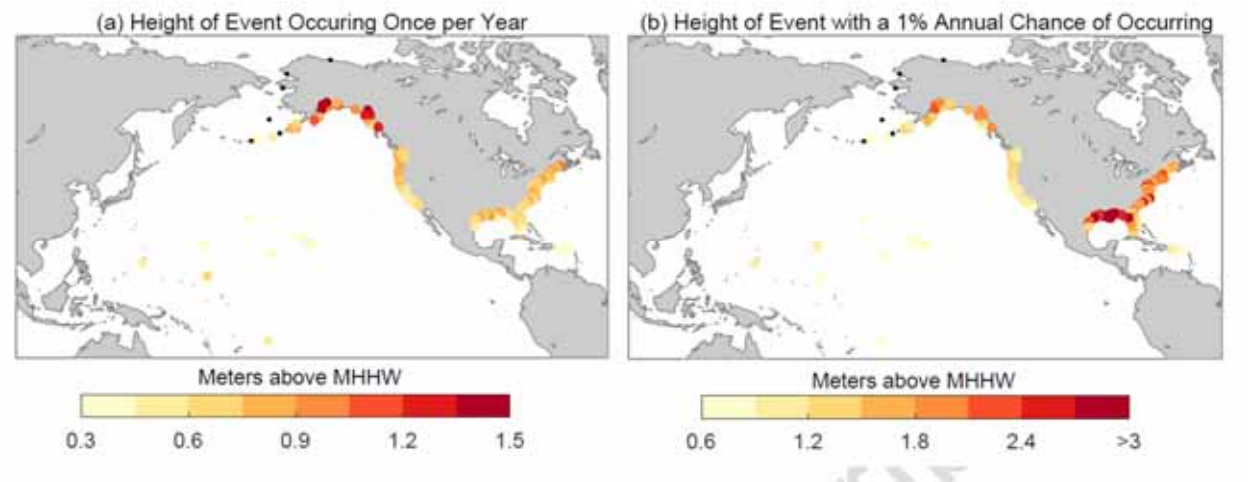

Figure 3.4: Contemporary (~2020 RSLs) EWL_{local} that a) occur annually on average and b) have a 0.01 year average event frequency (1% annual chance of occurring).

There are differences when comparing the RFA $EWLs_{local}$ from this study to current FEMA and NOAA governmental datasets. Comparisons to NOAA EWLs (Zervas, 2013) in Figure 3.5a-c show that the RFA EWL_{local} 1%, 10% and 50% annual chance events are about 6%, 9% and 13% higher across the board based upon linear regression, respectively. The bias between data sets is not unexpected, as the RFA typically increases median EWL probabilities and narrows the confidence intervals due to the regionalization process as compared to a single-gauge analysis (Sweet et al., 2020). Overall there is a fairly tight goodness-of-fit between datasets (high r^2 values), though less so at the 1% annual chance level (r^2=0.49) due in part of the large differences occurring along Gulf coastlines of Alabama, Mississippi and Louisiana where the RFA 1% annual chance EWL_{local} (~ 4 m above MHHW) are substantially higher (> 1 m) than the NOAA GEV estimates in a few locations .

The RFA EWL_{local} probabilities are also compared to the tide gauge-equivalent 'stillwater' component (tides, storm surge and wave setup, but not breaking wave effects) generated by FEMA used within their Flood Insurance Studies (Figure 3.5d-f). The FEMA EWLs vary in their construction by region, using a combination of singular and RFA tide gauge analyzes, storm-surge modeling and synthetic tropical storm modeling (East and Gulf Coasts) via a joint probability method - optimal sampling (JPM-OS) procedure. https://www.fema.gov/sites/default/files/2020-02/Coastal_Flood_Frequency_and_Extreme_Value_Analysis_Guidance_Nov_2016.pdf; https://www.fema.gov/sites/default/files/documents/fema_coastal-statistical-simulation-methods_nov-2016.pdf). The 1% and 10% annual chance RFA EWL_{local} are slightly lower (7% and 4%, respectively) with differences again noted along Gulf and Caribbean Island coastlines. At the 50% annual chance levels, both sets of EWLs are nearly the same based upon linear regression. The goodness-of-fit (r^2 values) are about the same as with the NOAA (2013) GEV results, though a little less at the 1% annual chance levels likely due to the inclusion of synthetic storm-surge modeling in the FEMA estimates, whereas the NOAA (2013) values are based upon tide gauge observations.

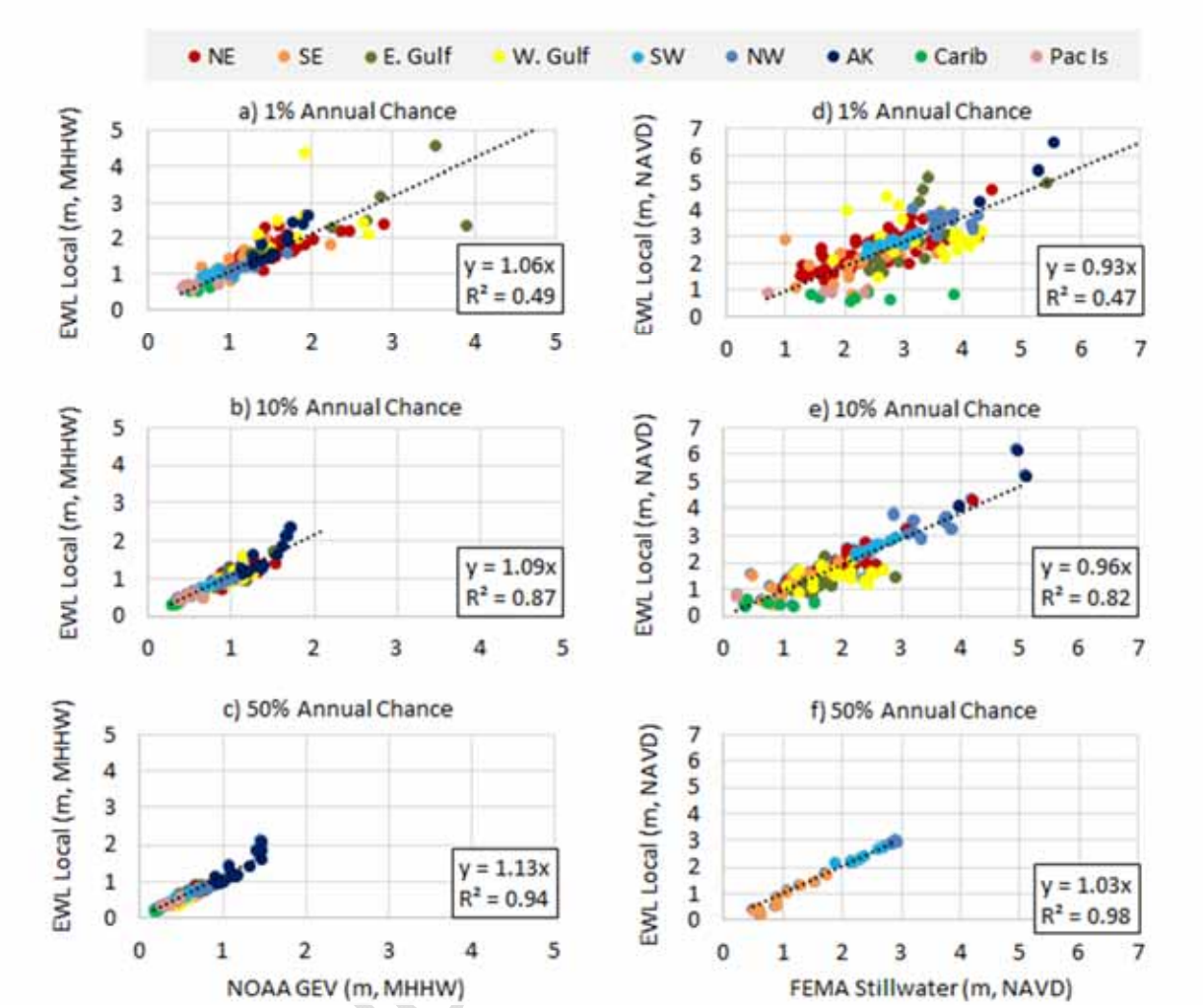

Figure 3.5: Comparison between this study's EWL_{local} to those of NOAA (Zervas, 2013) based upon a GEV fit of annual highest water levels a)-c) and to the stillwater (storm surge, tides, wave setup) components of FEMA used in their Flood Insurance Studies d)-f) at the 0.01 year, 0.1 year and 0.5 year average event frequency (1%, 10% and 50% annual chance) levels.

3.2 Methods to localize the Gridded extreme water Level (EWL) Event Probabilities

There are several ways to obtain EWL_{local} from the $EWL_{gridded}$. All require a local index (u), which can be obtained from 1) a NOAA tide gauge used in this study (e.g., shown in Figures 3.2), 2) alternative sources of water level/tide gauge data not used in this study (e.g., Figure A3 in Appendix) or 3) from tide range knowledge from measurements or models. When using short-term water level measurements (Figure 3.6a) additional uncertainty, dependent upon record length, is factored into the 95th confidence interval of the EWL_{local} estimate (see Equation 4 in the Appendix). This additional uncertainty relates to the fact that the local index (u=98th% of daily 'events'), will vary from year to year akin to how RSL vary through time (https://tidesandcurrents.noaa.gov/sltrends/sltrends.html). On a national scale (and most regions

as well, Figure A4), the RMSE in local index estimates are about 6-7 cm after 5 years and falls to less than 3 cm at 10 years, which is close to the standard error in tidal datum calculations themselves (see datum errors at https://tidesandcurrents.noaa.gov/pdf/).

Where local water level measurements are not available, another option to estimate a local index (u) and an EWL_{local} is based upon an underlying relationship between local index values and tide range (great diurnal tide range: GT) along U.S. coastlines. Additional uncertainty using this method will need to be factored into the results as well. This relationship (Figure 3.6b) builds off of the findings of Sweet et al. (2020) within the Pacific and globally of Merrifield et al. (2013) who found a strong global correlation between the range of water level variability and average annual highest water level across the globe. Nationally, there exists a strong positive relationship (r^2=0.72) though with fairly large uncertainty (RMSE of 0.11 m). But when quantified regionally, all the fits' RMSEs are less (Figure A5). As a whole, it takes about 6 years of measurement for the RMSE (Figure A4) in local index (u) estimates to match those based upon measured tide range (Figure A5). Tide range information can be obtained from NOAA Vertical Datum Transformation (VDatum: https://vdatum.noaa.gov/).

As an example, EWL_{local} probabilities are estimated for the NOAA tide gauge at Grand Bay, MS (https://tidesandcurrents.noaa.gov/stationhome.html?id=8740166), which is located within a NOAA National Estuarine Research Reserve (Figure 3.6c). This location falls within the EWL grid number 42811 with its gridded return level curves values provided by NOAA (NOAA API website). There is about 5 years of hourly data (see Figure A3 for more short-term NOAA tide gauges), of which 4 years is analyzed (2011, 2012, 2015, 2016) to obtain a local index (u) of 0.47 m above MHHW. As it turns out, the measured tide range at this location (0.49 m) leads to an estimated local index value also of 0.47 m through the regional regression (Figure A5: Apalachicola-Calcasieu Pass subplot). The RMSE based upon the tide range regression is 0.078 m (Figures A5) and is less than the 0.099 m RMSE based upon a 4-year water level record for this region (Figure A4). A contemporary (~2020) EWL_{local} return level curve (Figure 3.6d) is generated by substituting a local index value of 0.47 and a RMSE of 0.078 m (with a variance of 0.078^2) into Equation 1 and Equation 4 (see Method's Appendix), respectively. To update the curves to RSLs of 2020 from 1992, 0.12 m is added to the return level curve values (trend in 'u' of ~4.3 mm/yr x 28 years; Appendix Table A3).

Since the local index estimated for Grand Bay (0.47 m above MHHW) is similar to others computed at nearby tide gauges that share the same 1-degree $EWL_{gridded}$, (Figure 3.2), their return interval curve values are similar (Figure 3.4b). Less noticeable is that the 95th confidence intervals are more inflated by using this method (i.e., 0.5 m vs. 0.1 m at the 1-yr EWL). Nationally, the spread of the 95% confidence interval at the 1-yr EWL_{local} using a local index (u) estimated by tide range (Figure 3.6b and Figure A5) is 0.32 m as compared to 0.03 m when assessed across all NOAA tide gauges.

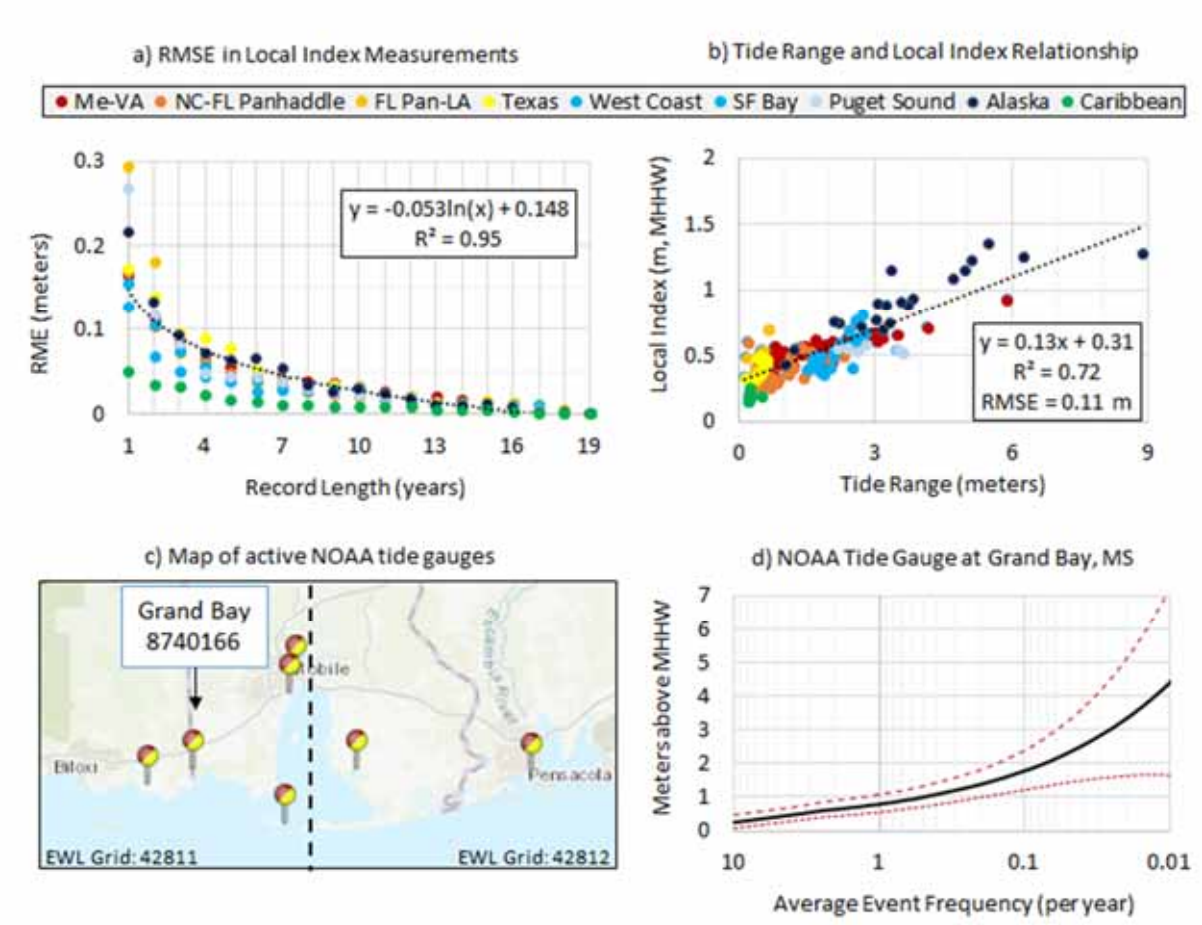

Figure 3.6: a) Root mean square error (RMSE) for estimates of u based upon 1–19 years of consecutive data over the 2001–2019 period based regional sets of tide gauges used in this study that mostly align with the National Climate Assessment, b) a national tide range to local index (u) regression with equations, goodness of fit (R^2) and associated RMSE, c) map showing active NOAA tide gauges indicating Grand Bay, which has about 5 years of hourly data and d) a 2020 EWL_{local} return level curve for Grand Bay using a local index (u) from tide range regression. Regional estimates for a) and b) are provided in Appendix Figures A4 and A5, respectively.

3.3 The Changing Nature of Coastal Flood Risk

To assess U.S. coastal flood risk using the EWL_{local} probabilities, we use the nationally calibrated coastal flood heights of NOAA (Sweet et al., 2018) and a modification of Sweet et al. (2020) for Alaska coastlines (see Methods Appendix). The NOAA flood heights include a minor, moderate and major category (national median) starting at about 0.55 m, 0.85 m and 1.20 (See Appendix and Figure A6) whose impacts are often disruptive, damaging and often destructive, respectively, under current flood defenses. NOAA provides data (e.g., (https://coast.noaa.gov/arcgis/rest/services/dc_slr/Flood_Frequency/MapServer) and maps (Figure 3.7) in its SLR Viewer of exposure to HTF to help communities recognize potential flood risk associated with weather-water level forecasts and for vulnerability assessments associated with sea level rise.

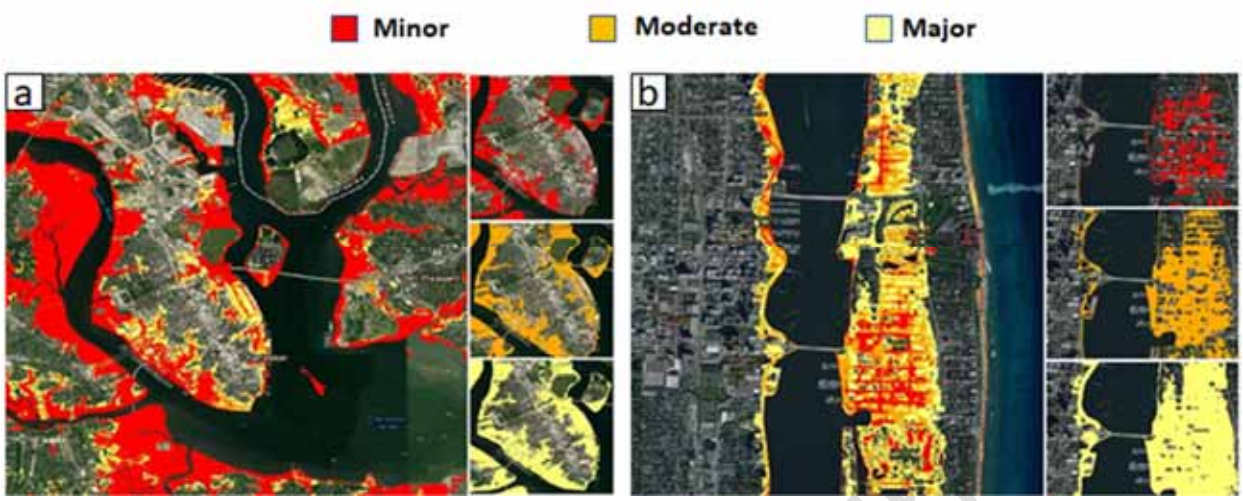

Figure 3.7: NOAA minor (red layer: land between MHHW and minor HTF flood height above MHHW), moderate and major HTF maps showing a regional layered map with individual layer panes to the right for a) Charleston, SC and b) West Palm Beach, FL. 1983-2001 MHHW is the shoreline edge.

Currently, (with EWL_{local} normalized to year 2020) minor flood events occur (median value) about 3 times/year along U.S. coastlines, and are highest (about 4 events/year) along the NE Atlantic, Western Gulf and NW Pacific coastlines and about 2 events/year along the SE Atlantic and Eastern Gulf coastlines (Figure 3.8a). A similar pattern emerges when comparing the 2020 NOAA high tide (minor) flood outlook (Sweet et al., 2020b) for the number of flood 'days' at about 100 of the tide gauges (Figure 3.8b). The NOAA Outlook for minor (high tide) flood days is based upon extrapolation of either linear or quadratic fits to days per year with a water level at or above the flood height. As a whole, there are about twice the number of 'days' of minor (high tide) flooding than the number of 'events' (Figure 3.8b insert) largely reflective of the 4-day event filtering used in the RFA process and GPD fitting. The national median HTF outlook for 2020 was 4-5 days, with about 8-9 days each along the NE Atlantic and Western Gulf Coasts and 3-5 days each along the SE Atlantic and Eastern Gulf Coasts (Sweet et al., 2020b).

Currently, moderate flooding in 2020 (Figure 3.8c) has about a (median value) a 30% annual chance of occurring nationally, and similarly (20-40% annual chance) along the SE Atlantic, Eastern Gulf and NW Pacific Coasts. It is highest along the NE Atlantic and Western Gulf coasts (60-70% annual chance). Major flooding (Figure 3.8d) nationally, and along the SE Atlantic Coasts, has about a 4% annual chance of occurring. Major flooding is most likely along the Western Gulf Coast (15% annual chance) and along the Northeast and Eastern Gulf Coasts has 8-9% annual chance of occurring. For a more-local reference (Figure 3.7), 2020 annual flood frequencies/probabilities of minor, moderate and major HTF in Charleston and West Palm Beach were about 2-3 events per year, a 15-25% annual chance and about a 2-4% annual chance event, respectively, based upon nearest tide gauge (see Table A2).

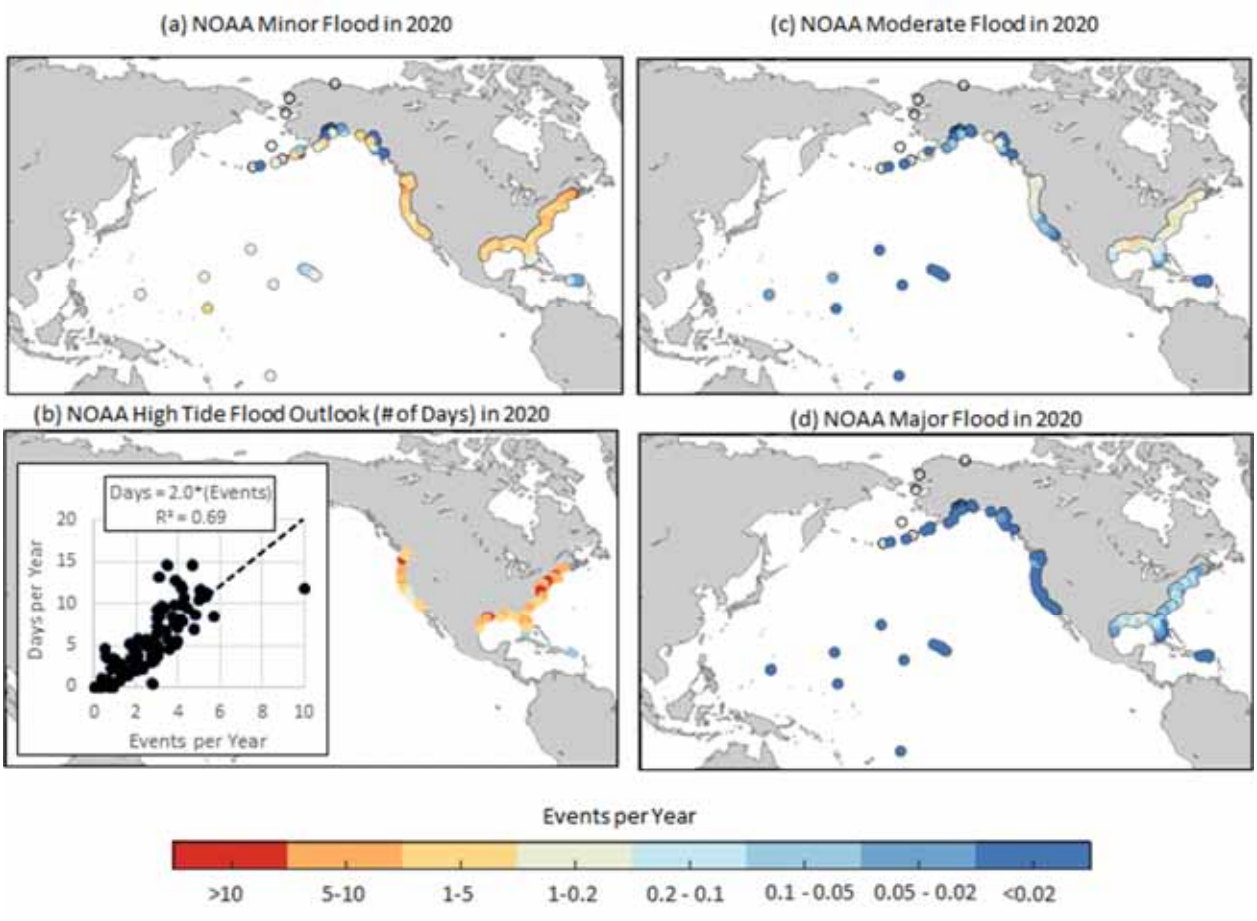

Figure 3.8: Average event frequencies in 2020 of a) minor high tide flooding (HTF) and b) number of days (as compared to 'events') of HTF estimated in NOAA's annual outlook and regression between events and days, c) average event frequencies of c) moderate HTF and d) major HTF using flood height-severity definitions of NOAA (Sweet et al., 2018) and Sweet et al. (2020b) for Alaska locations.

Changes in flood risk are projected to 2050 considering no additional flood mitigation or adaptation at NOAA tide gauges (Figure 3.9) using the scenario projections providing the upper bound to the regional trend extrapolations (Figure 2.3 and Table 2.2). Nationally, and along all regions except the Hawaii/Pacific (about 9 days), the Caribbean (about 6 days) and Alaskan (70% annual chance) coastlines, the median event frequency in minor (high tide) flooding is projected to increase to >10 events/year.

Moderate flooding (median) frequencies (Figure 3.9b) are projected by 2050 to increase nationally to about 4 events/year, >10 events/year along the Western Gulf, with 3-6 events/year along the NE and SE Atlantic and Eastern Gulf Coasts, about 1 event/year along the NW Pacific and a 70% annual chance along the SW Pacific. Major flooding frequencies (Figure 3.9c, f) are likely to increase to about a 20% annual change nationwide (median), occurring annually along the Western Gulf Coast, a 50% annual chance along the NE Atlantic Coast and between a 20-30% annual chance along SE Atlantic and Eastern Gulf Coasts. Again, for a more local frame-of-reference, 2050 projections of annual flood frequencies/probabilities of minor, moderate and major HTF collectively in Charleston and West Palm Beach are >10 events/year, 4-5 events/year and a 10-20% annual chance of occurring.

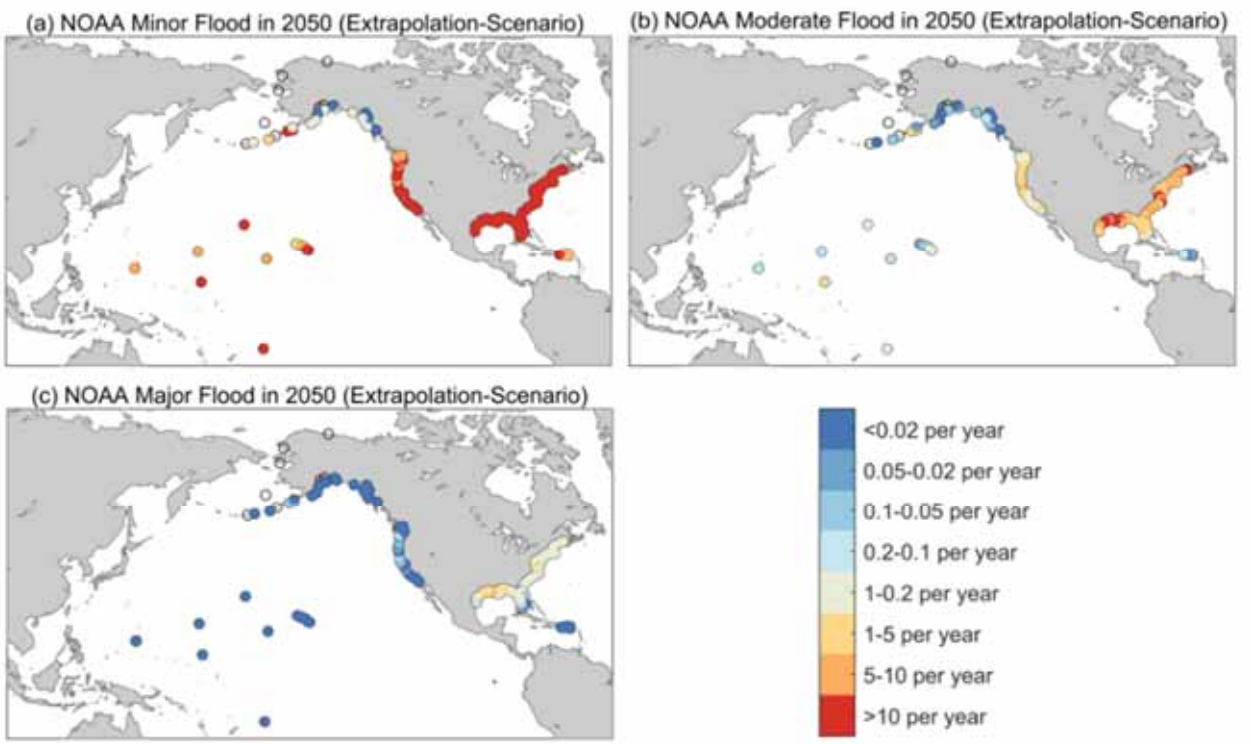

Figure 3.9: Coastal flood frequencies projected at 2050 using the sea level projection that upper-bounds the current trend extrapolations for a) minor flooding, b) moderate flooding and c) major flooding

For perspective and a summary assessment by region, Table 3.2 quantifies how minor, moderate and major flood frequencies have changed and are projected to change under the upper-bounding scenario of the regional trend extrapolations (Figure 3.9) using 1990, 2020 and 2050 time slices. Nationally, minor flood frequencies nearly tripled between 1990 and 2020, growing from about 1 to 3 per year. They are projected to more than triple by 2050 with >10 per year. Moderate flood frequencies experienced about a 50% increase (a 0.2 event/year frequency or 20% annual chance growing to a 30% annual chance) from 1990 to 2020, which is slightly higher than the frequency increase in major flood frequencies (3% annual chance growing to a 4% annual chance). By 2050, moderate flood frequencies are projected to increase by more than a factor of 10 (30% annual chance growing to about 4 events/year) with about a factor of 5 increase in major flood frequencies (4% annual chance growing to a 20% annual chance). In short, under current trends and summarized at the national level, a flood regime shift is projected by 2050, with moderate flooding occurring a bit more frequently than minor flooding events occur today and major flooding occurring in 2050 about/close to moderate flood frequencies.

Table 3.2: Average annual event frequencies for NOAA-defined minor, moderate and major flood heights by region that were typical (median values) in 1990, under current (2020) sea levels and projected to occur considering the upper-bounding scenario of the current trend extrapolations in 2050 (see Table 2.2).

U.S. Region	1990			2020			2050		
	Minor Flood	Moderate Flood	Major Flood	Minor Flood	Moderate Flood	Major Flood	Minor Flood	Moderate Flood	Major Flood
National	1	0.2	0.03	3	0.3	0.04	>10	4	0.2
*Hawaii/Pac Is	0.06	<0.02	<0.02	0.2	<0.02	<0.02	9	0.1	<0.02
NE Atlantic	2	0.3	0.06	4	0.6	0.09	>10	6	0.5
SE Atlantic	0.9	0.1	0.03	2	0.2	0.04	>10	4	0.2
E. Gulf	0.7	0.2	0.06	2	0.3	0.08	>10	3	0.3
W. Gulf	1	0.3	0.1	4	0.7	0.2	>10	>10	1
SW Pacifc	0.8	0.02	<0.02	1	0.04	<0.02	>10	0.7	<0.02
NW Pacific	3	0.3	<0.02	4	0.4	<0.02	>10	1	0.03
*Alaska	0.7	<0.02	<0.02	0.2	<0.02	<0.02	0.7	0.03	<0.02
US Carib	0.02	<0.02	<0.02	0.04	<0.02	<0.02	6	0.04	<0.02

*The Pacific Islands used the same scenario assigned to the Hawaiian Islands (see Table 2.2); *Alaska uses the Intermediate Low Scenario (see Table 2.1).

Call Out Box: Wave Contributions to Extreme Water Levels

Short of deterministic coastal flood mapping, water level elevation is a common proxy for coastal flood risk, and is comprised of a variety of components (Figure Box 1). This report is primarily focused on the contributions of relative sea level (RSL) rise together with tides and storm surge contributions to extreme water levels (EWLs). However, along exposed coasts, wave-driven water levels can play a significant role in coastal flooding during storm events and during lesser storm conditions as exacerbated by future sea level rise. Here we illustrate the relative influence of wave-driven water levels, broken down into the components set-up and swash, during extreme events across the United States, compared to tide and surge contributions.

Wave-set up is the quasi-static, superelevation of water level at the shoreline due to breaking waves (Longuet-Higgins and Stewart, 1963). Swash is the time-varying elevation of the leading edge of wave up rush, which varies in frequency from seconds (i.e., due to incident waves) to minutes (i.e., due to infragravity waves, a.k.a. surf beat) (Guza and Thornton, 1982). Wave-set up and swash components, collectively referred to as wave run-up, are dependent on wave height and period, and beach slope (Stockdon et al., 2006), and therefore controlled by local beach morphology and transient ocean conditions. To perform regional assessments of present day or future wave-driven water level contributions, wave conditions are typically determined via global wave models forced by wind-reanalysis studies (e.g., Reguero et al., 2012) or historical/future wind fields produced by Global Climate Models (GCMs) (e.g., Hemer et al., 2013).

Leveraging the global total water level assessment of Vitousek et al. (2017), which combines reanalysis models for waves, surge, and tides, the relative influence of waves on coastal water levels during extreme events is estimated (Figure Box 2). Even though the coarse resolution of this study (1° x 1° grid cells) cannot fully resolve tropical cyclones, which play a significant role in driving the most extreme water level events (~> 5-10 year-return intervals) for the Southeast Atlantic, Gulf Coast, Caribbean and Pacific Island regions, this analysis demonstrates the relevance of waves in contributing to coastal flood risk. Across the United States and territories, using the 10-year extreme water level return interval as an example, this study estimates that the water level contributions by wave set-up ranges from 22-75 cm (Figure Box 2A) and swash 37-127 cm (Figure Box 2B), together accounting for 23-92% of extreme water levels for open coast beaches (i.e., not for embayments or urbanized/hardened shorelines protected from ocean waves). Wave-driven water levels represent ~50% or more of the extreme water level contributions in areas with narrow continental shelves (reduces surge potential) and/or small tidal ranges, in particular the Pacific Islands and Caribbean, the Outer Banks (North Carolina), most of Florida and the U.S. West Coast, and portions of Louisiana, Texas and Alaska. While transient swash oscillations amplify coastal flooding, wave set-up represents a relatively sustained contribution during storm events and drives the most significant wave-driven flood risk, accounting for 10-82% of the extreme water levels relative to tide and surge contributions, with the highest values in the tropics (Figure Box 2D). Therefore, when omitting wave-driven processes, coastal flood risk can be significantly underestimated for open coast beaches. Henceforth, waves should be included in future regional and national coastal hazard assessments.

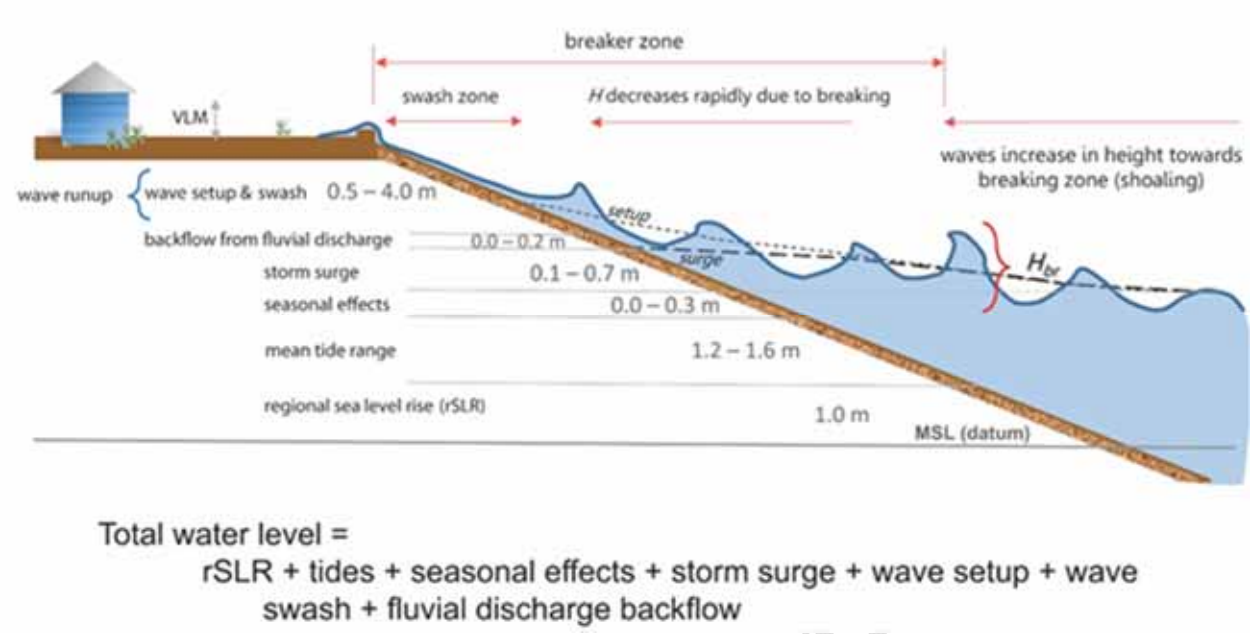

1193

1194 **Figure Box 1**. Water level components (PLACEHOLDER-NEEDS TO BE REDRAFTED).

1195

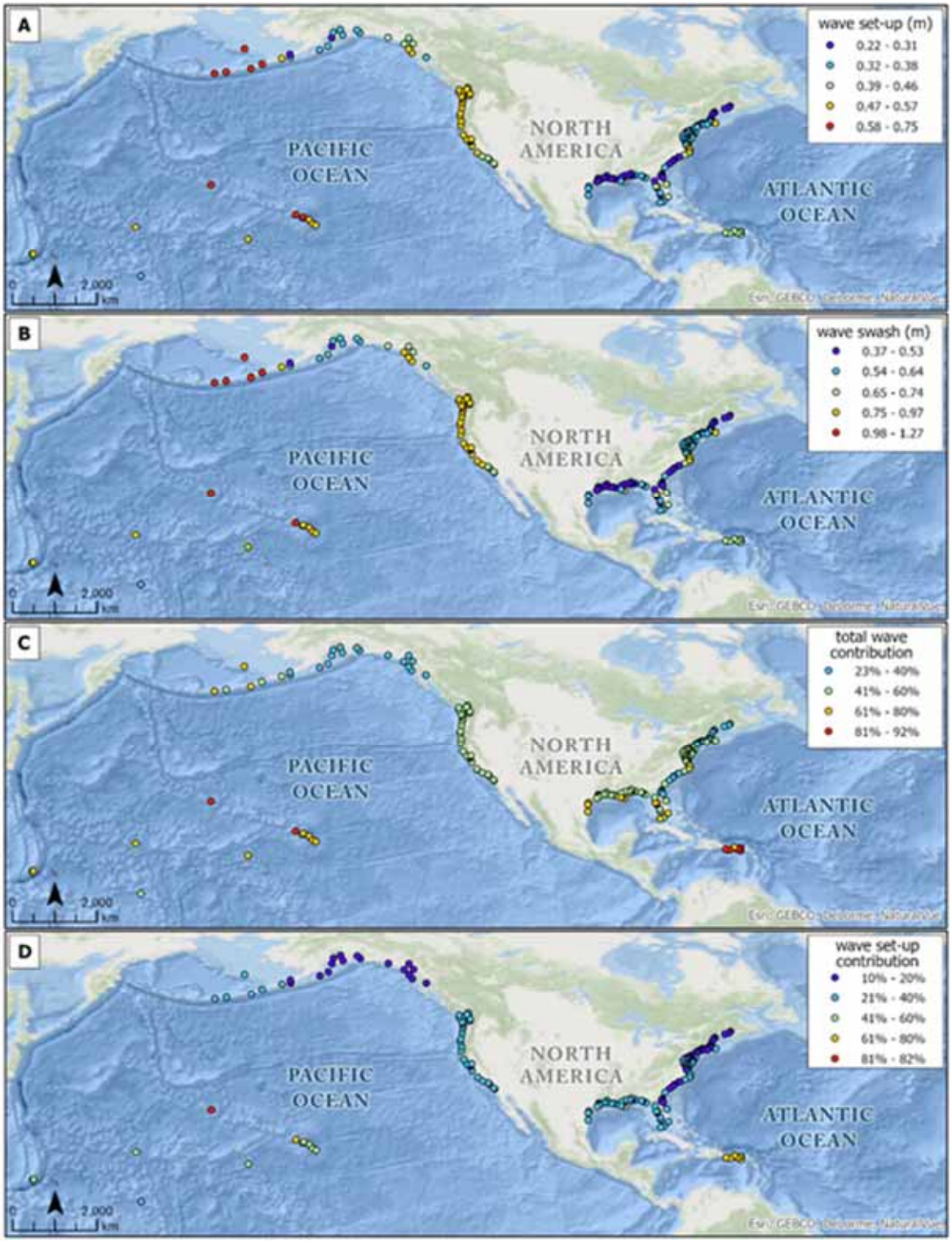

Figure Box 2. The relative influence of wave-driven processes on extreme water levels for the 10-year storm event along the outer coast of the United States and Territories, depicted at the most proximal tide station to the 1° x 1° grid cells from the model projections from Vitousek et al., (2017). A) Water level contribution due to wave set-up. B) Water level contribution due to wave swash. C) Percent

contribution of wave-driven water levels (wave set-up + swash) relative to all components: tide, storm surge, and waves. D) Percent contribution of wave set-up relative to the sum of tide, storm surge, and wave set-up.

Section 4 Use Cases

Below are four use cases, which

- map at city scales the coastal flood annual probabilities/frequencies for the NOAA minor (mostly disruptive), moderate (typically damaging) and major (often destructive) flood layer classifications that are currently used in weather-warning forecasting by NOAA

- incorporate nonstationarity (i.e., trend changes in environmental conditions) in engineering design criteria using the RSL scenario projections and EWL statistics for risk management and adaptive planning

- use maps of NOAA minor, moderate and major flood depth layers with the RSL rise projections and EWL statistics to assess current and future vulnerabilities to combined storm and wastewater systems

- consider new satellite technologies to estimate vertical land motion rates at very high spatial resolution to monitor current rates and localize projections of relative sea level rise

The goal is to provide context of how the emerging science and this report's data sets can assist in screening-level products suitable for framing and bounding important problems in coastal risk assessment and management.

4.1 Mapping of NOAA Flood Thresholds and Flood Frequencies

High-tide flooding, often referred to as "nuisance", "sunny day" or "king tide" flooding, is increasingly common due to years of RSL rise. NOAA has been 1) documenting changes in high-tide flooding patterns since 2015, with about 100 NOAA tide gauges along the U.S. coast and 2) providing a yearly coastal flood outlook for these locations for the coming year, as well as 3) projections for the next several decades based upon NCA4/Sweet et al., 2017 RSL projections. NOAA has also mapped the three HTF depth-severity (minor, moderate and major) catagories based upon the relationship with tide range (Sweet et al., 2018) to show spatial extent of associated impacts (see Figure 3.7). The minor HTF maps are provided in the NOAA SLR Viewer (https://coast.noaa.gov/slr/) under the high-tide flooding tab and all 3 map layers served through NOAA map services.

In an effort to provide better flood risk information, NOAA is developing a product with input from partners (e.g., FEMA) to assign exceedance probabilities to the three HTF categories and include this information via the existing mapped layers. For example, in Figure 4.1.1a and b are maps of Charleston, SC and West Palm Beach, FL showing annual event frequencies for the three NOAA coastal flood depth-severity categories. The annual event frequency shown for each NOAA coastal flood 'zone' is assigned to the height of the particular flood height. So for example, the moderate HTF zone in Charleston is shown as the orange-brown layer in Figure 4.1.1a, which includes all land elevations between the minor HTF

height threshold (0.570 m above MHHW; Table A2) and the moderate HTF threshold of 0.853 m above MHHW. This moderate HTF 'zone' layer is expected to be completely (up to 0.853 m above MHHW) at risk of flooding with an average event frequency between about once per year and a 20% annual change. A frequency range is provided to address inherent uncertainties in both the EWL statistics and the mapping data. In the case of local maps, like Charleston and West Palm Beach, the average event frequencies for each NOAA flood layer remained constant as binned.

These types of products will help to inform the probability of higher frequency, lower impact events. Several federal agencies (e.g., USACE, FEMA, and NOAA) currently develop and report out extreme water level information (e.g., 1% annual chance exceedance probability), often used to determine coastal flood risk. These are based on both historical data and modeled extremes. However, the primary focus has been on the more extreme, impactful events and less on the higher frequency (more recurrent), less impactful water levels. As agencies (e.g., FEMA) start to develop products based on a broader frequency distribution (e.g., graduated flood risk; see https://www.fema.gov/fact-sheet/future-flood-risk-data-ffrd) and considering today's impact -height thresholds in the face of sea level rise (Figure 1.3), higher resolution of event probabilities/frequencies that span the annual divide are needed (e.g., 10% to 50% annual chance events, 1-10 events per year). Such information would help differentiate risk e.g., within the 100-year floodplain, as the closer an individual structure is to the flooding source (or the lower its elevation), generally the higher the probability of flooding. FEMA and other agencies are working towards a graduated flood risk product that will inform floodplain managers about the range of probabilities across the entire floodplain. This information will be useful for risk rating as well as management decisions.

The NOAA HTF probability maps and data being developed here will help to fill the gap in existing products graduating risk within the coastal flood plain. The maps resolve the higher frequency water levels associated with chronic tidal flooding occurring today and starting to have impacts and economic consequences within many coastal cities. Long term exposure to salt water, for example, will jeopardize stormwater infrastructure, roads, vehicles, and cause more frequent loss of use and access issues.

How can this be done? The process to spatially assign probabilities again relies on a relationship to tide range (Figure A5), which is obtained via subtractingVDatum's MHHW and MLLW modeled tidal surfaces (vdatum.noaa.gov). Using VDatum's tide range and the regional regression equations to obtain a local index (u), the extreme water level return period curves are downscaled to individual VDatum grid cells (~100m) using Equation 1 in Section 3. With these downscaled curves, the HTF levels at each VDatum cell, also based on VDatum's GT relationship (Sweet et al., 2018), are intersected with the localized return period curve (expected values) for the cell in order to determine return periods on a cell-by-cell basis. The return periods are then associated with their respective mapped inundation footprints (3-5 m horizontal resolution) and classed based on the below classification. To refine the data, they were clipped to the coastal HUC 12 watersheds (USGS) that overlapped VDatum model data. This was done in order to only provide a probability in watersheds that contained source VDatum data.

The value of these data is that we can now provide not only the mapped inundation extent of each of the three HTF levels (Figure 3.7), but also the probability or return period for each level on high-resolution inundation data (Figure 4.1.1). By leveraging the relationship of u to GT on a regional basis, the extreme water level statistics can provide a return period for 1) most water levels or flood heights of interest and 2) most locations even if there is not a local gauge nearby to assist coastal managers when planning for potential impacts to their communities.

NOAA is currently investing in a more detailed (e.g., 40 year) hindcast modeling analysis of historical water levels to develop a more robust local index 'u' to further enhance the spatial granularity of the regional frequency analysis (RFA). This will serve to refine these HTF probabilities and continue the improvement of higher probability water levels and thus improve our understanding of our nation's coastal flood risk through products like FEMA's National Risk Index .

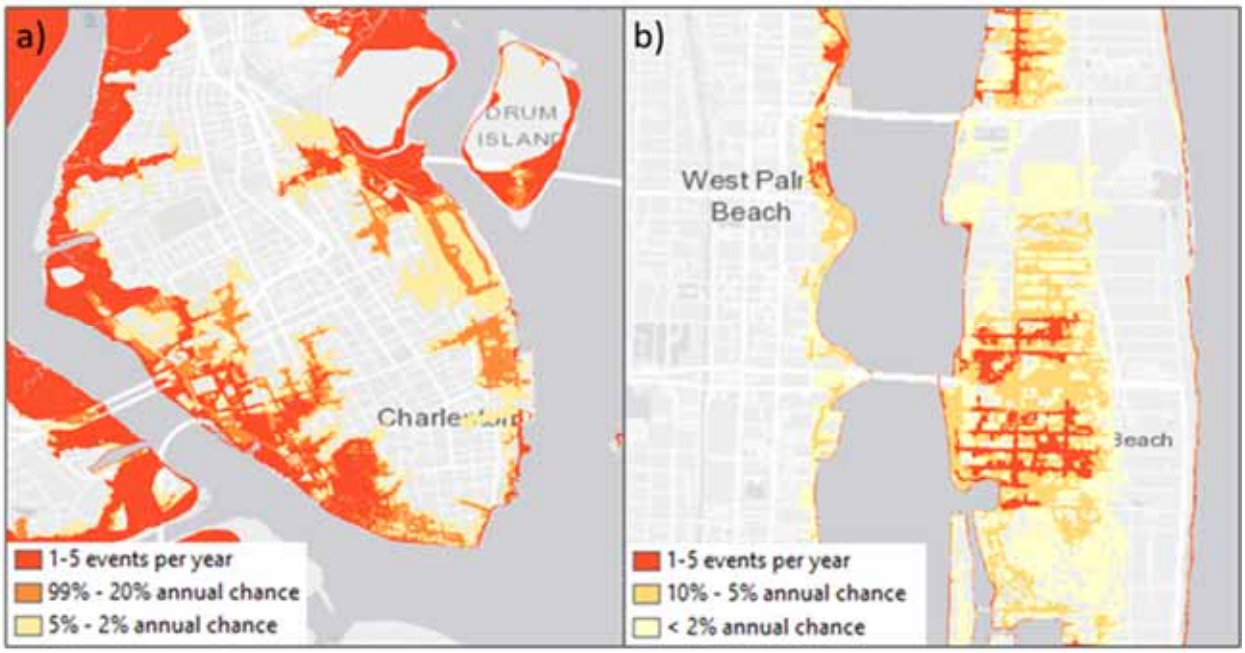

Figure 4.1.1: Maps of the NOAA minor, moderate, and major high tide flood (HTF) layers for a) Charleston, SC and b) West Palm Beach, FL as in Figure 3.7, but providing annual event frequencies for each layer

4.2 Exemplary application of Scenarios, Observation-Based Extrapolations, and Extreme Water Levels

Because future projections of sea level are inherently uncertain, resiliency planners who engage in addressing adaptation to future sea level rise in coastal communities, by necessity, have to adopt a scenario approach. Based on several national and regional sea level projections (Hall et al. 2019; Paris et al. 2012; USACE 2014; Hall et al. 2016; and Sweet et al. 2017), many communities have developed their own specific scenario sets and guidelines for how to use them. In this section, the application of the regional sea level scenarios (Section 2) that leverage the newly developed observation-based extrapolations (Section 2.3), and the extreme sea level projections produced using the Regional

Frequency Analysis (RFA, Section 3), are illustrated for representative locations around the United States.

This use case illustrated here is not meant to provide standardized guidelines for using the latest information on sea level rise projections, but rather, it is provided as an example of applying concepts of nonstationarity, risks, and adaptive planning that may be used in practice (Salas and Obeysekera 2014; Salas et al. 2019). One of the primary tasks in coastal infrastructure projects is to determine the design elevation (also known as return level) of a particular structure (e.g. seawall, building) and the corresponding design return period.

The term nonstationarity in the context of this section reflects the changing nature of extreme water level distributions due to sea level rise and possibly due to other factors associated with climate change (e.g. storminess).

Data

The use case is illustrated for ten tide gauges around the United States (Figure 4.2.1)

Figure 4.2.1: Tide gauges selected for the illustration of nonstationary methods

For illustration, the lower and upper bounding scenarios of the observation-based extrapolations for circa 2050 (Table 2.2) and the extreme value distribution parameters from the Regional Frequency Analysis, RFA (Section 3) are provided in Table 4.2.1. In the examples below, only the upper-bounding scenario is used and shown in Figure 4.2.2. The Peaks Over Threshold (POT) approach (Coles 2001) and the corresponding Generalized Pareto Distribution (GPD) developed for each tide gauge using RFA include four parameters: (a) Local Index, u; (b) rate of exceedances above the local index, λ; (c) Scale, σ_{RFA}; and (d) Shape, ξ. Because the exceedances are assumed to follow a homogeneous Poisson process, the approach is referred to as the Poisson-GPD model. The corresponding return level curves for the selected tide gauge locations are shown in Figure 4.2.3.

Table 4.2.1: Tide gauge locations, scenarios bounding the observation-based extrapolations, and the extreme value distribution parameters estimated using the Regional Frequency Analysis (RFA)

Tide gauge location details			Scenarios bounding the circa 2050 observation extrapolations		RFA based Poison-GPD parameters			
NOAA ID	Location	Region	Lower Bound	Upper Bound	u	λ	σ_{RFA}	ξ
1612340	Honolulu, HI	H	Int Low	Int	0.248	3.19	0.218	0.066
8518750	The Battery, NY	NE	Int Low	Int	0.546	2.98	0.261	0.179
8638610	Sewells Point, VA	NE	Int Low	Int	0.502	2.95	0.332	0.067
8723214	Virginia Key, FL	SE	Int	Int High	0.284	3.00	0.152	0.251
8726520	St Petersburg, FL	EG	Int High	High	0.337	2.99	0.266	0.354
8729840	Pensacola, FL	EG	Int High	High	0.345	2.85	0.212	0.456
8771450	Galveston Pier 21, TX	WG	Int	Int High	0.366	2.75	0.289	0.340
9410660	Los Angeles, CA	SW	Int	Int High	0.472	3.21	0.150	-0.063
9414290	San Francisco, CA	SW	Int	Int High	0.375	3.15	0.211	0.038

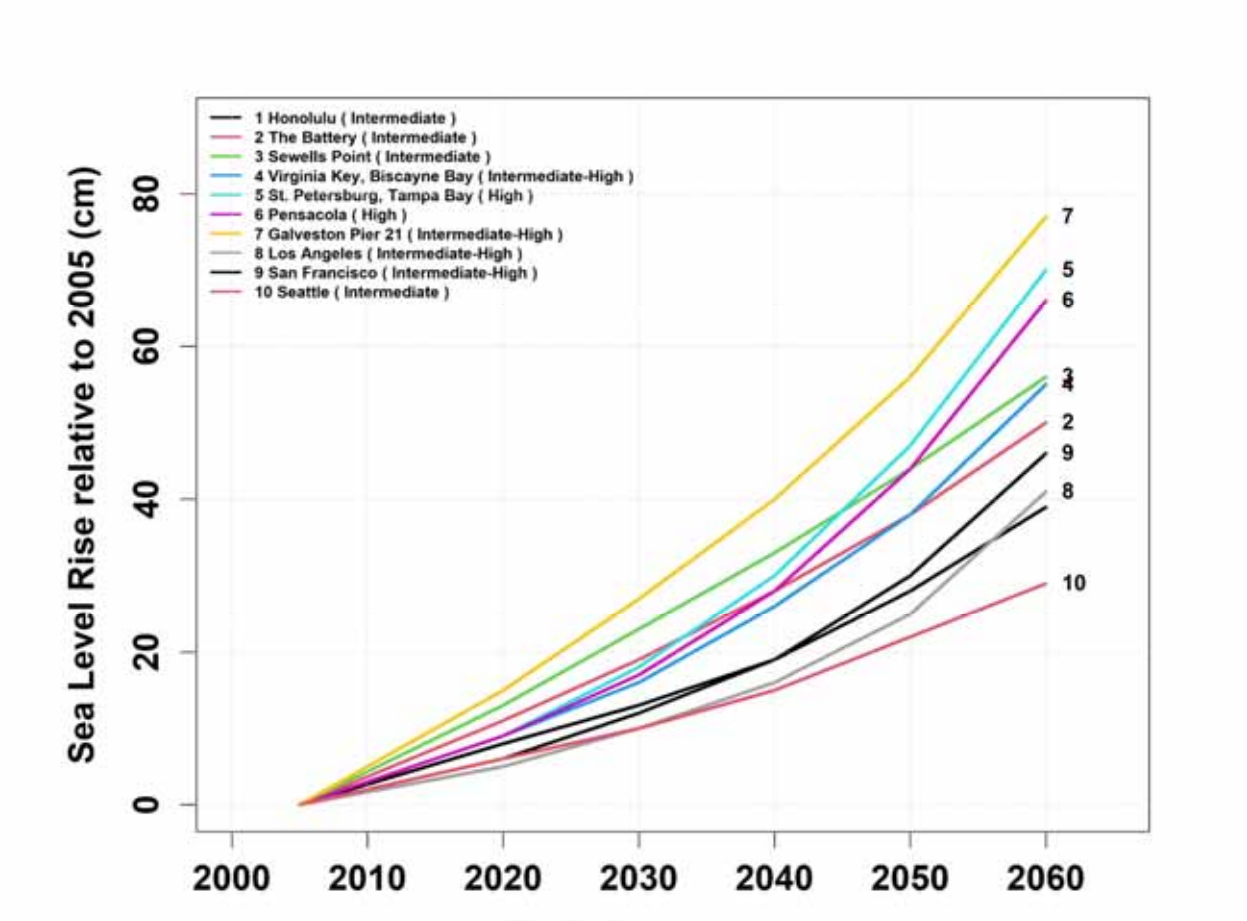

Figure 4.2.2: Relative sea level (RSL) projections for the scenarios providing the upper bound to observation-based extrapolation to about 2060 for the selected tide gauges. The corresponding scenario for each tide gauge is shown in parenthesis in the legend. For the use cases, it was assumed that the extrapolations are valid upto about the 2060 although methods described below can be used with any projection scenario.

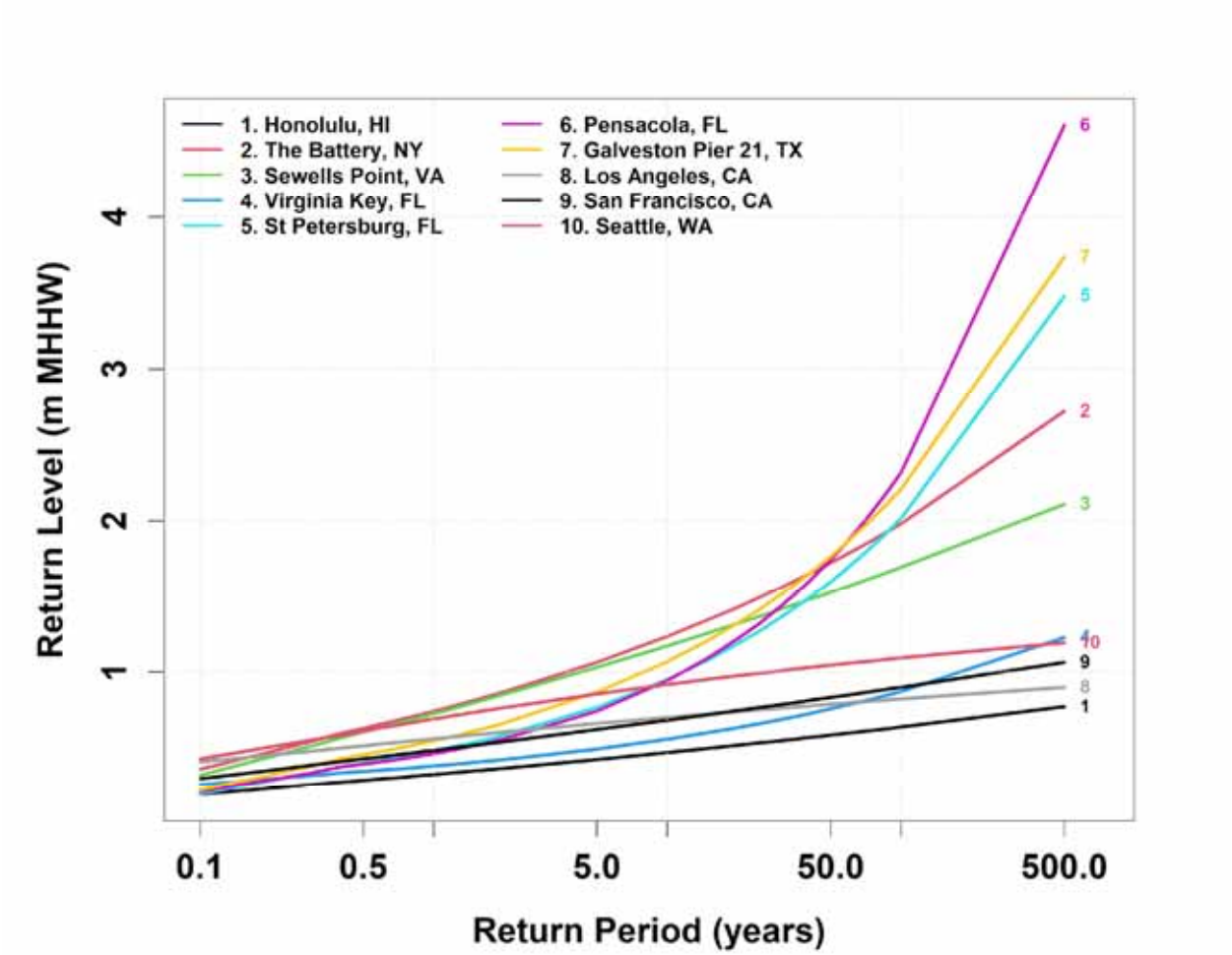

Figure 4.2.3: Extreme Value Distributions derived from RFA (see Section 3) developed by using the Peaks Over Threshold (POT) approach and the Generalized Pareto Distribution (GPD).

As shown in Figure 4.2.2, the "reference year" for the projection scenarios is the year 2005. However, the return level curves shown in Figure 4.2.3 are referenced to the year 2000. The return level curves are first adjusted to the year 2005 by raising the curves by an amount equivalent to the local trend in the flood index (u) from 2000 to 2005 (see Appendix Table A3).

Nonstationary Approach

A particular scenario depicts the changes in the Mean Sea Level (MSL) at a selected location. A common assumption is that, as MSL increases, the extremes also increase and that must be accounted for in the changing behavior of the probability distribution of the extreme sea level. One approach for developing a time-varying extreme value distribution is to assume that one or more parameters (location, scale, and shape) are functions of time or some other covariate (e.g. ENSO index). When a parameter evolves with time, the paradigm shifts from a "stationary" approach, typically used for planning infrastructure until

recently, to one reflecting "nonstationarity." For simplicity, it is assumed that only the location parameter (i.e local index, u in GPD) is a function of MSL (of a particular projection scenario). This may be expressed as

$$F(z) \sim GPD(u(MSL), \sigma, \xi)$$

where u is the GPD local index, and σ, ξ are scale and shape parameters respectively, assumed to be constant over time. However, this assumption does not preclude the analysis of using a higher degree of nonstationarity (e.g. both u and σ are functions of MSL or some other covariate). As a consequence of the above assumption, the local index u is adjusted by a magnitude δ (i.e. the sea level change from the reference year) obtained from a selected projection scenario.

For planning infrastructure using the scenario's RSL projections and the extreme water level probabilities, two approaches are illustrated:

1. Recurrent Flood Frequency
2. Nonstationary Return Period and Risk

One or both of the above approaches may be used to determine the sizing of future infrastructure (e.g. height of a sea wall, or base-flood elevation).

Designs based on Recurrent Flood Frequency

In many coastal locations, the frequency of flooding is increasing, mostly due to rising sea levels. A community may tolerate infrequent flooding initially, but at some point in time when the sea level rise is significant, the flooding frequency will increase, which in turn, may exceed that community's risk tolerance. Using the extreme value distributions and the sea level rise scenarios, it is possible to predict the time-varying change in frequency. In case of GPD, the Recurrent Flood Frequency (RFF: number of exceedances above a return level, z) may be computed as (Buchanan et al. 2017):

$$N(z, \delta) = \lambda \left(1 + \frac{\xi(z - [u + \delta])}{\tilde{\sigma}}\right)^{\frac{-1}{\xi}} \text{ for } \xi \neq 0$$

where δ is the change in MSL (relative to the project construction year). The value of δ may be obtained from the selected regional sea level scenarios (Figure 4.2.2).

In the example used here, the planning problem may be stated as follows: What should be the initial return level (used for the design), so that, at the end of the Design Life (say 50 years), the Recurrent Flood Frequency (RFF) is limited to a specified number of events (e.g. N=1)?. It is now possible to lay this out graphically as shown in Figure 4.2.4 for two tide gauges (Sewells Points and Galveston Pier 21).

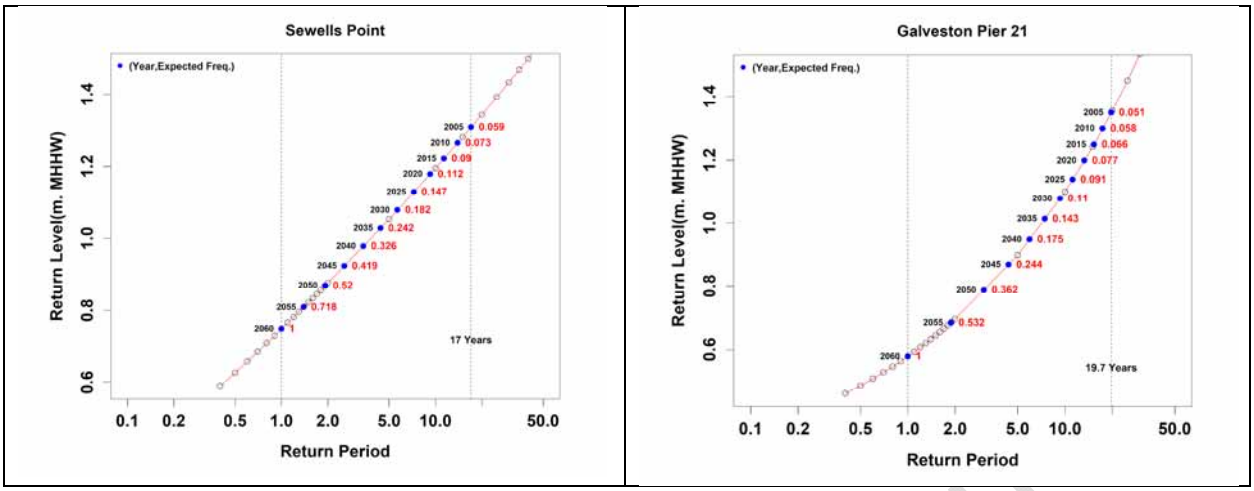

Figure 4.2.4: Recurrent Flood Frequency estimates for (a) Sewells Point; and (b) Galveston Pier 21. For both, the RSL projection for the scenarios in Table 4.2.1) and the return level curves in Figure 4.2.3 are used.

In Figure 4.2.4, the number to the right of each point along the curve shows the RFF, N corresponding to the year indicated on the left. In this case, it was assumed that, by 2060, the desired value of N=1. The design return period necessary for this criterion is indicated in the figures (17 years for Sewells Point and 19.7 years for Galveston Pier 21). The corresponding design return levels are 1.31 m and 1.35 m respectively, relative to MHHW datum. A summary of results for all 10 tide gauges is shown in Table 4.2.2. The design return period required in 2005 to meet the flood frequency criteria shows significant variability across the sites. The design return level (and the design return period) depends on two factors: (a) the magnitude of the sea level rise from 2005 to 2060 (end of the design life); and (b) the slope (a function of the scale and shape parameters) of the return level curve Figure 4.2.4.

Table 4.2.2: Summary of design parameters (with numbers rounded) to constrain the recurrent flood frequency, N to 1 per year by 2060 (end-year of the design life)

NOAA ID	Location	Sea Level Rise (from 2005 to 2060)	Return Level corresponding to Return Period=1 year	Return Level required in 2005 to ensure N=1 by 2060	Design Return Period required in 2005 to ensure N=1 by 2060
1612340	Honolulu, HI	0.39	0.33	0.72	250
8518750	The Battery, NY	0.5	0.76	1.26	10
8638610	Sewells Point, VA	0.56	0.75	1.31	15
8723214	Virginia Key, FL	0.55	0.41	0.96	130

8726520	St Petersburg, FL	0.7	0.49	1.19	20
8729840	Pensacola, FL	0.66	0.47	1.13	15
8771450	Galveston Pier 21, TX	0.77	0.58	1.35	20
9410660	Los Angeles, CA	0.41	0.57	0.98	500+
9414290	San Francisco, CA	0.46	0.49	0.95	155

Design Based on Nonstationary Return Period

Projects with a longer design life (> 25 years) typically use larger design return periods (> 10 years or more). At high return periods, the Peaks Over Threshold (POT) and the annual maxima return levels converge (Langbein 1949). It is more convenient to convert the POT Poisson-GPD model to an equivalent Annual Maxima (AM) model which in this case is the Generalized Extreme Value Distribution (GEV). The equivalent AM model will facilitate the direct application of risk and return period concepts already developed for nonstationary situations (Salas and Obeysekera 2014).

The Cumulative Distribution Function (CDF) of the GEV is expressed as

$$F(z) = exp\left\{-\left[1+\xi\left(\frac{z-\mu}{\sigma}\right)\right]^{-1/\xi}\right\}$$

where μ, σ, ξ, are the location, scale, and shape parameters (Coles 2001). The equivalency of the Poisson-GPD model for POT and the GEV model for AM may be expressed as

$$\lambda = \left(1+\ \xi\frac{u-\mu}{\sigma}\right)^{-\frac{1}{\xi}} \qquad \text{and} \qquad \sigma = \tilde{\sigma}\lambda^{\xi}$$

where $u, \tilde{\sigma},\ \lambda$ are the GPD local index, scale, and event occurrence rate respectively. The shape parameter is identical in both models. The above expressions are used to compute the equivalent GEV parameters μ, σ, ξ for all tide gauge locations. The at-site scale parameter $\tilde{\sigma}$, is first computed as $\tilde{\sigma} = \sigma_{RFA} * u$. For computing μ, the local index is further adjusted to reflect the translation of the return level curve from 2000 to the reference year (i.e. 2005). For this use case, the adjusted local index is computed as $u_{adj} = u * s\ (2005 - 2000)$ where s is the trend of the local index u at the site (see Appendix Table A3). If desirable, ther adjustment procedures may be used. Finally, the nonstationary GEV assumes that only the location parameter, μ changes with sea level change, δ and the time varying annual extreme value distribution is given by

$$F^t(z,\delta) = exp\left\{-\left[1+\xi\left(\frac{z-(\mu+\delta)}{\sigma}\right)\right]^{-1/\xi}\right\}$$

With sea level rise, the exceedance probability, p_t, corresponding to an initial return level ($z_{q0,}$initial design), changes with time because of the nonstationarity introduced by the rising sea level, δ (Figure

4.2.5) Consequently, the return period is not a fixed measure but decreases with increasing sea level (see also Fig. 4.2.5.)

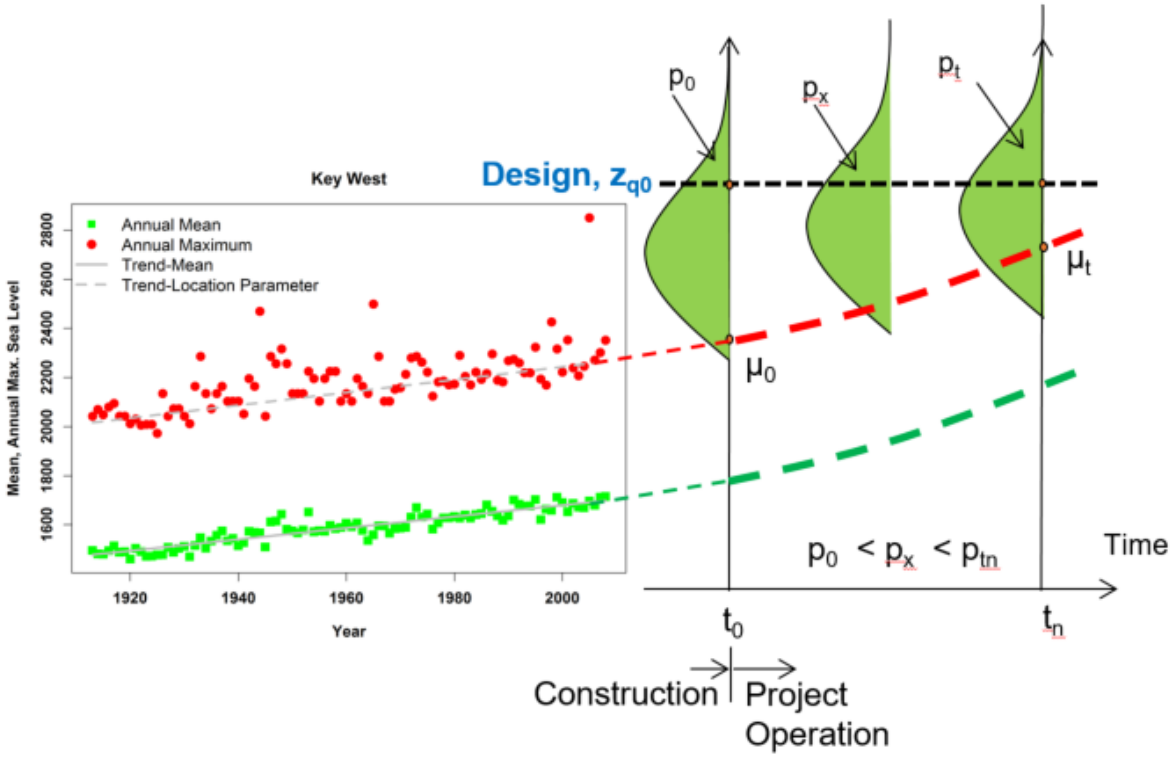

Figure 4.2.5: Conceptual illustration of increasing exceedance probability (hence decreasing return period) assumes the location parameter is a function of the magnitude of the sea level rise.

The traditional concept of the return period is the expected waiting time (EWT) for the first exceedance of the design return level. Using EWT as the definition, an equivalent measure under nonstationarity may be derived as (Cooley, 2013; Salas and Obeysekera, 2014)

$$T = EWT = 1 + \sum_{x=1}^{\infty} \prod_{t=1}^{x} (1 - p_t) \quad (4.2.5)$$

Where $p_t = 1 - F^t(z, \delta)$ is the time-varying exceedance probability. With rising sea level, if a project is designed for a return period, T_0, then T < T_0 which implies that the level of protection for the structure is less depending on the rate of sea level rise.

The methods described in the preceding paragraphs are applied to the ten tide gauge locations. For the illustration of nonstationary return period curves, it was assumed that the projection scenario for each tide gauge was assumed to continue beyond 2060. However, the methodology described above can be used with any other scenario, if necessary. The derived GEV parameters for each gauge is shown in Table 4.2.3

Table 4.2.3: The parameters of GEV computed using the POT, Poisson-GPD model

NOAA ID	Location	At-site scale parameter	Local Index adjustment from 2000-2005 (m)	GEV location parameter,	GEV scale parameter	GEV shape parameter
1612340	Honolulu, HI	0.054	0.007	0.330	0.058	0.066
8518750	The Battery, NY	0.142	0.016	0.757	0.173	0.179
8638610	Sewells Point, VA	0.167	0.023	0.748	0.179	0.067
8723214	Virginia Key, FL	0.043	0.026	0.405	0.057	0.251
8726520	St Petersburg, FL	0.090	0.014	0.494	0.132	0.354
8729840	Pensacola, FL	0.073	0.012	0.474	0.118	0.456
8771450	Galveston Pier 21, TX	0.106	0.033	0.579	0.149	0.340
9410660	Los Angeles, CA	0.071	0.005	0.565	0.066	-0.063
9414290	San Francisco, CA	0.079	0.010	0.492	0.083	0.038

The nonstationary return period curves, T , as a function of T_0 for all locations are shown in Figure 4.2.6. This figure demonstrates that the actual EWT is less than the design return period. For instance, for a location near Pensacola, Florida, if a project is designed for T_0 = 100 years, the actual level of protection (measured in this case as EWT) is only about 50 years. As another example, for a location near The Battery, NY, a project may need to be designed for T_0 ~ 90 years if the desired EWT=40 years.

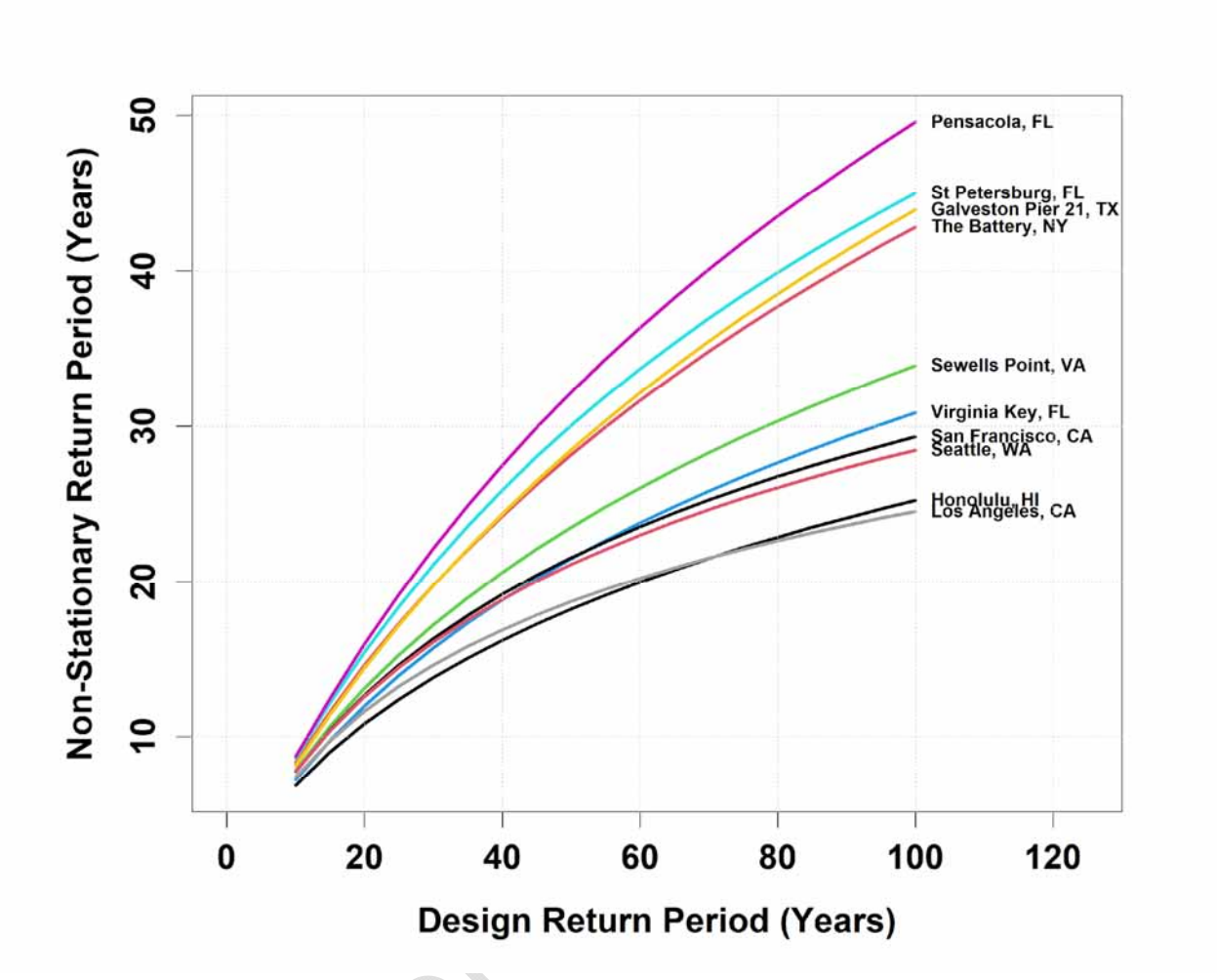

Figure 4.2.6: Nonstationary return level curves (T versus T_0) at each tide gauge using the selected scenario's RSL projection (Table 4.2.1)

Risk Based Design

Under stationary conditions, the risk of "failure" (one or more exceedances above the design elevation) is a function of the life of the project, n. The risk formula under stationarity is given by $R = 1 - (1 - \frac{1}{T_0})^n$. As the length of the design life increases, risk also increases. In case of nonstationarity, time-varying exceedance probability,p_t, the Risk formula is (Salas and Obeysekera, 2014)

$$R = 1 - \prod_{t=1}^{n} (1 - p_t)$$

With rising sea levels, p_t increases and the failure risk is higher than that under stationarity. This increase in risk is illustrated in Figure 4.2.7 for the case when the initial design, T_0=50 yrs. The black curve in Figure 4.2.7 shows the increasing risk as the design life becomes longer even under stationarity. However, when the nonstationarity due to sea level rise is incorporated, the risk of failure over a given

life of the project increases more rapidly exceeding the corresponding risk under stationarity (see red curve in Figure 4.2.7). Moreover, the rising sea level causes the risk to approach 100% failure (R=1) when the design life is about 50 years or more. In the risk-based design approach, one can specify the tolerable risk and determine the initial design period (or return level).

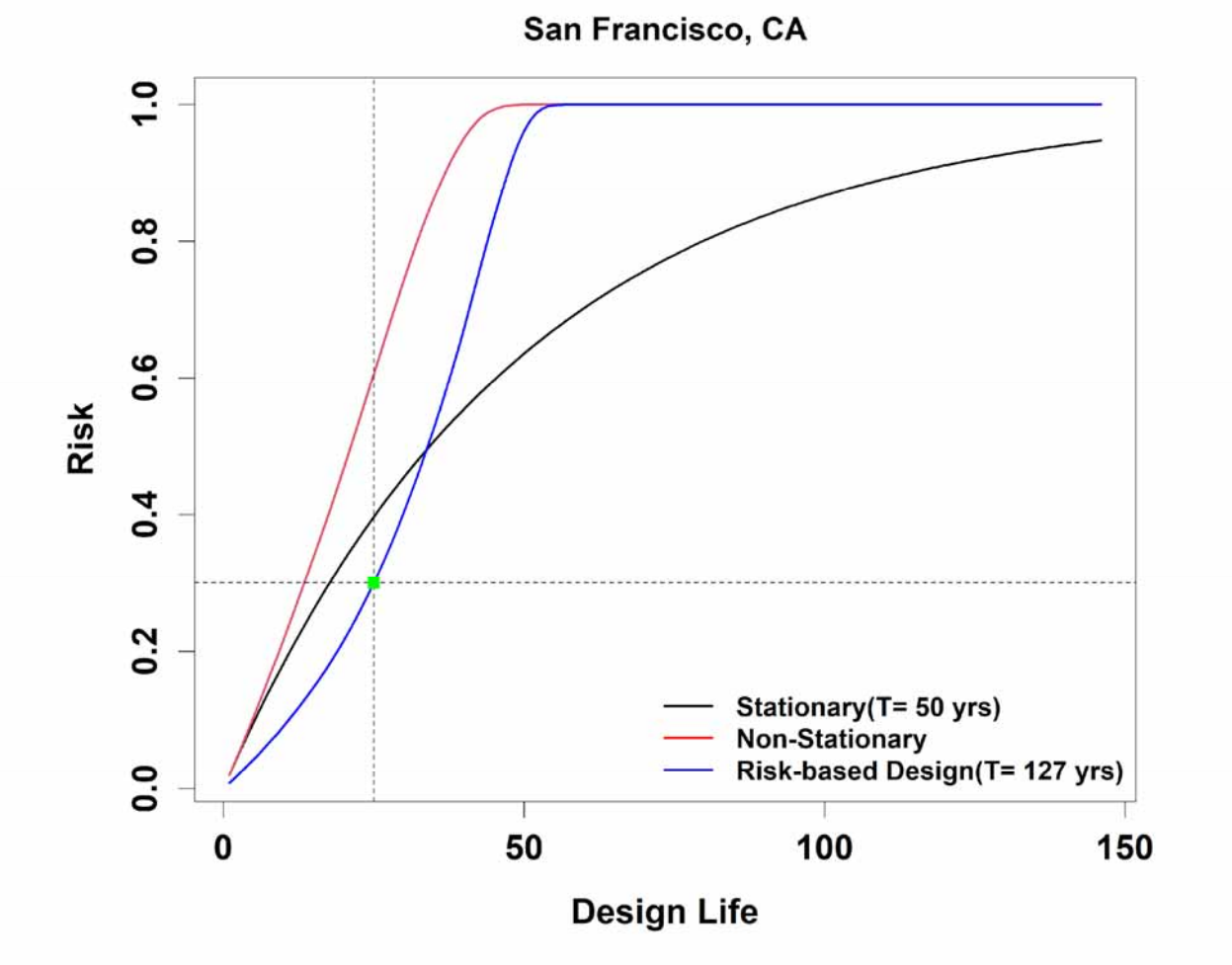

Figure 4.2.7: Risk curves as a function design life: (a) stationary (black curve); (b) nonstationarity resulting from sea level rise (red curve); and (c) nonstationary design for a specific risk (blue curve)

One option is to design a project in such a way that the resulting nonstationary risk profile is at or below that under stationarity. Considering uncertainty in the sea level rise projections, one may wish to approach the problem using concepts of dynamically adaptive planning. In the example shown in Figure 4.2.7 (blue curve), two parameters are specified to illustrate this concept. First, it is assumed that the project will be constructed in, e.g., two or more phases. Considering such a planning assumption, phase I is 25 years long and the maximum tolerable risk during this phase is 0.3 (30%). The blue curve shows the risk profile for such a design. In this approach, one must also assume that the project will be expanded after that initial period, and measures must be adopted not to lock in the design preempting the

planners from expanding it into a bigger project after the initial 25-year period. For example, the foundation design of the project may need to assume the eventual capacity expansion and allow for it in the initial design. This approach of dynamically adaptive planning is becoming increasingly popular as a way to deal with deep uncertainties associated with sea level rise.

Table 4.2.4: The above approach is used for all the sites and the results

NOAA ID	Location	Design Return Level for T_0 = 50 years	Design Return Level to constrain Risk to 30% over a 25-year period	Return Period of the deign to constraint Risk to 30% over a 25-year period
1612340	Honolulu, HI	0.59	0.69	175
8518750	The Battery, NY	1.74	1.95	90
8638610	Sewells Point, VA	1.55	1.75	115
8723214	Virginia Key, FL	0.78	0.92	110
8726520	St Petersburg, FL	1.61	1.88	80
8729840	Pensacola, FL	1.75	2.09	75
8771450	Galveston Pier 21, TX	1.79	2.13	85
9410660	Los Angeles, CA	0.79	0.86	200
9414290	San Francisco, CA	0.84	0.93	125

The above table shows that with a relatively small increase in initial design elevation, the risk can be managed to a desirable level. In this example, however, the ultimate design (at the end of the full design life, say 50 or 100 years) needs to be assessed to ensure that resources (e.g. land) may be needed for the build-out.

4.3 Growing Risk to Combined Storm and Wastewater Systems from Sea Level Rise

Sea level rise is causing HTF to become more severe--frequent, deeper and more widespread--in terms of its impacts (Sweet et al., 2021). Coastal areas that are not exposed to HTF now may become so in the coming decades. As the footprint of flooding expands, water from adjacent estuaries and bays will flood into communities, encountering previously unaffected urban infrastructure.

Many places already see backflow from tidal waters through stormwater pipes that spill out of catch basins into neighborhood streets. Cities with combined sewer systems often have backflow preventers on their vulnerable outfall pipes (EPA, 1995a, b: https://www.epa.gov/sites/default/files/2015-10/documents/owm0030_2.pdf; https://www.epa.gov/sites/default/files/2015-10/documents/owm0272_0.pdf)—however combined sewers will be open to inflow from surface flooding. If flood water in the streets encounter a catch basin that connects to a combined sewer system, then high tide waters will enter the sewer. At best, the tide waters will be on their way to the sewage treatment plant; at worst, a combined sewer outflow would be triggered if the sewer pipes cannot handle the volume of water.

Whereas Camden has taken action to prevent runoff from entering its system (https://www.epa.gov/arc-x/camden-new-jersey-uses-green-infrastructure-manage-stormwater) tidal inflow is a novel problem. Identification of risks like this can provide lead time to take mitigation actions. Still, in some combined sewer communities, such as Camden, N.J., the onset of risk can arrive well before mid-century. Mapping shows that minor HTF at a height of 0.58 m (1.9 feet) above current MHHW tidal datum begins to have a footprint in Camden in neighborhoods (red shade in Figure 4.3.1 spanning from MHHW to 0.58 m above MHHW) served by combined sewers (locations provided here: https://njdep.maps.arcgis.com/apps/Viewer/index.html?appid=70dd49de342949ca933e840d0c530fc7). By the time the tide reaches the moderate (0.86 m or 2.8 feet above MHHW) and major (1.24 m or 4.1 feet above MHHW) HTF levels, the extent of flooding increases dramatically and many intersections will be flooded.

The Camden, NJ region currently (circa 2020) experiences:

- about 2 events/year (or about 4 days/year per relationship in Figure 3.8b) of minor HTF,
- a 20% annual chance of a moderate flooding event,
- a 3% annual chance of a major flooding

based upon the ESL_{local} directly across the Delaware River at the NOAA tide gauge in Philadelphia. For reference, in 2020 the Camden/Philadelphia region experienced 4 days of HTF with 4-8 days projected to occur in 2021 (Sweet et al., 2021).

Considering the Intermediate scenario, which is the upper-bounding scenario for this region's RSL trend extrapolations (Table 2.2), a rise of 0.19 m by 2030 (measured since 2005) is projected to have:

- 5-10 events per year (on the order of 10-20 days per year) of minor HTF occuring
- a 60% annual chance of moderate HTF
- a 7% annual chance of major HTF

By 2050, a 0.38 m RSL rise is projected to have:

- >10 per year (>20 days per year) of minor HTF
- about 3 events per year (6 days per year) of moderate HTF
- a 30% annual chance of major HTF

So, within about the next 30 years (by 2050), a (surface) flood regime shift is projected to occur within Camden, NJ considering current RSL rise trajectories. By then moderate and major flooding (flooding upwards of 3 and 4 feet above MHHW, respectively) are projected to occur with similar frequencies/probabilities as minor (about 2 feet above MHHW) and moderate flooding occur today. With nearly 4 high tides per event (1 event lasts about 2 days; 2 high tides occur almost every day), this implies that by 2050, upwards of 80 tides per year or more at the minor flood level is projected, with about 12 of those tides per year exceeding the moderate flood level and a 30% chance that 1 event (with perhaps 4 distinct high tides) will exceed the major flood level causing tidal waters to flow into the combined system (Figure 4.3.1). Beyond 2050, HTF frequency, depth and extent will continue to grow. It is unclear how this increased flood frequencies will affect the combined system's functionality and surrounding water quality.

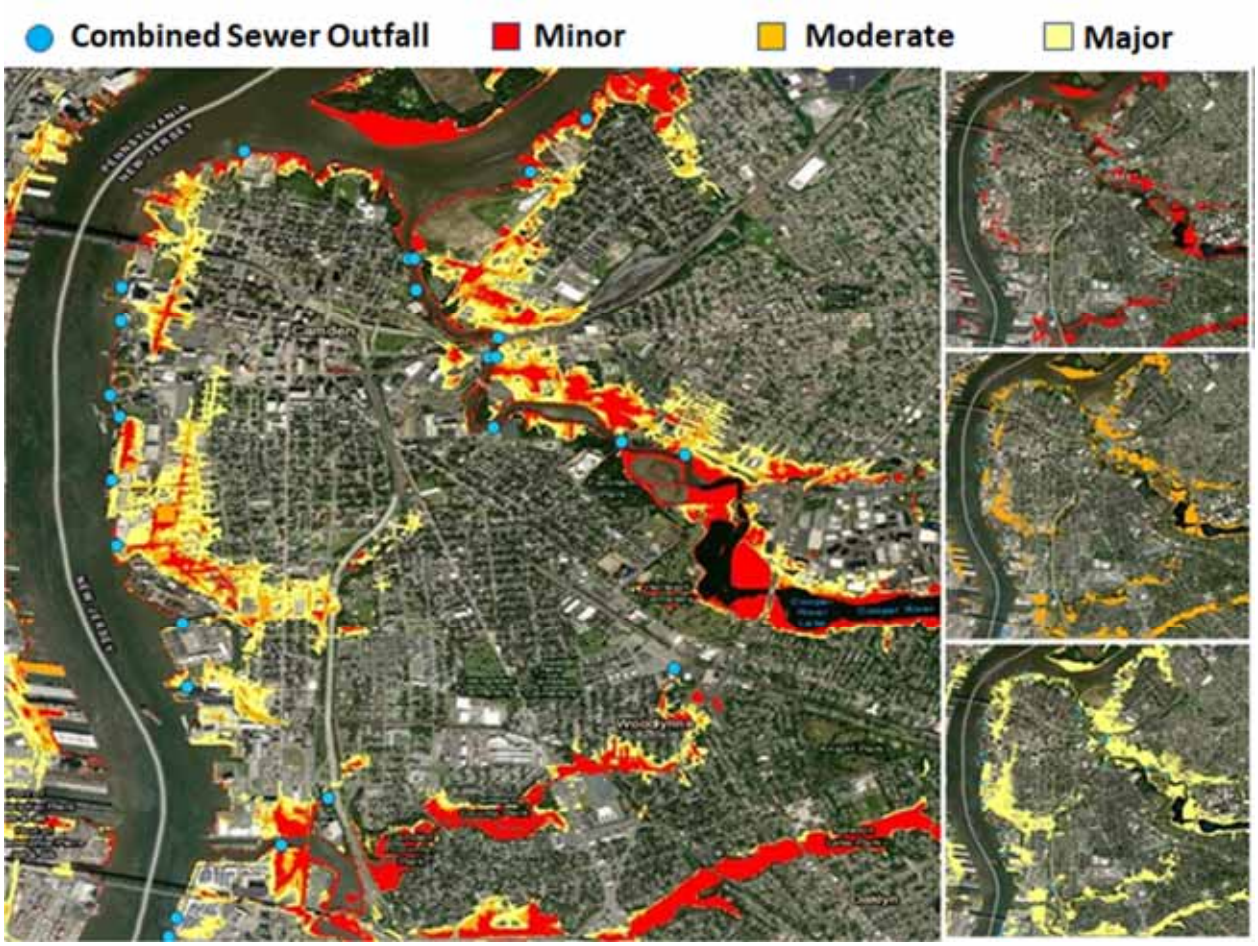

Figure 4.3.1: Location of combined stormwater and sewer system outfalls within the Camden, NJ region with the minor (red: MHHW to 0.58 m or 1.9 feet above MHHW), moderate (orange layers: MHHW to

0.86 m or 2.8 feet above MHHW) and major (yellow layer: MHHW to 1.25 m or 4.1 feet above MHHW) flood layers stacked in the enlarged map and individual layers mapped to the right.

4.4: Using InSAR technology for determining regional vertical land motion rates and suitability for using to compute long-term sea level rise projections.

Vertical land motion (VLM) is an important component of relative sea level (RSL) rise, leading to changes in the height of the ocean relative to land. VLM is not a singular phenomenon, but instead results from various processes that display different patterns in space and time. These patterns have different impacts from place to place, especially in coastal settings where many of them operate at the same time, and can serve to either increase RSL (subsidence) or decrease RSL (uplift). For much of the coastal U.S., subsidence is driven on local scales by groundwater and fossil fuel withdrawal and on larger scales by glacial isostatic adjustment (GIA). On the other hand, in some regions like southern Alaska, GIA leads to high rates of uplift in coastal regions. For example, Grand Isle, LA has experienced over 0.9 m (3 feet) of RSL rise, whereas Juneau, AK has experienced over 1.2 m (4 feet) of RSL fall based upon a 100-year historical linear trend value (https://tidesandcurrents.noaa.gov/sltrends/) in large part due to VLM. For perspective, the national median RSL rise along U.S. coastlines during this 100-year period was about 0.25--slightly less than 1 foot (Figure 1.2b).

Accurate future projections of VLM require an understanding of and accounting for the underlying processes and the time and space scales on which they vary. In this report, VLM projections are based in part on analysis of past observations. VLM rates are estimated at tide gauge locations as well as at 1-degree grids using a statistical model of tide gauge observations (Kopp et al., 2014; Sweet et al., 2017, Fox-Kemper et al., 2021; Garner et al., 2021). The model assesses RSL change across the global tide gauge network (https://www.psmsl.org/data/) with data through about 2019 and decomposes the tide gauge observations into 3 modes: 1) a global rise signal (Dangendorf et al., 2019), 2) a long-term linear-- but regionally varying--trend, and 3) local effects that vary in time and by region. It is the second mode which defines this report's linear VLM rates , which have been incorporated into the RSL projections for each GMSL rise scenario. These rates are assumed to be linear over the past record and that they will persist linearly into the future over the length of the projected record. As shown in Fig. 4.4.1A, high rates of subsidence are estimated along the Gulf Coast and moderate rates of subsidence are assessed along the East coast. On the other hand, high rates of uplift are estimated for the southern coast of Alaska.

Over the past couple of decades, GPS stations have provided estimates of VLM in coastal areas across the U.S. These GPS-based VLM estimates provide a comparison to the VLM rates in this report, albeit with a couple caveats. First, the record lengths over which the GPS-based estimates are computed are significantly shorter than the tide gauge data records used to infer the VLM rates in this report. Second, many tide gauge locations do not have a collocated GPS station. While it is not possible to extend the record lengths of the available GPS, the second challenge has been addressed using the GPS imaging technique discussed in Hammond et al. (2021), which leverages the GPS network in coastal areas of the U.S. to generate VLM estimates at all tide gauge locations (Fig. 4.4.1B). Broadly, the GPS-based estimates are consistent with the VLM estimates contained in this report. However, when subtracting the VLM rates in this report from the GPS-derived rates, differences become apparent (Fig.

4.4.1C). The largest differences are found in Alaska where rates of uplift are very large and along the Gulf Coast where subsidence rates are large. The rates are further compared in Fig. 4.4.1D, which again reflects general agreement between the two sets of estimates, although at roughly 75% of the gauges, the tide gauge-based VLM estimate in this report is greater than that from GPS. In other words, there is generally higher subsidence indicated in the GPS rates when compared to the VLM estimates in this report.

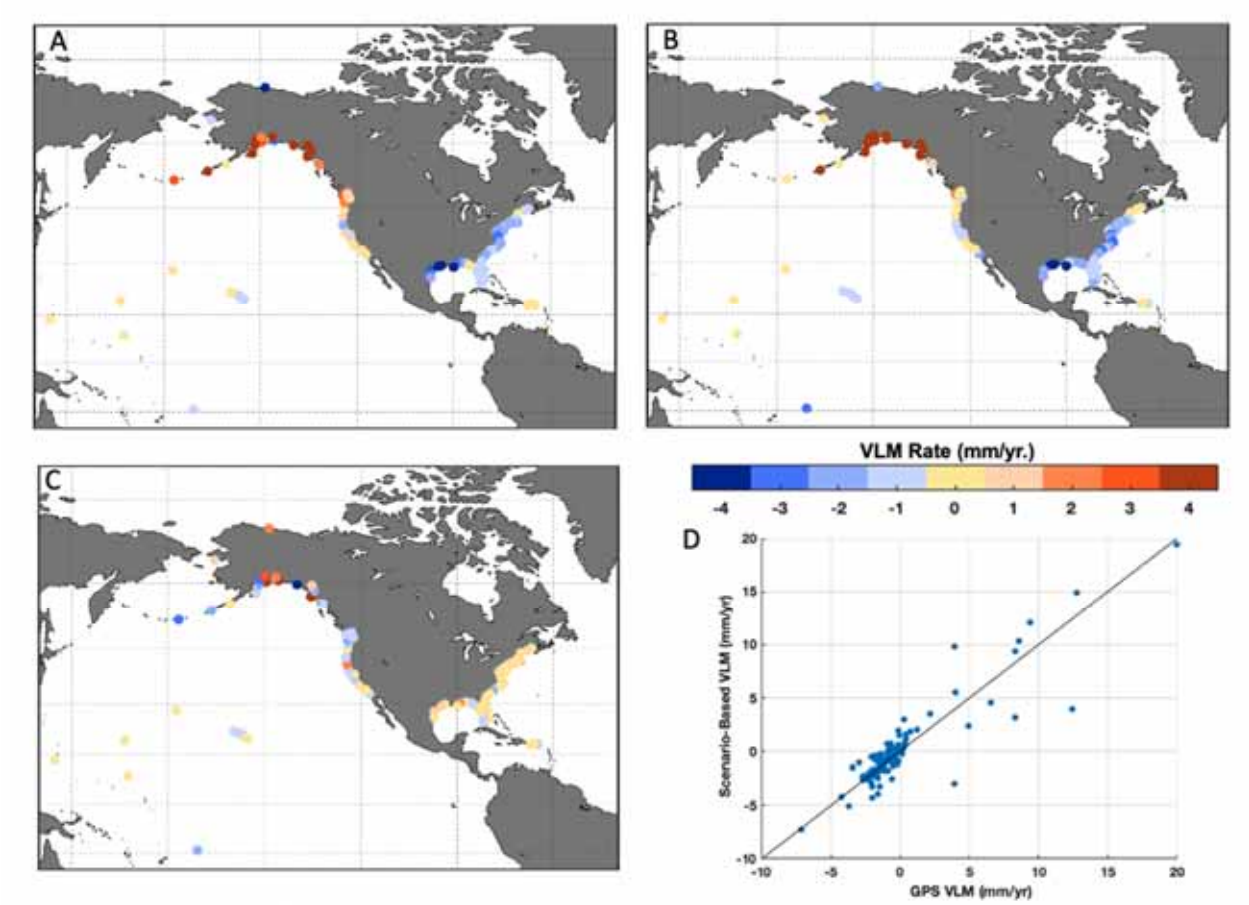

Figure 4.4.1. Comparison of VLM rate estimates (mm/year) from (A) scenario-based framework used in this report, and (B) GPS imaging estimates from Hammond et al. (2021). The difference between GPS-derived rates and scenario-derived rates (C) and comparison between the VLM estimates at the U.S. tide gauge locations (D) are also shown.

This comparison with the GPS is not intended to be an assessment of the accuracy of VLM rates and associated projections included in this report. Instead, it highlights some of the challenges associated with both estimating VLM rates at the coast and then projecting these into the future, particularly away from the tide gauge and GPS stations. The spatial variability and local drivers of VLM are clear in Fig. 4.4.1, and extending the tide gauge-centered estimates to fill in spatial gaps either through the projection framework in this report or with GPS imaging is challenging to validate, particularly as these methods are not intended to capture VLM varying on small spatial scales. An opportunity is provided, however, by new technologies using satellite-based Advanced Interferometric

Synthetic Aperture Radar (InSAR) analysis that can provide higher spatial resolution measurements of VLM rates. Calibrated to land GPS station estimates, measurements of land elevations over time by InSAR are producing VLM rates for large swaths or the U.S. coastal plain (e.g Bekaert et al., 2016; Buzzanga et al. 2020; Bekaert et al., 2020; Shirzaei et al., 2020). Having a higher resolution assessment of VLM rates can in turn help communities understand where VLM is occurring at very fine scales (e.g., street block level) now and help make informed decisions of how continued VLM will contribute to future RSL projections. Furthermore, InSAR provides an additional component to the coastal VLM observing network. Integrated assessments across tide gauges, GPS and InSAR are likely to be most useful for inferring VLM rates and projecting these rates forward at the spatial scales key to coastal communities. Here, a case study of InSAR VLM is presented and connected to this observing network. In general, as there is the possibility of using a user-defined VLM rate within the RSL projections, we examine other sources of VLM that may offer options.

Hampton Roads, VA

The historic long-term linear RSL rise trend at the Sewells Point, VA tide gauge is about 4.7 mm/yr. More than half this trend is estimated to be from VLM/subsidence with a rate of about 2.9 mm/yr, which is close to previous estimates (Zervas, 2013; Kopp et al., 2014; Sweet et al., 2017). This subsidence is driven by both glacial isostatic adjustment and more localized groundwater withdrawal. If assumed to be linear and persistent into the future, VLM will contribute about 0.29 m or 1 foot to projections of RSL over the next 100 years. For example, by 2050 under the Intermediate Low and Intermediate Scenarios, the amount of RSL rise is projected to be between about 0.4-5 m, respectively, with about 35% and 25% of that rise amount, respectively, from VLM. However, VLM rates across the Hampton Roads region are not uniform. A past study (Eggleston et al., 2013) leveraged a variety of in-situ observations to find a spatially varying pattern of subsidence ranging from 1.8-4.4 mm/year in the region from 1940 to 1971. The variations were connected to groundwater withdrawal in the region, which was captured via this assessment even with an effective spatial resolution on the order of tens of kilometers. More recently, InSAR rate maps have shown a range of subsidence from about 1-5 mm/year in the region over the time period from 2014 to present with locally higher rates (Figure 4.4.2; Buzzanga et al., 2020). Importantly, the satellite-based assessment revealed spatial variations on sub-kilometer scales with some of the most prominent features in the spatial map connected to specific construction projects and land-use. With an average rate of subsidence around 3 mm/year, over the course of the 21st century, VLM could contribute about 0.3 m to projected RSL with locally higher amounts elsewhere in the region. Furthermore, comparing the InSAR-derived spatial pattern of VLM to that in either Eggleston et al. (2013) or the gridded rates in this report provides important information about the linearity of VLM and the timescales on which VLM varies. There are considerable differences between the different assessments, indicating a shift in rates over the time periods considered. While it is necessary to consider the uncertainty in the VLM rate estimates and differences in measurement type, users of VLM information should assess land-use changes over the time periods considered along with the relevant processes driving VLM in the region. InSAR-derived VLM maps will play an increasingly key role in this assessment due to the spatial coverage and resolution provided by the satellites.

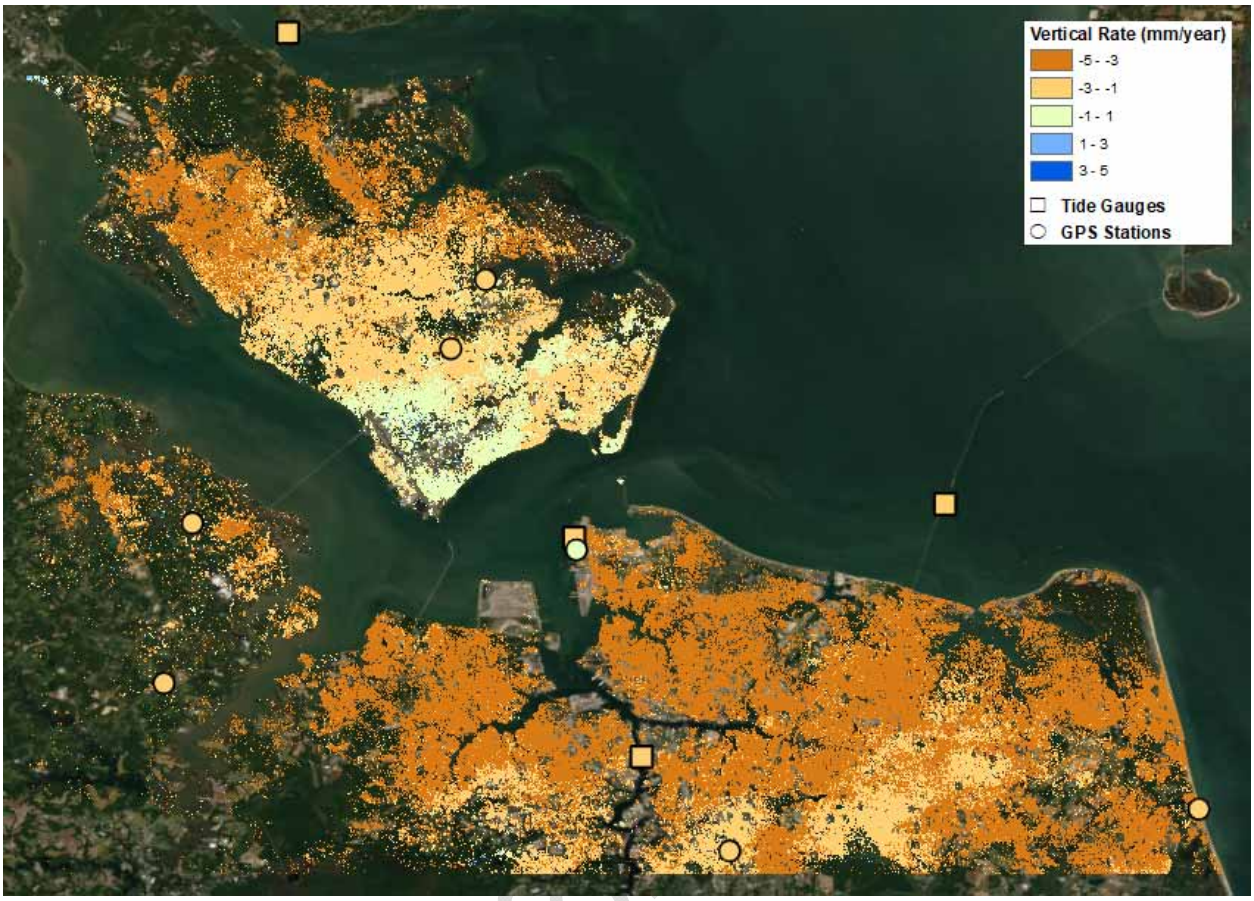

Figure 4.4.2: Map showing VLM rates (mm/year) for the Hampton Roads region, displayed on top of satellite imagery. Higher rates of subsidence are indicated by darker beige colors. Of particular interest to note is the range of rates in such a small region, e.g., on the order of up to 5 mm/yr difference in places. Based on Buzzanga et al. (2020).

Observing and Projecting Coastal Vertical Land Motion

While InSAR-measured VLM provides advantages over other measurement platforms in terms of spatial coverage and resolution, it should be considered in the context of the larger observing network when assessing VLM at the coast. In particular, InSAR serves two potential roles. First, InSAR can be used to provide ongoing monitoring of VLM at high spatial resolutions. InSAR has the potential to generate time series of VLM on a fine spatial scale. Subsidence 'hotspots' can be identified along with abrupt shifts in VLM, which can assist in planning and executing adaptation or mitigation efforts.. For coastal communities attempting to alleviate subsidence in their region through efforts like groundwater reinjection, InSAR provides a potentially better alternative to in situ monitoring to assess effectiveness of these efforts. Second, InSAR can serve to assess spatial variability in VLM, filling in the gaps between tide gauges and GPS stations in coastal regions. The observations can then be combined in a statistical framework to provide more accurate projections of VLM with better estimates of uncertainty.

Assessing VLM with InSAR is not without challenges, however, although many of these are being addressed in ongoing and planned efforts. To be useful for assessing long-term VLM rates with the still relatively short satellite records, the shorter term VLM rates can be calibrated and tied into existing National Spatial Reference System (NSRS) to improve accuracy and representativeness of long-term changes. Additionally, the availability and coverage of GPS in coastal regions impacts the accuracy of VLM by InSAR. To provide a measurement of absolute VLM, InSAR needs to be tied to available GPS measurements. In areas with large gaps between GPS stations, this can lead to reduced accuracy of the InSAR estimates. Ideally, analysis would be conducted to determine optimal GPS station spacing for maintaining integrity of the InSAR-derived velocity field in various environments including but not limited to regions of coastal subsidence, landslide/earthquake/volcanic activity, high plains aquifer depletion, and aquifer depletion in a tectonic area. Finally, InSAR VLM estimates are computationally expensive to perform over large regions, making national coverage a challenge. Efforts are underway, however, to generate a consistent surface displacement product (a preliminary step to estimating VLM) for the United States. A generalized approach for generating absolute VLM estimates from this product could then be created, paving the way for ongoing monitoring of VLM along the U.S. coastlines at high spatial resolutions.

To improve projections of VLM, InSAR alone is not sufficient. Instead, InSAR should be analyzed in tandem with available tide gauge, GPS and any other available in situ observations to assess both the spatial variability of VLM rates and potential non-linearities in the VLM rates estimated over these records. These non-linearities are critical for determining the future contribution of VLM to RSL. For example, the long-term rate assessed at a tide gauge as done in this report could differ significantly from the rate of VLM over the past decade because of a sustained land-use change. The comparison between the two types of VLM estimates in Fig. 1 indicate that these shifts may be present at some locations along the U.S. coastlines and need to be assessed to improve projections of VLM.

Section 5: Conclusions

Sea level rise driven by global climate change is a clear and present risk to the United States, now and for the foreseeable future. It is the goal of the Sea Level Rise and Coastal Flood Hazard Scenarios and Tools Interagency Task Force to continue to provide actionable scenarios of the future to assist decision making for both planning and risk bounding purposes. Both the IPCC AR6-based projections and extrapolations of observed trends agree on the amount of sea level rise in the next 30 years. Relative sea levels (RSL) along most U.S. coastlines (some in Alaska are the exception) are projected to rise 0.3 - 0.5 meters (1 - 1.6 feet) by 2050 as measured since 2000. Measured since 2020, the rise projected matches that over the last 100 years (1920-2020). At the regional scale, over this time period, RSLs may rise above or fall below this range by about 0.15 m (0.5 foot) with vertical land motion (VLM) largely responsible (with Southern Alaska an exception). These best-estimate, near-term projections (~30 years) represent a narrowing of uncertainty compared to the previous iteration of this report (Sweet et al., 2017). Though they will continue to evolve over time with new observations and analysis, they should help inform both near-term decisions and projects that may require decades worth of planning prior to actual implementation.

A major consequence of sea level rise projected over the next 30 years is that coastal flooding will continue to increase in frequency and severity, with potentially significant repercussions without additional widespread risk reduction measures. Using NOAA's coastal flood (emergency response) criteria with the regionalized extreme water level probabilities developed here, HTF is projected to hit 'moderate' severity stages routinely by 2050, which stands to be outright damaging to U.S. coastal infrastructure. By 2050, moderate flooding events that today pose a serious risk to life and property are projected to occur 4 times/year (about 8 days per year), which is more often than minor 'nuisance' high tide flooding occurs today (about 3 events or 6 days per year). Similarly, major flooding by 2050 is projected to have a (median value) 20% annual chance of occurring within a typical coastal community, which is quite close to the annual chance (30%) that moderate flooding has today. In short, a coastal flood regime shift is projected to occur along U.S. coastlines in the next 30 years.

Beyond 2050, the amount of sea level rise is strongly affected by future global warming. By reducing greenhouse gas emissions, severe and transformative impacts occurring later this century or early next century along U.S. coastlines are more likely to be avoided. As greenhouse gas emissions and global temperatures continue to rise, the likelihood of very high U.S. sea level rise does too. If global warming reaches 2° C (warming levels are already >1° C), there is about a 50% chance that U.S. sea level as a whole will rise 0.7 m by 2100 and 1.2 m by 2150, with higher/lower values regionally. If that were to occur, by 2100 'major' flooding would become tidally driven and as frequent as minor HTF occurs today in many coastal communities if risk-reduction action is not taken. For perspective, 3-7 days of minor HTF are projected as likely to occur along U.S. coastlines during 2021/2022 (Sweet et al., 2021). If global mean temperatures were to rise as high as about 3-5° C, much larger amounts of sea level rise become increasingly possible as instabilities in ice sheet dynamics potentially come into play, with 2.2 m by 2100 and 3.7 m by 2150 considered a possibility. Constant monitoring of global to local sea levels and their source contributions will be key to help assess potential trajectory divergence for triggering adaptive management plans.

The refreshed sea level scenario projection and the extreme water level probability datasets are being delivered or planned via several agency data servers, tools and associated guidance products. The

datasets are available through NOAA's Center for Operational Products and Services data API services, NOAA's Sea Level Rise Viewer and NASA's Sea Level Rise Portal. Eventual downstream guidance products include inclusion within NOAA Storm Water Assess tool, NOAA's County Snapshots, NOAA High Tide Flood Outlook and Projections the USACE SLR Calculator, USACE SLCT, USGS CoSMoS, EPA water utilities, FEMA National Risk Hazard among others. In addition, this report is a key technical input to NCA5, underway, and the datasets and derived information are being delivered to the NCA5 author teams.

In terms of next steps, the U.S. Sea Level Rise and Coastal Flood Hazard Scenarios and Tools Interagency Task Force will continue to refine these sea level projections and extreme (high tides, storms) water level probabilities, while working to improve understanding of the implications of these projections for coastal hazards (e.g., flooding and erosion), societal exposure and risk, infrastructure vulnerability, ecosystem health, and cascading societal impacts. In order to do so, more sophisticated modeling approaches that incorporate the relevant physical processes will be needed at the regional scale, with local granularity to assess the impacts of these coastal hazards. Such information is expected to ultimately feed into the next generation of interagency reports and assessments to enable informed climate adaptation planning. Specific focus areas include (also see the Section 3 'waves' callout box):

- Modeling long-term coastal evolution of beaches, dunes and cliffs coupled with storms and sea level rise, as these coastal changes can significantly affect future water levels and community flood exposure compared to static approaches (i.e., where topographic changes are not included; Barnard et al., 2019). Modeling of future dynamics such as changes in tide range will also be important under future sea levels (Passeri et al., 2016), as well as considering both dynamical changes in topography/landscape and physical forcing can be critical for assessing flood and inundation potential as compared to an assumed static coastal landscape (Lentz et al., 2016).
- Groundwater changes and, in particular, the potential shoaling and emergence of coastal water tables at the land surface in response to sea level rise. Several studies are signaling that climate-driven groundwater hazards could have impacts on coastal communities and ecosystems of comparable magnitude to overland flooding. In addition, there are direct impacts from rising water tables, including flooding of basements, liberating pollutants, disrupting septic systems, salt water intruding into agricultural soils and municipal wells, corroding buried infrastructure, and undermining structural foundations and roads; shallower water tables also reduce the infiltration capacity of soils, and therefore can amplify overland flooding.

There are a suite of federal agency tools that have been developed to begin to directly address these coastal hazards with more advanced approaches, as well as the associated societal exposure. The NOAA Sea Level Rise Viewer (https://coast.noaa.gov/slr/), which provides consistent national coverage of RSL rise-driven high tide flood risk, marsh migration projections, and social vulnerability; the USGS Coastal Change Hazards Portal (https://marine.usgs.gov/coastalchangehazardsportal/), which provides select, regionally-relevant projections of RSL rise-driven shoreline change, landscape response, and salt marsh vulnerability, as well as real-time and scenario-based storm-induced coastal change; and the USGS Coastal Storm Modeling System (CoSMoS; www.usgs.gov/cosmos; Barnard et al., [2019]), which

provides select regional coastal hazards coverage with projected sea level rise + CMIP5/6-derived storm-driven coastal flooding, beach and bluff erosion, and groundwater hazards, with fine-resolution to support local climate adaptation planning (www.ourcoastourfuture.org). What this combination of tools so far lacks, however, are nationally consistent, but locally resolved, total water and coastal change mapping and projections with coverage of the entire U.S. Over the course of its operations, the Task Force has worked toward this goal for RSL rise, first, and then extreme water levels, while simultaneously integrating the most up-to-date sea level rise science. Accomplishing this for total water levels and associated coastal change is the next step in this progression aimed at informing planning and decision-making in the coastal zone.

6. References

Bamber, J.L., Oppenheimer, M., Kopp, R.E., Aspinall, W.P. and Cooke, R.M., 2019. Ice sheet contributions to future sea-level rise from structured expert judgment. *Proceedings of the National Academy of Sciences*, *116*(23), pp.11195-11200.

Barnard, P. L., Erikson, L. H., Foxgrover, A. C., Hart, J. A. F., Limber, P., O'Neill, A. C., ... & Jones, J. M. (2019). Dynamic flood modeling essential to assess the coastal impacts of climate change. *Scientific reports*, *9*(1), 1-13.

Befus, K.M., Barnard, P.L., Hoover, D.J., Finzi Hart, J.A. and Voss, C.I., 2020. Increasing threat of coastal groundwater hazards from sea-level rise in California. *Nature Climate Change*, Volume 10, p. 946-952, https://doi.org/10.1038/s41558-020-0874-1

Bloemen, P., Reeder, T., Zevenbergen, C., Rijke, J., & Kingsborough, A. (2018). Lessons learned from applying eadaptation pathways in flood risk management and challenges for the further development of this approach. *Mitigation and Adaptation Strategies for Global Change*, *23*(7), 1083-1108.

Buchanan, M.K., Kopp, R.E., Oppenheimer, M. *and C. Tebaldi.* Allowances for evolving coastal flood risk under uncertain local sea-level rise. *Climatic Change* **137,** 347–362 (2016). https://doi.org/10.1007/s10584-016-1664-7

Church, J. A., Clark, U., Cazenave, A., Gregory, J. M., Jevrejeva, S., Levermann, A., et al. (2013). "Sea Level Change," in Climate Change 2013: The Physical Science Basis. Contribution of Working Group I to the Fifth Assessment Report of the Intergovernmental Panel on Climate Change, eds T. F. Stocker, D. Qin, G.-K. Plattner, M. Tignor, S. K. Allen, J. Boschung, et al. (Cambridge: Cambridge University Press), 1137–1216.

Coles, S., 2001. *An Introduction to statistical modeling of extreme values*. Springer-Verlag, London, 208 pages.

Cooley, D. (2013). "Return periods and return levels under climate change." Chapter 4 in Extremes in a Changing Climate: Detection, Analysis and Uncertainty, A. AghaKouchak et al. eds., Springer Science + Business media Dordrecht.

Dangendorf, S. et al., 2019: Persistent acceleration in global sea-level rise since the 1960s. Nature Climate Change, 49 9(9), 705–710, doi:10.1038/s41558-019-0531-8

Dokka, R. (2011). The role of deep processes in late 20th century subsidence of New Orleans and coastal areas of southern Louisiana and Mississippi. Journal of Geophysical Research. 116. doi: 10.1029/2010JB008008.

DeConto, R. M., Pollard, D., Alley, R. B., Velicogna, I., Gasson, E., Gomez, N., ... & Dutton, A. (2021). The Paris Climate Agreement and future sea-level rise from Antarctica. *Nature*, *593*(7857), 83-89.

Edwards, T. L., Nowicki, S., Marzeion, B., Hock, R., Goelzer, H., Seroussi, H., ... & Zwinger, T. (2021). Projected land ice contributions to twenty-first-century sea level rise. *Nature*, *593*(7857), 74-82.

Farrell, W.E. and Clark, J.A., 1976. On postglacial sea level. *Geophysical Journal International*, *46*(3), pp.647-667.

Fasullo, J. T., & Nerem, R. S. (2018). Altimeter-era emergence of the patterns of forced sea-level rise in climate models and implications for the future. *Proceedings of the National Academy of Sciences*, *115*(51), 12944-12949.

Frederikse, T., Landerer, F., Caron, L., Adhikari, S., Parkes, D., Humphrey, V.W., Dangendorf, S., Hogarth, P., Zanna, L., Cheng, L. and Wu, Y.H., 2020. The causes of sea-level rise since 1900. *Nature*, *584*(7821), pp.393-397.

Frederikse, T., K. Simon , C. A. Katsman, and R. Riva (2017). The sea-level budget along the Northwest Atlantic coast: GIA, mass changes, and large-scale ocean dynamics, J. Geophys. Res. Oceans, 122, 5486–5501, doi:10.1002/2017JC012699.

Fu, X. (2020). Measuring local sea-level rise adaptation and adaptive capacity: A national survey in the United States. *Cities*, *102*, 102717.

Guza, R.T., Thornton, E.B., 1982. Swash oscillations on a natural beach. Journal of Geophysical Research 87 (C1), 483–491.

Hall, J. W., Harvey, H., & Manning, L. J. (2019). Adaptation thresholds and pathways for tidal flood risk management in London. *Climate Risk Management*, *24*, 42-58.

Hall, J. A., Gill, S., Obeysekera, J., Sweet, W., Knuuti, K., and Marburger, J. (2016). Regional Sea Level Scenarios for Coastal Risk Management: Managing the Uncertainty of Future Sea Level Change and Extreme Water Levels for Department of Defense Coastal Sites Worldwide. Virginia: U.S. Department of Defense, 224.

Hemer, M.A., Fan, Y., Mori, N., Semedo, A. & Wang, X.L. Projected changes in wave climate from a multi-model ensemble. *Nature Climate Change.* **3** - 5, 471-476 (2013).

Hinkel, J., Aerts, J. C., Brown, S., Jiménez, J. A., Lincke, D., Nicholls, R. J., ... & Addo, K. A. (2018). The ability of societies to adapt to twenty-first-century sea-level rise. *Nature Climate Change*, *8*(7), 570-578.

Hosking, J. R. M., and Wallis, J. R. (1997). *Regional Frequency Analysis: An Approach Based on L-Moments.* Cambridge: Cambridge Univ. Press.

Karegar, M.A., T.H.Dixon, and S. E. Engelhart (2016). Subsidence along the Atlantic Coast of North America: Insights from GPS and late Holocene relative sea level data, Geophys. Res. Lett., 43, 3126–3133, doi:10.1002/2016GL068015.

Kopp, R. E., Gilmore, E. A., Little, C. M., Lorenzo-Trueba, J., Ramenzoni, V. C., & Sweet, W. V. (2019). Usable science for managing the risks of sea-level rise. Earth's Future, 7, 1235–1269. https://doi.org/10.1029/2018EF001145

Kopp, R.E., Horton, R.M., Little, C.M., Mitrovica, J.X., Oppenheimer, M., Rasmussen, D.J., Strauss, B.H. and Tebaldi, C., 2014. Probabilistic 21st and 22nd century sea-level projections at a global network of tide-gauge sites. *Earth's future*, *2*(8), pp.383-406.

Langbein W. B.,1949. Annual floods and the partial-duration flood series, Transactions, American Geophysical Union, Vol. 30, No. 6.

Longuet-Higgins, M.S., Stewart, R.W., 1963. A note on wave set-up. Journal of Marine Research 21, 4.

Lyu, K., Zhang, X., Church, J. A., Slangen, A. B., & Hu, J. (2014). Time of emergence for regional sea-level change. *Nature Climate Change*, *4*(11), 1006-1010.

McKenzie, T., Habel, S., & Dulai, H. (2021). Sea-level rise drives wastewater leakage to coastal waters and storm drains. Limnology and Oceanography Letters.

Milne, G.A. and Mitrovica, J.X., 1998. Postglacial sea-level change on a rotating Earth. *Geophysical Journal International*, *133*(1), pp.1-19.

Mitrovica, J.X., Tamisiea, M.E., Davis, J.L. and Milne, G.A., 2001. Recent mass balance of polar ice sheets inferred from patterns of global sea-level change. *Nature*, *409*(6823), pp.1026-1029.

Nadal-Caraballo, N.C.; Campbell, M.O.; Gonzalez, V.M.; Torres, M.J.; Melby, J.A., and Taflanidis, A.A., 2020. Coastal Hazards System: A Probabilistic Coastal Hazard Analysis Framework. In: Malvárez, G. and Navas, F. (eds.), Global Coastal Issues of 2020. Journal of Coastal Research, Special Issue No. 95, pp. 1211-1216. Coconut Creek (Florida), ISSN 0749-0208.

National Geodetic Survey (NGS) (2001). *Geodetic Program Needs of Louisiana and Wisconsin: Report to Congress*, Silver Spring, MD, U.S. Dept. of Commerce, National Oceanic and Atmospheric Administration, National Ocean Service. https://www.ngs.noaa.gov/PUBS_LIB/NGSreport_823.pdf

NOAA (2020). National Weather Service Instruction 10-320. Surf Zone Forecast and Coastal/Lakeshore Hazard Services. http://www.nws.noaa.gov/directives/sym/pd01003020curr.pdf

Obeysekera, J and J. Salas, 2020. Hydrologic Designs for Extreme Events under Nonstationarity, Engineering Methods for Precipitation under a Changing Climate . 2020

Oppenheimer, M., Glavovic, B. C., Hinkel, J., van de Wal, R., Magnan, A. K., Abd-Elgawad, A., et al. (2019). “Sea level rise and implications for low-lying islands, coasts and communities,” in IPCC Special Report on the Ocean and Cryosphere in a Changing Climate, eds H.-O. Pörtner, D. C. Roberts, V. Masson-Delmotte,
P. Zhai, M. Tignor, E. Poloczanska, et al.

Parris, A., P. Bromirski, V. Burkett, D. Cayan, M. Culver, J. Hall, R. Horton, K. Knuuti, R. Moss, J. Obeysekera, A. Sallenger, and J. Weiss. 2012. Global Sea Level Rise Scenarios for the US National Climate Assessment. NOAA Tech Memo OAR CPO-1. 37 pp. 2012.

Reguero, B.G., Menéndez, M., Méndez, F.J., Mínguez, R. & Losada, I.J. A Global Ocean Wave (GOW) calibrated reanalysis from 1948 onwards. *Coastal Engineering.* **65**, 38-55 (2012).

Richter, K., Meyssignac, B., Slangen, A. B., Melet, A., Church, J. A., Fettweis, X., ... & Champollion, N. (2020). Detecting a forced signal in satellite-era sea-level change. *Environmental Research Letters*, *15*(9), 094079.

Perica, S., Pavlovic, S., St Laurent, M., Trypaluk, C., Unruh, D., and Wilhite, O. (2018). Precipitation-Frequency Atlas of the United States. Texas: Version 2.0, 11. Silver Spring, MD: National Oceanic and Atmospheric Administration, National Weather Service.

Rueda, A., Vitousek, S., Camus, P., Tomás, A., Espejo, A., Losada, I. J., et al. (2017). A global classification of coastal flood hazard climates associated with large-scale oceanographic forcing. Sci. Rep. 7, 1–8.

Rydlund, P. H. Jr., B. J. Densmore (2012). "Methods of Practice and Guidelines for Using Survey-Grade Global Navigation Satellite Systems (GNSS) to Establish Vertical Datum in the United States Geological Survey, " Chapter 1 of Section D, Field Survey Methods, Book 11, Collection and Delineation of Spatial Data. U. S. Department of the Interior, U.S. Geological Survey, Reston, Virginia. http://pubs.usgs.gov/tm/11d1/

Salas, J.D. and Obeysekera, J., 2014. Revisiting the concepts of return period and risk for nonstationary hydrologic extreme events. *ASCE Journal of Hydrologic Engineering*, 19 (3), 554-568.

Salas, J.D., J. Obeysekera, and R. Vogel. 2018. Techniques for assessing water infrastructure for nonstationary extreme events: a review. Hydrologic Science Journal, Vol. 63, Issue 3,325-352

Stockdon, Hilary F., et al. Empirical parameterization of setup, swash, and runup. *Coastal engineering* 53.7 (2006): 573-588.

Sweet, W. V., & Park, J. (2014). From the extreme to the mean: Acceleration and tipping points of coastal inundation from sea level rise. *Earth's Future*, *2*(12), 579-600.

Sweet, W. V., Park, J., Gill, S., & Marra, J. (2015). New ways to measure waves and their effects at NOAA tide gauges: A Hawaiian-network perspective. *Geophysical Research Letters*, *42*(21), 9355-9361.

Sweet, W.V., G. Dusek., J. Obeysekera, J. Marra (2018). Patterns and Projections of High Tide Flooding Along the U.S. Coastline Using a Common Impact Threshold. NOAA Tech. Rep. NOS CO-OPS 086. National Oceanic and Atmospheric Administration, National Ocean Service, Silver Spring, MD. 44p. https://tidesandcurrents.noaa.gov/publications/techrpt86_PaP_of_HTFlooding.pdf

Sweet, W. V., Genz, A. S., Obeysekera, J., & Marra, J. J. (2020). A Regional Frequency Analysis of Tide Gauges to Assess Pacific Coast Flood Risk. Frontiers in Marine Science, 7, 883.

Sweet, W. V., Dusek, G., Carbin, G., Marra, J. J., Marcy, D., and Simon, S. (2020b). 2019 State of US High Tide Flooding With a 2020 Outlook. NOAA Tech. Rep. NOS CO-OPS., Vol. 92. Silver Spring, MD: National Oceanic and Atmospheric Administration, 17.

Thompson, P. R., Widlansky, M. J., Hamlington, B. D., Merrifield, M. A., Marra, J. J., Mitchum, G. T., & Sweet, W. (2021). Rapid increases and extreme months in projections of United States high-tide flooding. *Nature Climate Change*, 1-7.

USACE. 2014. Procedures to evaluate sea level change: Impacts, responses, and adaptation. Engineer Technical Letter 1100–2–1. Washington, DC: USACE.

Vitousek, S., Barnard, P.L., Fletcher, C., Frazer, N., Erikson, L.H. and Storlazzi, C.D., 2017. Doubling of coastal flooding frequency within decades due to sea-level rise. *Nature Scientific Reports*, Volume 7 (Number 1399), 9 pp., http://dx.doi.org/10.1038/s41598-017-01362-7

Werner, S. E., Wise, R. M., Butler, J. R., Totin, E., & Vincent, K. (2021). Adaptation pathways: A review of approaches and a learning framework. *Environmental Science & Policy*, *116*, 266-275.

Wuebbles, D.J., Fahey, D.W., Hibbard, K.A., Arnold, J.R., DeAngelo, B., Doherty, S., Easterling, D.R., Edmonds, J., Edmonds, T., Hall, T. and Hayhoe, K., 2017. Climate science special report: Fourth national climate assessment (NCA4), Volume I.

Zervas, C. (2013). NOAA Technical Report NOS Co-OPS 067: Extreme Water Levels of the United States 1893–2010. Silver Spring, MD: National Ocean Service.

2017 Appendix Tables and Figures
2018
2019 **Table A1:** Projections methods employed

Driver of GMSL or RSL change	**Kopp et al. (2014) projection method (used in Sweet et al., 2017)**	**AR6 (Fox-Kemper et al., 2021) projection methods (used here)**
Thermal expansion	CMIP5 ensemble drift-corrected *zostoga*	Two-layer model with climate sensitivity calibrated to the IPCC assessment and expansion coefficients calibrated to emulate CMIP6 models
Greenland ice sheet	*Likely* range from AR5 assessment, with shape of tails based on structured expert judgement (Bamber and Aspinall, 2013)	1. Emulated ISMIP6 simulations through 2100 (Edwards et al., 2021), extended after 2100 based on constant post-2100 rates 2. Structured expert judgement (Bamber et al., 2019)
Antarctic ice sheet	*Likely* range from AR5 assessment, with shape of tails based on structured expert judgement (Bamber and Aspinall, 2013)	1. Emulated ISMIP6 simulations through 2100 (Edwards et al., 2021), extended after 2100 with constant rates based on the IPCC AR5 parametric AIS model (Church et al., 2013) 2. LARMIP-2 simulations (Levermann et al., 2020) augmented by AR5 surface mass balance model (Church et al., 2013), extended past 2100 based on constant rates 3. Single ice-sheet model incorporated Marine Ice Cliff Instability (DeConto et al,. 2021) 4. Structured expert judgement (Bamber et al., 2019)
Glaciers	Distribution based on Marzeion et al. (2012) surface mass balance model	Emulated GlacierMIP (Marzeion et al., 2020; Edwards et al., 2021) extended after 2100 with AR5 parametric model re-fit to GlacierMIP (Marzeion et al., 2020)

Land water storage	Groundwater depletion: Population/groundwater depletion relationship calibrated based on (Konikow, 2011; Wada et al., 2012) Water impoundment: Population/dam impoundment relationship calibrated based on (Chao et al., 2008)	Groundwater depletion: Updated population/groundwater depletion relationship calibrated based on (Konikow, 2011; Wada et al., 2012, 2016) Water impoundment: Population/dam impoundment relationship calibrated based on (Chao et al., 2008), adjusted for new construction following (Hawley et al., 2020) for 2020 to 2040
Ocean dynamic sea level	Distribution derived from CMIP5 ensemble *zos* field	Distribution derived from CMIP6 ensemble zos field after linear drift removal
Gravitational, rotational, and deformational effects	Sea-level equation solver (Mitrovica et al,. 2011) driven by projections of ice sheet and glacier changes	Sea-level equation solver (Slangen et al., 2014a) driven by projections of ice sheet, glacier, and land water storage changes
GIA and other drivers of VLM	Spatiotemporal statistical model of tide-gauge data (updated from Kopp et al., 2014)	Spatiotemporal statistical model of tide-gauge data (updated from Kopp et al., 2014)

Table A2. Offsets, in meters, for different time periods and for each region considered in section 2. These offsets are assessed using the trajectory determined from the available tide gauge data in each region.

	1992-2000	2000-2005	2005-2020
Contiguous U.S.	0.02	0.02	0.07
Northeast	0.03	0.02	0.09
Southeast	0.03	0.02	0.09
Eastern Gulf	0.03	0.02	0.1
Western Gulf	0.05	0.04	0.14
Southwest	0.01	0.01	0.05
Northwest	0.01	0.01	0.04
Hawaiian Islands	0.02	0.02	0.06
Caribbean	0.02	0.01	0.06

Table A3: Tide Gauge , Extreme Water Level Metadata and Flood Heights

US Region	EWL Grid No.	NOAA ID	Location	Latitude	Longitude	Tide Range (m)	Flood Index 'ν' (m, MHHW)	ν' Trend (mm/yr)	Epoch of 'ν'	Minor Flood (m, MHHW)	Moderate Flood (m)	Major Flood (m)
Pacific	39509	1611400	Nawiliwili, HI	21.95	-159.36	0.558	0.244	1.7	1983-2001	0.522	0.817	1.192
	39511	1612340	Honolulu, HI	21.31	-157.87	0.580	0.248	1.3	1983-2001	0.523	0.817	1.193
	39511	1612480	Mokuoloe, HI	21.43	-157.79	0.646	0.265	2.0	1983-2001	0.526	0.819	1.196
	39153	1615680	Kahului, HI	20.90	-156.48	0.686	0.252	2.1	1983-2001	0.527	0.821	1.197
	39154	1617433	Kawaihae, HI	20.04	-155.83	0.659	0.237	7.9	1983-2001	0.526	0.820	1.196
	38795	1617760	Hilo, HI	19.73	-155.06	0.731	0.272	3.1	1983-2001	0.529	0.822	1.199
	37704	1619000	Johnston Atoll	16.74	-169.53	0.674	0.295	2.2	1983-2001	0.527	0.820	1.197
	42004	1619910	Midway Islands	28.21	-177.36	0.381	0.303	1.9	1983-2001	0.515	0.811	1.185
	36941	1630000	Apra Harbor, Guam	13.44	144.65	0.715	0.249	4.2	1983-2001	0.529	0.821	1.199
	36941	1631428	Pago Bay, GUAM	13.43	144.80	0.525	0.287	4.2	1983-2001	0.521	0.816	1.191
	26574	1770000	American Samoa	-14.28	189.32	0.848	0.338	3.8	1983-2001	0.534	0.825	1.204
	35169	1820000	Kwajalein	8.73	167.74	1.194	0.446	3.1	1983-2001	0.548	0.836	1.218
	39117	1890000	Wake Island	19.29	166.62	0.718	0.295	2.1	1983-2001	0.529	0.822	1.199
NE	47859	8410140	Eastport, ME	44.90	-66.98	5.874	0.930	2.1	1983-2001	0.735	0.976	1.405
	47858	8411250	Cutler Naval Base, ME	44.64	-67.30	4.133	0.716	2.4	1983-2001	0.665	0.924	1.335
	47857	8413320	Bar Harbor, ME	44.39	-68.21	3.465	0.657	2.1	1983-2001	0.639	0.904	1.309
	47496	8418150	Portland, ME	43.66	-70.25	3.019	0.605	1.9	1983-2001	0.621	0.891	1.291
	47496	8419317	Wells, ME	43.32	-70.56	2.914	0.667	3.5	1983-2001	0.617	0.887	1.287
	47496	8423898	Fort Point, NH	43.07	-70.71	2.864	0.662	3.5	1983-2001	0.615	0.886	1.285
	47136	8443970	Boston, MA	42.35	-71.05	3.131	0.634	2.8	1983-2001	0.625	0.894	1.295
	46777	8447386	Fall River, MA	41.70	-71.16	1.456	0.566	3.5	1983-2001	0.558	0.844	1.228
	46778	8447930	Woods Hole, MA	41.52	-70.67	0.672	0.446	3.2	1983-2001	0.527	0.820	1.197
	46778	8449130	Nantucket Island, MA	41.29	-70.10	1.089	0.418	3.8	1983-2001	0.544	0.833	1.214
	46777	8452660	Newport, RI	41.51	-71.33	1.174	0.478	2.8	1983-2001	0.547	0.835	1.217
	46777	8452944	Conimicut Light, RI	41.72	-71.34	1.398	0.560	3.5	1983-2001	0.556	0.842	1.226
	46777	8454000	Providence, RI	41.81	-71.40	1.476	0.549	2.3	1983-2001	0.559	0.844	1.229
	46777	8454049	Quonset Point, RI	41.59	-71.41	1.249	0.547	3.5	1983-2001	0.550	0.837	1.220
	46776	8461490	New London, CT	41.36	-72.09	0.930	0.468	2.6	1983-2001	0.537	0.828	1.207
	46776	8465705	New Haven, CT	41.28	-72.91	2.045	0.603	3.5	1983-2001	0.582	0.861	1.252
	46775	8467150	Bridgeport, CT	41.17	-73.18	2.231	0.555	3.0	1983-2001	0.589	0.867	1.259
	46777	8510560	Montauk, NY	41.05	-71.96	0.771	0.487	3.4	1983-2001	0.531	0.823	1.201
	46416	8514560	PORT JEFFERSON, NY	40.95	-73.08	2.181	0.527	2.5	1983-2001	0.587	0.865	1.257
	46416	8516945	Kings Point, NY	40.81	-73.76	2.378	0.638	2.5	1983-2001	0.595	0.871	1.265
	46415	8518750	The Battery, NY	40.70	-74.01	1.542	0.546	3.1	1983-2001	0.562	0.846	1.232
	46415	8519483	Bergen Point, NY	40.64	-74.14	1.681	0.549	4.4	1983-2001	0.567	0.850	1.237
	46415	8531680	Sandy Hook, NJ	40.47	-74.01	1.593	0.552	2.7	1983-2001	0.564	0.848	1.234
	46056	8534720	Atlantic City, NJ	39.36	-74.42	1.403	0.534	4.1	1983-2001	0.556	0.842	1.226
	45697	8536110	Cape May, NJ	38.97	-74.96	1.659	0.486	4.7	1983-2001	0.566	0.850	1.236
	46055	8537121	Ship John Shoal, NJ	39.31	-75.38	1.894	0.578	3.5	1983-2001	0.576	0.857	1.246
	46055	8540433	Marcus Hook, PA	39.81	-75.41	1.871	0.563	3.5	1983-2001	0.575	0.856	1.245
	46055	8545240	Philadelphia, PA	39.93	-75.14	2.039	0.462	3.1	1983-2001	0.582	0.861	1.252
	46055	8551762	Delaware City, DE	39.58	-75.59	1.830	0.540	3.5	1983-2001	0.573	0.855	1.243
	46055	8551910	Reedy Point, DE	39.56	-75.57	1.779	0.423	4.1	1983-2001	0.571	0.853	1.241
	45696	8555889	Brandywine Shoal, DE	38.99	-75.11	1.676	0.616	3.5	1983-2001	0.567	0.850	1.237
	45696	8557380	Lewes, DE	38.78	-75.12	1.418	0.530	3.5	1983-2001	0.557	0.843	1.227
	45696	8570280	OCEAN CITY, MD	38.33	-75.08	1.187	0.413	3.5	1983-2001	0.547	0.836	1.217
	45696	8570283	Ocean City Inlet, MD	38.33	-75.09	0.751	0.360	3.5	1983-2001	0.530	0.823	1.200
	45695	8571421	Bishops Head, MD	38.22	-76.04	0.624	0.503	3.5	1983-2001	0.525	0.819	1.195
	45695	8571892	Cambridge, MD	38.57	-76.07	0.622	0.414	4.9	1983-2001	0.525	0.819	1.195
	46054	8573364	Tolchester Beach, MD	39.21	-76.25	0.527	0.484	2.5	1983-2001	0.521	0.816	1.191
	46055	8573927	Chesapeake City, MD	39.53	-75.81	0.980	0.470	3.8	1983-2001	0.539	0.829	1.209
	46054	8574070	Havre De Grace, MD	39.54	-76.09	0.746	0.482	3.5	1983-2001	0.530	0.822	1.200
	46054	8574680	Baltimore, MD	39.27	-76.58	0.506	0.443	3.2	1983-2001	0.520	0.815	1.190
	45695	8575512	Annapolis, MD	38.98	-76.48	0.438	0.430	3.7	1983-2001	0.518	0.813	1.188
	45695	8577330	Solomons Island, MD	38.32	-76.45	0.449	0.398	6.0	1983-2001	0.518	0.813	1.188
	45694	8594900	Washington, DC	38.87	-77.02	0.965	0.461	3.3	1983-2001	0.539	0.829	1.209
	45337	8631044	Wachapreague, VA	37.61	-75.69	1.376	0.508	5.4	1983-2001	0.555	0.841	1.225
	45337	8632200	Kiptopeke, VA	37.17	-75.99	0.896	0.435	4.7	1983-2001	0.536	0.827	1.206
	45695	8635150	Colonial Beach, VA	38.25	-76.96	0.591	0.406	4.7	1983-2001	0.524	0.818	1.194
	45336	8635750	Lewisetta, VA	38.00	-76.46	0.458	0.420	5.6	1983-2001	0.518	0.814	1.188
	45336	8636580	Windmill Point, VA	37.62	-76.29	0.424	0.419	5.2	1983-2001	0.517	0.813	1.187
	45336	8637689	Yorktown, VA	37.23	-76.48	0.786	0.567	3.5	1983-2001	0.531	0.824	1.201
	44977	8638610	Sewells Point, VA	36.95	-76.33	0.841	0.502	4.6	1983-2001	0.534	0.825	1.204
	44977	8638863	CBBT, VA	36.97	-76.11	0.885	0.503	6.0	1983-2001	0.535	0.827	1.205
	44977	8639348	Money Point, VA	36.78	-76.30	0.977	0.528	5.6	1983-2001	0.539	0.829	1.209

US Region	EWL Grid No.	NOAA ID	Location	Latitude	Longitude	Tide Range (m)	Flood Index 'u' (m, MHHW)	u' Trend (mm/yr)	Epoch of 'u'	Minor Flood (m, MHHW)	Moderate Flood (m)	Major Flood (m)
SE	44978	8651370	Duck, NC	36.18	-75.75	1.124	0.494	4.6	1983-2001	0.545	0.834	1.215
	44619	8652587	Oregon Inlet, NC	35.80	-75.55	0.360	0.384	4.6	1983-2001	0.514	0.811	1.184
	44619	8654400	Cape Hatteras, NC	35.22	-75.64	1.056	0.412	3.2	1983-2001	0.542	0.832	1.212
	44619	8654467	USCG Hatteras, NC	35.21	-75.70	0.186	0.598	3.2	1983-2001	0.507	0.806	1.177
	44259	8656483	Beaufort, NC	34.72	-76.67	1.079	0.362	3.8	1983-2001	0.543	0.832	1.213
	44258	8658120	Wilmington, NC	34.23	-77.95	1.427	0.327	2.3	1983-2001	0.557	0.843	1.227
	44258	8658163	Wrightsville Beach, NC	34.21	-77.79	1.366	0.564	3.2	1983-2001	0.555	0.841	1.225
	43898	8661070	Springmaid Pier, SC	33.66	-78.92	1.707	0.493	2.9	1983-2001	0.568	0.851	1.238
	43897	8662245	Oyster Landing, SC	33.35	-79.19	1.561	0.496	3.2	1983-2001	0.562	0.847	1.232
	43558	8665530	Charleston, SC	32.78	-79.93	1.757	0.453	3.3	1983-2001	0.570	0.853	1.240
	43537	8670870	Fort Pulaski, GA	32.03	-80.90	2.287	0.500	3.3	1983-2001	0.591	0.869	1.261
	42818	8720030	Fernandina Beach, FL	30.67	-81.47	1.999	0.473	2.3	1983-2001	0.580	0.860	1.250
	42818	8720218	Mayport, FL	30.40	-81.43	1.508	0.378	2.6	1983-2001	0.560	0.845	1.230
	42818	8720357	St Johns River, FL	30.19	-81.69	0.312	0.333	3.2	1983-2001	0.512	0.809	1.182
	42459	8720587	St. Augustine Beach, FL	29.86	-81.26	1.569	0.531	3.2	1983-2001	0.563	0.847	1.233
	42101	8721604	Trident Pier, FL	28.42	-80.59	1.193	0.407	5.1	1983-2001	0.548	0.836	1.218
	41024	8723214	Virginia Key, FL	25.73	-80.16	0.667	0.284	5.1	1983-2001	0.527	0.820	1.197
	40664	8723970	Vaca Key, FL	24.71	-81.11	0.297	0.249	4.2	1983-2001	0.512	0.809	1.182
	40664	8724580	Key West, FL	24.56	-81.81	0.551	0.262	2.5	1983-2001	0.522	0.817	1.192
E Gulf	41382	8725110	Naples, FL	26.13	-81.81	0.875	0.323	2.9	1983-2001	0.535	0.826	1.205
	41382	8725520	Fort Myers, FL	26.65	-81.87	0.401	0.325	3.1	1983-2001	0.516	0.812	1.186
	41740	8726384	Port Manatee, FL	27.64	-82.56	0.669	0.260	6.6	1983-2001	0.527	0.820	1.197
	41740	8726520	St Petersburg, FL	27.76	-82.63	0.688	0.337	2.8	1983-2001	0.528	0.821	1.198
	41740	8726607	Old Port Tampa, FL	27.86	-82.55	0.749	0.304	3.2	1983-2001	0.530	0.822	1.200
	41740	8726667	Mckay Bay Entrance, FL	27.91	-82.43	0.814	0.320	3.2	1983-2001	0.533	0.824	1.203
	41740	8726724	Clearwater Beach, FL	27.98	-82.83	0.841	0.294	7.1	1983-2001	0.534	0.825	1.204
	42457	8727520	Cedar Key, FL	29.14	-83.03	1.157	0.415	2.2	1983-2001	0.546	0.835	1.216
	42456	8728690	Apalachicola, FL	29.73	-84.98	0.492	0.390	3.0	1983-2001	0.520	0.815	1.190
	42814	8729108	Panama City, FL	30.15	-85.67	0.409	0.368	2.5	1983-2001	0.516	0.812	1.186
	42814	8729210	Panama City Beach, FL	30.21	-85.88	0.420	0.348	4.3	1983-2001	0.517	0.813	1.187
	42812	8729840	Pensacola, FL	30.40	-87.21	0.383	0.345	2.4	1983-2001	0.515	0.811	1.185
	42812	8732828	Mobile Bay, AL	30.42	-87.83	0.490	0.519	4.3	1983-2001	0.520	0.815	1.190
	42811	8735180	Dauphin Island, AL	30.25	-88.08	0.367	0.354	4.3	1983-2001	0.515	0.811	1.185
	42811	8736897	Mobile, AL	30.69	-88.06	0.517	0.535	4.3	1983-2001	0.521	0.816	1.191
	42811	8737048	Mobile State Docks, AL	30.71	-88.04	0.501	0.439	4.3	1983-2001	0.520	0.815	1.190
	42811	8741533	Pascagoula NOAA Lab, MS	30.37	-88.56	0.466	0.494	4.3	1983-2001	0.519	0.814	1.189
	42810	8747437	Bay Waveland Yacht Club, MS	30.33	-89.33	0.529	0.498	4.6	1983-2001	0.521	0.816	1.191
W Gulf	42092	8760922	Pilots Station East, SW Pass, LA	28.93	-89.41	0.356	0.399	4.3	2012-2016	0.514	0.811	1.184
	42451	8761724	Grand Isle, LA	29.26	-89.96	0.323	0.309	7.8	2012-2016	0.513	0.810	1.183
	42809	8761927	New Canal Station, LA	30.03	-90.11	0.164	0.485	5.6	1983-2001	0.507	0.805	1.177
	42450	8762075	Port Fourchon, LA	29.11	-90.20	0.368	0.298	4.3	2012-2016	0.515	0.811	1.185
	42449	8764227	Amerada Pass, LA	29.45	-91.34	0.487	0.535	4.3	1983-2001	0.519	0.815	1.189
	42449	8765251	Cypremort Point, LA	29.71	-91.88	0.518	0.458	4.3	1983-2001	0.521	0.816	1.191
	42448	8766072	Freshwater Canal Locks, LA	29.56	-92.31	0.657	0.696	4.3	1983-2001	0.526	0.820	1.196
	42806	8767816	Lake Charles, LA	30.22	-93.22	0.427	0.494	4.3	1983-2001	0.517	0.813	1.187
	42447	8768094	Calcasieu Pass, LA	29.77	-93.34	0.589	0.465	6.1	1983-2001	0.524	0.818	1.194
	42447	8770570	Sabine Pass North, TX	29.73	-93.87	0.488	0.368	6.1	1983-2001	0.520	0.815	1.190
	42446	8770613	Morgans Point, TX	29.68	-94.99	0.398	0.488	3.1	1983-2001	0.516	0.812	1.186
	42446	8771013	Eagle Point, TX	29.48	-94.92	0.338	0.331	13.8	1983-2001	0.514	0.810	1.184
	42446	8771341	Galveston Bay Entrance, TX	29.36	-94.72	0.510	0.499	6.1	1983-2001	0.520	0.815	1.190
	42446	8771450	Galveston Pier 21, TX	29.31	-94.79	0.429	0.366	6.5	1983-2001	0.517	0.813	1.187
	42446	8771510	Galveston Pleasure Pier, TX	29.29	-94.79	0.622	0.425	6.5	1983-2001	0.525	0.819	1.195
	42086	8772440	Freeport, TX	28.95	-95.31	0.536	0.391	9.0	1983-2001	0.521	0.816	1.191
	42086	8772447	USCG Freeport, TX	28.94	-95.30	0.549	0.460	6.1	1983-2001	0.522	0.816	1.192
	42084	8774770	Rockport, TX	28.02	-97.05	0.111	0.336	5.7	2002-2006	0.504	0.803	1.174
	41725	8775870	Corpus Christi, TX	27.58	-97.22	0.497	0.391	4.8	1983-2001	0.520	0.815	1.190
	41366	8779770	Port Isabel, TX	26.06	-97.22	0.418	0.337	4.0	1983-2001	0.517	0.813	1.187
SW	43500	9410170	San Diego, CA	32.71	-117.17	1.745	0.490	2.2	1983-2001	0.570	0.852	1.240
	43500	9410230	La Jolla, CA	32.87	-117.26	1.624	0.468	2.1	1983-2001	0.565	0.849	1.235
	43858	9410660	Los Angeles, CA	33.72	-118.27	1.674	0.472	1.0	1983-2001	0.567	0.850	1.237
	44217	9410840	Santa Monica, CA	34.01	-118.50	1.654	0.489	1.8	1983-2001	0.566	0.850	1.236
	44216	9411340	Santa Barbara, CA	34.41	-119.69	1.645	0.485	0.6	1983-2001	0.566	0.849	1.236
	44574	9412110	Port San Luis, CA	35.18	-120.76	1.623	0.449	1.0	1983-2001	0.565	0.849	1.235
	44932	9413450	Monterey, CA	36.61	-121.89	1.627	0.431	1.6	1983-2001	0.565	0.849	1.235
	45290	9414290	San Francisco, CA	37.81	-122.47	1.780	0.375	1.9	1983-2001	0.571	0.853	1.241
	45290	9414523	Redwood City, CA	37.51	-122.21	2.501	0.400	2.7	1983-2001	0.600	0.875	1.270
	45290	9414750	Alameda, CA	37.77	-122.30	2.010	0.411	0.4	1983-2001	0.580	0.860	1.250
	45290	9414863	Richmond, CA	37.93	-122.40	1.846	0.359	3.1	1983-2001	0.574	0.855	1.244
	45290	9415020	Point Reyes, CA	38.00	-122.98	1.758	0.447	2.1	1983-2001	0.570	0.853	1.240
	45649	9415144	Port Chicago, CA	38.06	-122.04	1.498	0.388	1.4	1983-2001	0.560	0.845	1.230

2032
2033

US Region	EWL Grid No.	NOAA ID	Location	Latitude	Longitude	Tide Range (m)	Flood Index 'a' (m, MHHW)	a' Trend (mm/yr)	Epoch of 'a'	Minor Flood (m, MHHW)	Moderate Flood (m)	Major Flood (m)
SW con't	45648	9416841	Arena Cove, CA	38.91	-123.71	1.787	0.500	0.6	1983-2001	0.571	0.854	1.241
	46365	9418767	North Spit, CA	40.77	-124.22	2.090	0.491	4.8	1983-2001	0.584	0.863	1.254
	46724	9419750	Crescent City, CA	41.75	-124.18	2.095	0.548	-0.8	1983-2001	0.584	0.863	1.254
	47083	9431647	Port Orford, OR	42.74	-124.50	2.220	0.594	0.2	1983-2001	0.589	0.867	1.259
	47442	9432780	Charleston, OR	43.35	-124.32	2.323	0.586	1.1	1983-2001	0.593	0.870	1.263
	47801	9435380	South Beach, OR	44.63	-124.04	2.543	0.579	1.7	1983-2001	0.602	0.876	1.272
	48161	9437540	Garibaldi, OR	45.55	-123.92	2.536	0.597	2.4	1983-2001	0.601	0.876	1.271
	48520	9439040	Astoria, OR	46.21	-123.77	2.624	0.629	-0.2	1983-2001	0.605	0.879	1.275
NW	48520	9440910	Toke Point, WA	46.71	-123.97	2.720	0.807	0.6	1983-2001	0.609	0.882	1.279
	48519	9441102	Westport, WA	46.90	-124.11	2.786	0.670	1.9	1983-2001	0.611	0.884	1.281
	48878	9442396	La Push, WA	47.91	-124.64	2.577	0.766	1.9	1983-2001	0.603	0.877	1.273
	49237	9443090	Neah Bay, WA	48.37	-124.61	2.425	0.688	-1.7	1983-2001	0.597	0.873	1.267
	49238	9444090	Port Angeles, WA	48.13	-123.44	2.153	0.562	0.2	1983-2001	0.586	0.865	1.256
	49239	9444900	Port Townsend, WA	48.11	-122.76	2.597	0.538	1.7	1983-2001	0.604	0.878	1.274
	48880	9446484	Tacoma, WA	47.27	-122.41	3.595	0.517	3.4	1983-2001	0.644	0.908	1.314
	48880	9447130	Seattle, WA	47.60	-122.34	3.462	0.541	2.1	1983-2001	0.638	0.904	1.308
	49239	9449424	Cherry Point, WA	48.86	-122.76	2.788	0.585	0.4	1983-2001	0.612	0.884	1.282
	49238	9449880	Friday Harbor, WA	48.55	-123.01	2.364	0.554	1.2	1983-2001	0.595	0.871	1.265
Alaska	51743	9450460	Ketchikan, AK	55.33	-131.63	4.708	1.086	-0.4	1983-2001	2.059	2.359	2.759
	52099	9451054	Port Alexander, AK	56.25	-134.65	3.329	0.738	-5.8	1983-2001	1.031	1.331	1.731
	52457	9451600	Sitka, AK	57.05	-135.34	3.029	0.768	-2.4	1983-2001	0.883	1.183	1.583
	52817	9452210	Juneau, AK	58.30	-134.41	4.970	1.152	-15.1	2012-2016	2.319	2.619	3.019
	53175	9452400	Skagway, AK	59.45	-135.33	5.100	1.218	-19.9	2012-2016	2.456	2.756	3.156
	52815	9452634	Elfin Cove, AK	58.19	-136.35	3.360	1.149	-5.8	1983-2001	1.048	1.348	1.748
	53171	9453220	Yakutat, Yakutat Bay, AK	59.55	-139.73	3.070	0.891	-10.7	2012-2016	0.902	1.202	1.602
	53524	9454050	Cordova, AK	60.56	-145.75	3.838	0.937	0.8	1983-2001	1.344	1.644	2.044
	53882	9454240	Valdez, AK	61.13	-146.36	3.702	0.878	-5.8	1983-2001	1.253	1.553	1.953
	53520	9455090	Seward, AK	60.12	-149.43	3.238	0.884	-4.0	1983-2001	0.983	1.283	1.683
	53159	9455500	Seldovia, AK	59.44	-151.72	5.499	1.350	-9.8	2012-2016	2.906	3.206	3.606
	53518	9455760	Nikiski, AK	60.68	-151.40	6.262	1.254	-9.9	2012-2016	NaN	NaN	NaN
	53879	9455920	Anchorage, AK	61.24	-149.89	8.889	1.269	-2.7	1983-2001	NaN	NaN	NaN
	52440	9457292	Kodiak Island, AK	57.73	-152.51	2.675	0.715	-9.2	2012-2016	0.743	1.043	1.443
	52079	9457804	Alitak, AK	56.90	-154.25	3.578	0.908	-5.8	2012-2016	1.174	1.474	1.874
	51714	9459450	Sand Point, AK	55.34	-160.50	2.204	0.737	1.4	1983-2001	0.615	0.915	1.315
	51712	9459881	King Cove, AK	55.06	-162.33	2.082	0.753	-5.8	1983-2001	0.592	0.892	1.292
	50262	9461380	Adak Island, AK	51.86	-176.63	1.131	NaN	NaN	NaN	0.572	0.872	1.272
	50623	9461710	Atka, AK	52.23	-174.17	1.041	0.424	-5.8	1983-2001	0.584	0.884	1.284
	50629	9462450	Nikolski, AK	52.94	-168.87	1.213	0.537	-5.8	1983-2001	0.563	0.863	1.263
	50990	9462620	Unalaska, AK	53.88	-166.54	1.098	NaN	NaN	NaN	0.576	0.876	1.276
	51714	9463502	Port Moller, AK	55.99	-160.57	3.175	0.697	-5.8	1983-2001	0.952	1.252	1.652
	52422	9464212	Village Cove, AK	57.13	-170.29	1.005	NaN	NaN	NaN	0.589	0.889	1.289
	54940	9468756	Nome, AK	64.50	-165.43	0.464	NaN	NaN	NaN	0.719	1.019	1.419
	56018	9491094	Red Dog Dock, AK	67.58	-164.07	0.269	NaN	NaN	NaN	0.787	1.087	1.487
	57111	9497645	Prudhoe Bay, AK	70.40	-148.53	0.214	NaN	NaN	NaN	0.808	1.108	1.508
Carib	38168	9751364	St Croix, VI	17.75	-64.71	0.226	0.205	2.4	1983-2001	0.509	0.807	1.179
	38527	9751381	St John, VI	18.32	-64.72	0.252	0.210	2.4	1983-2001	0.510	0.808	1.180
	38168	9751401	Lime Tree Bay, VI	17.69	-64.75	0.216	0.154	3.0	1983-2001	0.509	0.806	1.179
	38527	9751639	Charlotte Amalie, VI	18.34	-64.92	0.240	0.172	2.3	1983-2001	0.510	0.807	1.180
	38526	9752695	Vieques Island, PR	18.09	-65.47	0.225	0.190	2.4	1983-2001	0.509	0.807	1.179
	38525	9755371	San Juan, PR	18.46	-66.12	0.481	0.191	2.4	1983-2001	0.519	0.814	1.189
	38165	9759110	Magueyes Island, PR	17.97	-67.05	0.204	0.157	1.9	1983-2001	0.508	0.806	1.178
	38524	9759938	Mona Island, PR	18.09	-67.94	0.247	0.257	2.4	1983-2001	0.510	0.807	1.180

2034
2035

Method's Appendix: Extreme Water Levels and Alaskan Coastal Flood Height

1. Data and Regional Frequency Analysis. A regional frequency analysis (RFA) of NOAA tide gauges is used to estimate extreme water levels (EWLs) along U.S. coastlines at and away from tide gauge. The RFA method (Hosking and Wallis, 1997) is based upon the assumption that similar physical forcing across a region will produce a similar frequency of events and a probability density up to a 'local index (u)', which is a local scaling factor that captures response peculiarities (Dalrymple, 1960). A RFA uses regional sets of data that have been locally normalized by their respective local index with a statistical heterogeneity test (H value) to assess the extent that the data are sufficiently similar. Using statistical L-moments, heterogeneity is a measure of the variation between sites of a location's summary distribution statistics relative to the amount of dispersion expected if the locations were indeed a homogeneous region (Hosking and Wallis, 1997). If $H < 1$, the region is considered acceptably homogeneous. If $1 \leqslant H < 2$, the region is considered possibly heterogeneous, but acceptable for our study. If $H \leqslant 2$, then the TG group is definitely heterogeneous and not suitable for analysis. Once the regional bounds are established whose data is acceptably homogeneous, the aggregated data is fit with an extreme value distribution.

In this study, hourly and 'top ten' data from all NOAA tide gauges (tidesandcurrents.noaa.gov) with 10 years of record (Figure A1) are used. Water levels are put onto the mean higher high water (MHHW) tidal datum and detrended relative to the midpoint of the current national datum tidal epoch (1983-2001) similar for NOAA extreme water level procedures using a single-gauge analysis (Zervas, 2013: https://tidesandcurrents.noaa.gov/est/). From the data sets, daily highest water levels are picked and declustered at each tide gauge using a 4-day storm window to ensure event independence. The 98th percentile of the declustered daily highest levels at each tide gauge is used as the local index to normalize the data for the RFA process.

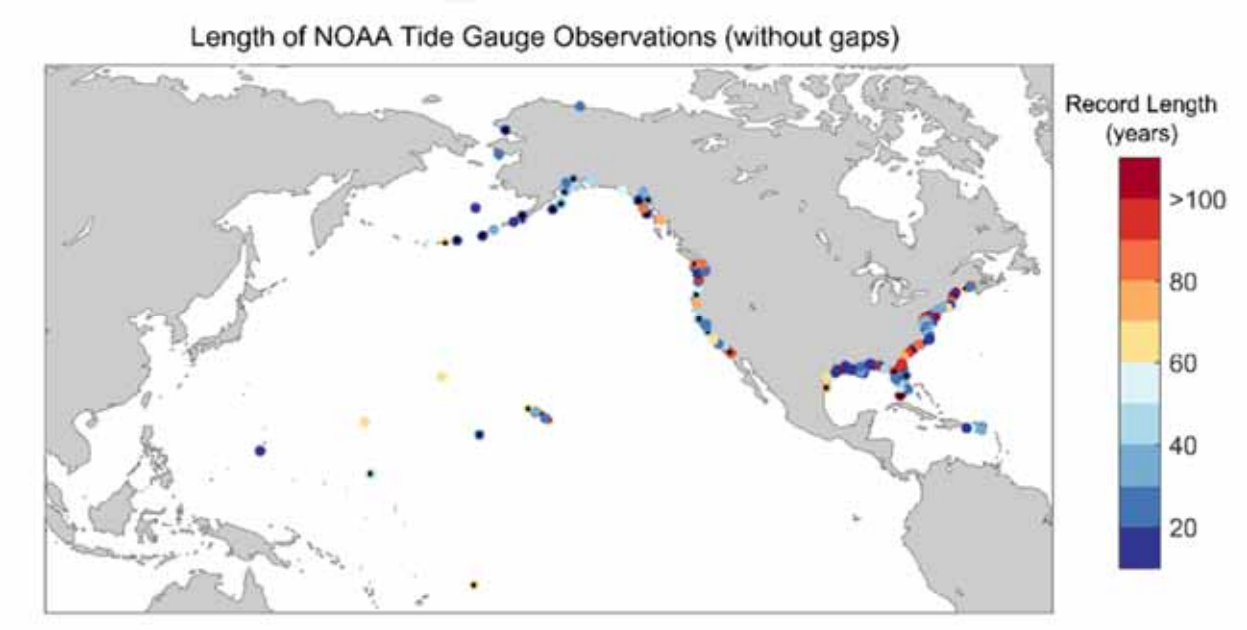

Figure A1. NOAA tide gauges used in the Regional Frequency Analysis (RFA) to generate extreme water level (EWL) probabilities for the U.S coastline.

To form regions, the tide gauge data is aggregated across a 250-mile radius similar to methods of Hall et al. (2016), but from the mid-point of a continuous set of coastline-intersecting 1-degree grids instead of site-specific installations. A maximum of 10 and a minimum of 3 tide gauges are included for each grid. These grids align with those of the sea level rise projections in this report. Next, the regional data are spatially declustered with an additional 4-day event (i.e., storm) window to ensure that only the maximum water level within a region is retained (keep only the highest peak water levels for a particular event). Then, the statistical heterogeneity measure is estimated to ensure that the grouped tide gauge data are sufficiently homogeneous ($H < 2$). In some instances, when a region about its grid centroid has $H > 2$, tide gauges furthest away are sequentially dropped until homogeneity is achieved. In the end, all 1-degree grids along the continental U.S. had $H < 2$ (considered acceptably homogeneous) except a grid (number 48519) along the Pacific Northwest Coast, which along with the Hawaiian and other Pacific Islands, uses the much larger physical-process regions identified and quantified in Sweet et al. (2020). The Alaskan coastline is fairly well quantified except along the western and northern coasts.

An example is shown for grid number 46415, which is where the NOAA Tide Gauge at The Battery in NYC is located (Figure A2). Four tide gauges are included in this grid (Kings Point, The Battery, Bergen Point and Sandy Hook in Figure A2a-d) and their data are considered homogeneous (H value of 0.32). After the 4-day spatial filtering for events, each of the tide gauge data sets are normalized (divided by) by its respective local index (u) value and aggregated as shown in Figure A2e.

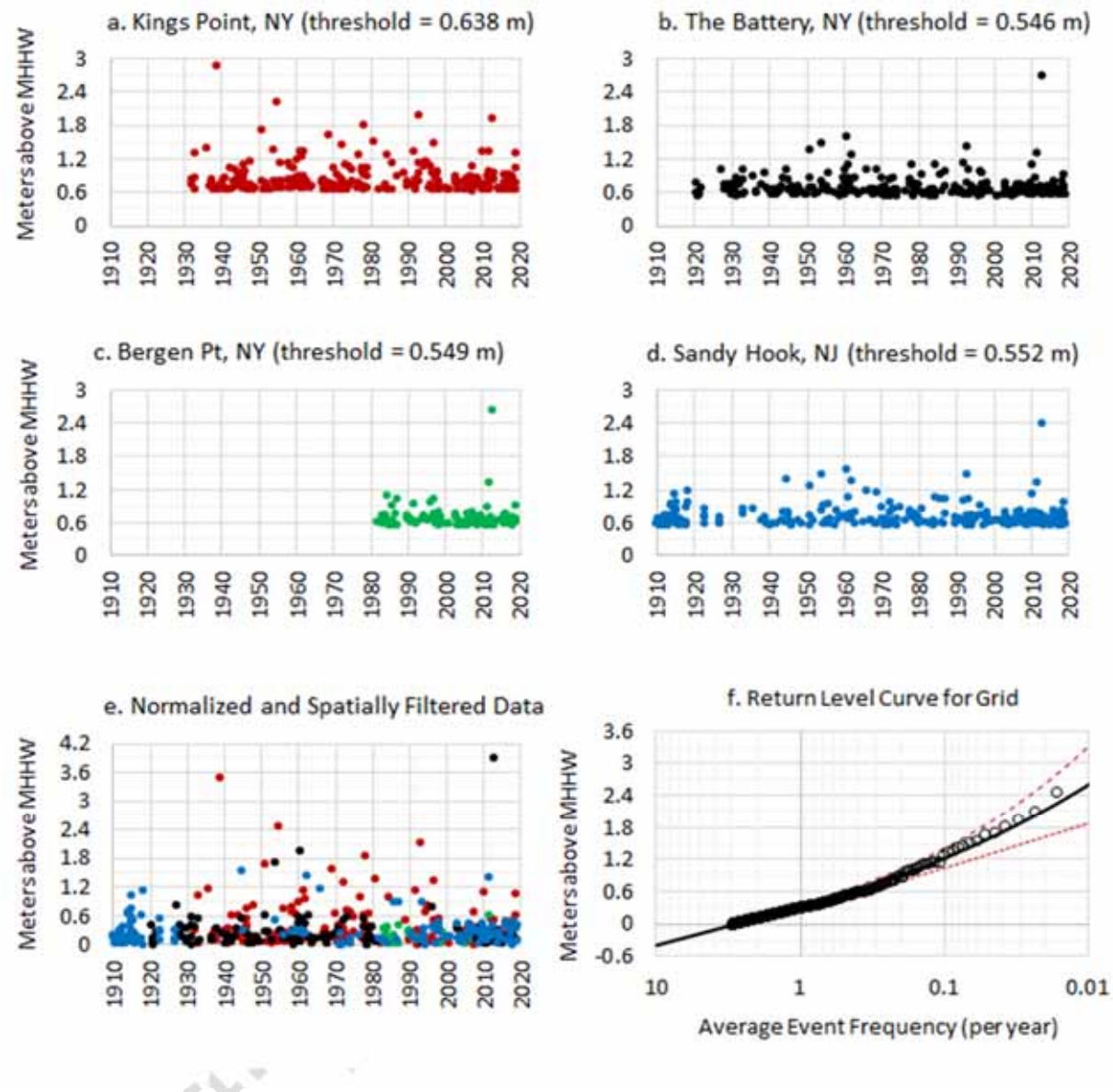

Figure A2: Example of data from grid number 46415 showing exceedances above each local index (u: 98th % of daily highest water level with a 4-day event filter) relative to the 1983-2001 MHHW tidal datum at a) Kings Point, NY, b) The Battery, NY, c) Bergen Point, NY and d) Sandy Hook, NJ that are e) aggregated into a single dataset and f) fit by a GPD to form a return level interval curve for the grid.

2. Gridded (Regional) Extreme Water Level Probabilities.

With the tide gauges identified for each 1-degree grid, the aggregated and normalized datasets are fit with a Generalized Pareto Distribution (GPD; Coles, 2001). Using the penalized maximum likelihood method (Coles and Dixon, 1999; Frau et al., 2018; Sweet et al., 2020), expected and 95% confidence interval (2.5 and 97.5th % levels) values are estimated for the gridded EWL probabilities defined as:

2092 1) $G\ (Z;\ u, \alpha, \xi)\ =\ \lambda\left[1 + \xi(\frac{z-u}{\alpha})\right]^{\ -1/\xi}$

2093 where G is the exceedance probability (P[Z > z]), λ is the probability of an individual (normalized)
2094 observation exceeding the local index (u), α is the scale parameter, and ξ is the shape parameter. It is
2095 assumed that the distribution of the number of exceedances per year follows a Poisson distribution and
2096 the return level (e.g., 2% annual chance event often referred to as 50-yr event) for an EWL of height (Z)
2097 is given by:

2098 2) $Z_N = u + \frac{\alpha}{\xi}\left[(Nn_y\ \ \lambda)^{\xi} - 1\right]$

2099 where N is the average recurrence interval (referred to in this study as the average event frequency), n_y
2100 is number days per year (365.25) and λ is the average number of event exceedances/year (about 3 on
2101 average across all tides gauges in the study). To estimate EWLs with return levels down to a 0.1-year
2102 interval (10 events/year), we extrapolate the gridded GPD model with a logarithmic fit for return levels
2103 between 2 years and the ~0.3 years ($1/\lambda$) limit. A return level interval curve (following common
2104 engineering practice) fit to the aggregated data (Figure A2e) for the grid where NYC is located is shown
2105 in Figure A2f.

2106

2107 3. Localized Extreme Water Level Probabilities

2108 When fitting a GPD to the RFA of aggregated tide gauge data, the local EWL (EWL_{local}) probabilities
2109 including the model of expected values and their 95% confidence interval at a particular location is given
2110 as:

2111 3) $EWL_{local} = EWL_{gridded} * u_{local} + u_{local}$

2112 where $EWL_{gridded}$ is the gridded return level for a particular coastal 1-degree grid and 'u_{local}' is the local
2113 index used in both the RFA and GPD process. The value of u is a height (98th% of 4-day event filtered
2114 daily highest water level) above the local MHHW tidal datum on the current 1983-2001 national tidal
2115 datum epoch (NTDE) or for a modified 5-year epoch. The associated uncertainty of the $EWL_{gridded}$
2116 estimated during the RFA is expressed as $\sigma_{gridded}$. When localized at a tide gauge used in the formulation
2117 of the grids (Figure A1), u is assumed to have no uncertainty. Though, just as the location parameters in
2118 Generalized Extreme Value (GEV) have time-dependent characteristics (Menéndez and Woodworth,
2119 2010), it is recognized that u would experience similar behavior, but that is not quantified in this study.

2120 In this RFA framework, it is possible to estimate EWL_{local} from the $EWL_{gridded}$ probabilities (expected
2121 values and 95% confidence interval) through use of other sources of data. Specifically, the local indices
2122 needed to localize the $EWL_{gridded}$ values can be obtained from either 1) short-term tide gauge data (or by
2123 targeted deployments) within a particular grid that is not included in the RFA formulation (<10 years,
2124 Figure A3) or 2) based upon an underlying relationship between regional sets of local index (u) values
2125 and tide range available, e.g., from NOAA VDatum (https://vdatum.noaa.gov/). In both cases, we
2126 establish large U.S. coastal regions that are aligned (though not exactly) with those of the National

Climate Assessment that encompass several 1-degree grids to quantify information needed to obtain local indices and/or estimate variance/uncertainties (e.g., root mean squared error [RMSE]). These alternative methods may be of interest to coastal communities that are not co-located to a tide gauge used in this study, but have predictions of tide range or have access to or are planning temporary tide gauge installations to establish tidal datums and/or EWLs.

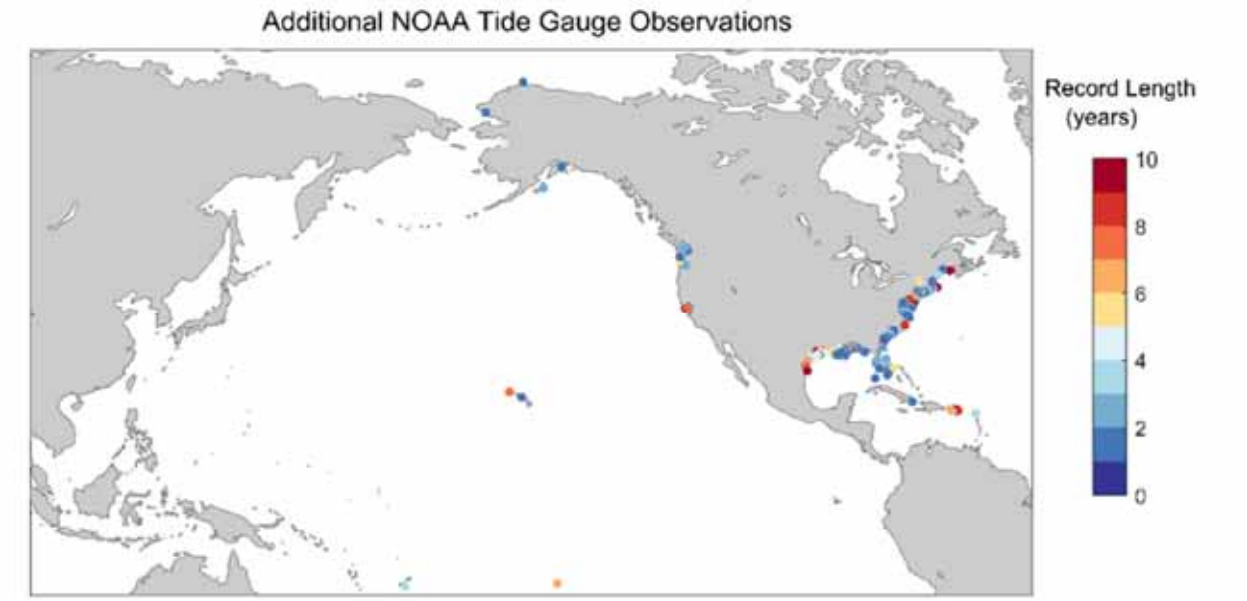

Figure A3: Additional tide gauge data available from NOAA (tidesandcurrents.noaa.gov) that can be used to localize the 1-degree gridded set of RFA EWL probabilities.

3.1 Local Index Estimates from Short Term Installations

When other sets of tide/water level data are available, a local index can be directly estimated to obtain EWL_{local} probabilities from the $EWL_{gridded}$ probabilities. The first step in using these data would be to estimate a local MHHW tidal datum, e.g., using NOAA on-line datum tool (https://access.co-ops.nos.noaa.gov/datumcalc/) if the data is not from NOAA. Following Equation 3 above, there will be some uncertainty in the local index value dependent upon record length (e.g., 1-10 years). To account for short-record uncertainty in the local indices (u), root mean square error (RMSE: 1 standard error) are estimated for regional estimates of u for the tide gauges used in the RFA (Figure A1). RMSE is estimated using a logarithmic fit over a 19-year record length (Figure A4). To compute the RMSE, first the maximum absolute differences are computed between u derived over the entire record and for progressively longer consecutive record lengths between 2001 and 2019 at each tide gauge (e.g., 19 discrete 1-year records; 18 consecutive 2-year records, etc.). The maximum (absolute) difference is used to account for interannual variability that can be extreme (e.g., during phases of ENSO). This difference is considered the error in estimating u for shorter records and the average of the absolute differences across the regional set of tide gauges is considered the bias. The standard deviation of the absolute differences is also computed across all tide gauges and an estimate of the RMSE is then computed as the

square root of the sum of the square of the bias and the standard deviation (variance). The estimates for Hawaii and U.S. Pacific Islands follow estimates of Sweet et al. (2020).

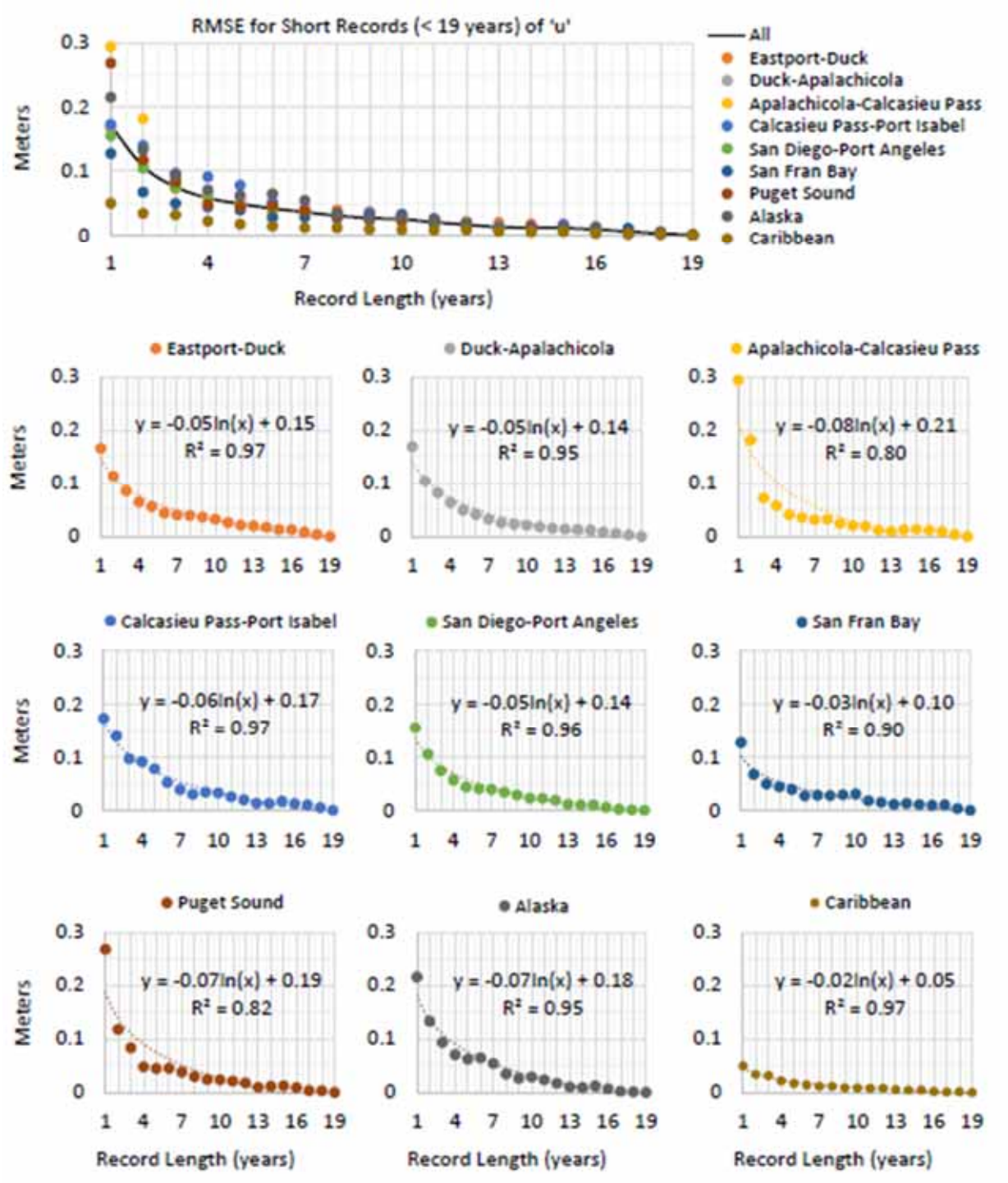

Figure A4: Root mean square error (RMSE) for regional estimates of flood indices (u) based upon 1–19 years of consecutive data over the 2001–2019 period based sets of tide gauges used in this study that mostly align with the National Climate Assessment (NCA, e.g., NCA Northeast U.S. region spans from ME to MD and the Southeast U.S. region spans from VA to LA).

3.2 Obtaining a Local Index from Tide Range Information

Another method to obtain an estimate of a local index (u) and its uncertainty is based upon a dependency (correlation) that exists with tide range (great diurnal [GT]) along most coastal regions similar to findings of Merrifield et al. (2013). In essence, tide range, which represents the spread between MHHW and mean lower low water (MLLW), partially quantifies the variance of the daily highest water level distribution and the height of the local index u (98th%). Figure A5 illustrates the regression-based relationships between tide range and u along U.S. coastal regions. All regressions are significant above the 90% significance level (p values < 0.1) and applicable for the 1983-2001 tidal epoch. For the Hawaiian and U.S. Pacific Islands, the Pacific-wide regression of Sweet et al. (2020) are used.

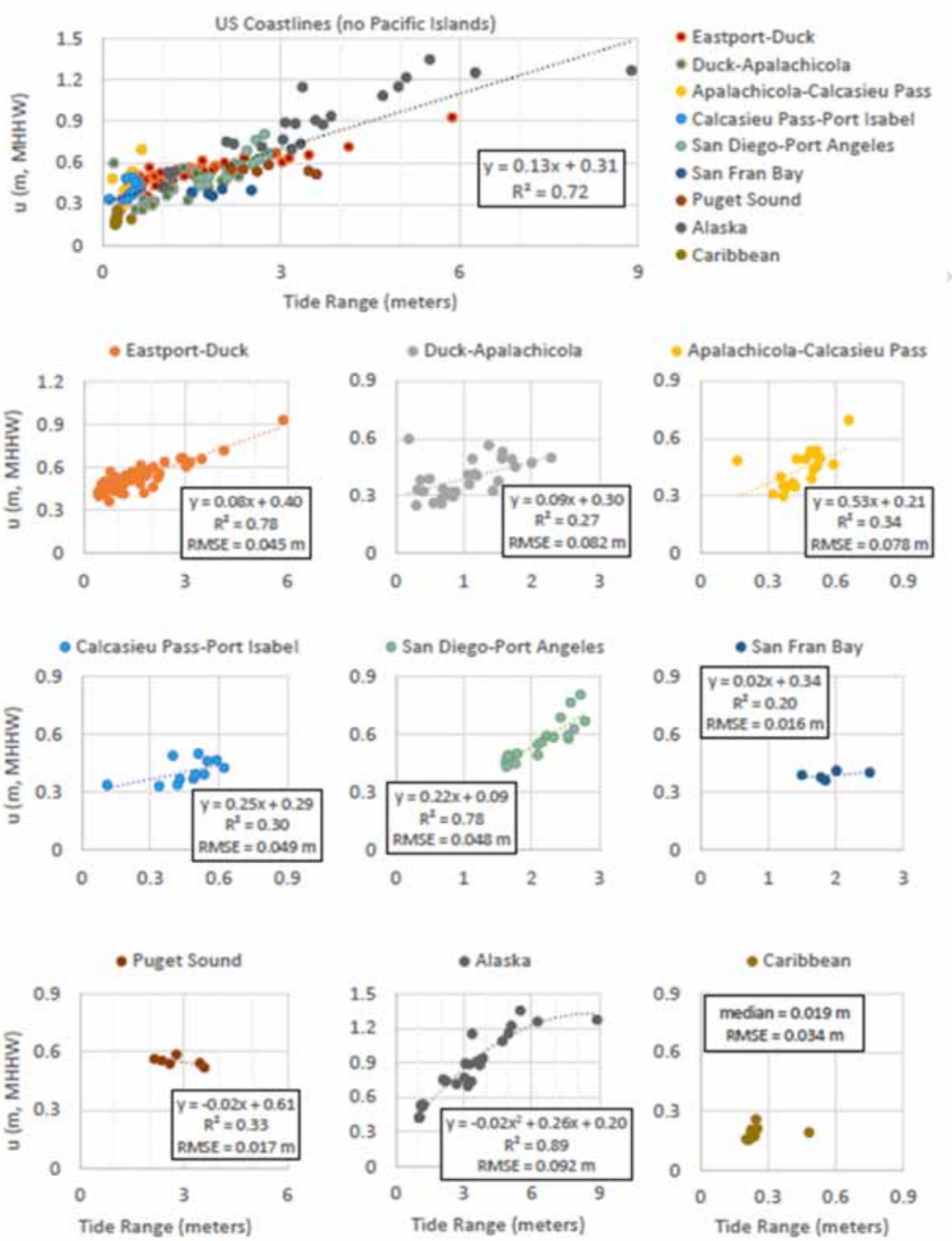

Figure A5: Tide range to local index (u) regressions with equations, goodness of fit (R^2) and root mean squared error (RMSE) shown by regions.

3.3 Uncertainties using Alternative Methods to Estimate EWL_{local} Probabilities

When using either alternative methods (tide range of or short-record estimates) to obtain a local index (u), the uncertainty estimates of EWL_{local} probabilities will include additional uncertainty in u (σ_u). Following methods of Sweet et al. (2020), it can be shown that:

4) $$\sigma_{EWL(local)} = [(1 + \mu_{EWLgridded})^2 + \sigma^2_{EWLgridded}]\sigma_u^2 + \mu_u^2\sigma^2_{EWLgridded}$$

where $\mu_{EWLgridded}$ and μ_u are the expected values of the gridded return levels and the expected value of u, for example, predicted by the tide-range and u dependency (Figure A5), respectively, σ_u^2 is the uncertainty inherent to any u-prediction relationship (e.g., RMSE). Thus, there is an additive uncertainty in u as estimated from this relationship would introduce additional uncertainty in estimates of EWL_{local}.

3.4 Adjusting Local Extreme Water Level Probabilities to Different Sea Levels

To adjust the EWL_{local} probabilities to a different sea level than under the current tidal epoch (e.g., 1983-2001 or modified 5-year epoch), trends inherent in the local index (u) need to be applied to the epoch-specific EWL_{local} probabilities themselves. For tide gauges used in the RFA and with more than 20 years of data (e.g., with missing data accounted for), the local u trend is used; otherwise, a median regional (i.e., Eastport to Duck) trend is used. For example, to estimate probabilities for year 2000, the EWL_{local} probabilities value would be increased by an amount equal to the trend in 'u' (or the median u trend value for the region) multiplied by 8 years 1992 (the midpoint of the 1983-2001 epoch). The same procedure is used to adjust EWL_{local} probabilities estimated via the tide range regression (Figure A5), using the regional median trend in the local indices. In the case of a short-term estimate of 'u', if local tidal datums have been computed and adjusted to the national tidal datum epoch (e.g., using https://access.co-ops.nos.noaa.gov/datumcalc/index.jsp), then regional median trend in the local indices can be applied; in the case where no epoch can be established (see https://access.co-ops.nos.noaa.gov/datumcalc/index.jsp for guidance), then the measurements will be assumed to be referenced to the period of collection and trend adjustment may be less straightforward.

4. Alaska Coastal Flood Heights

To assess flood risk, the coastal flood heights of Sweet et al. (2018) are used for all U.S. coastlines outside of Alaska. Used in NOAA annual outlooks (e.g., Sweet et al., 2020b; https://tidesandcurrents.noaa.gov/HighTideFlooding_AnnualOutlook.html), these heights are a best-fit solution (regression) to the dozens of National Weather Service (NWS) emergency response warning thresholds established at many (but not all) NOAA tide gauges along the country's coastline. The NWS thresholds are used to communicate expected or on-going coastal flood hazards to the public (NOAA, 2020), but often their depth/severity varies according to specific features near the tide gauge that affects both the associated flood frequency and broader vulnerabilities. Along the Alaskan coastline, we follow methodologies of Sweet et al. (2020) who used a slight modification to assess 'damaging flood heights' for the Pacific Basin coastlines. Here, the Alaskan flood heights are based upon a quadratic

regression model using Pacific Coast NWS minor flood heights and considered for only tide ranges below 6 meters (Fig S6a). To obtain moderate and major flood heights for Alaska, 0.3 and 0.7 m are added to the regression, which is approximately the median difference between these heights and those for minor flooding along the continental U.S. (Sweet et al., 2018). With flood heights defined nationally, minor, moderate and major high tide flooding (HTF) are defined as occurring when water level reach or exceed heights of about (median values) 0.55 m, 0.85 m and 1.2 m above MHHW, respectively, and linearly varies with tide range (Figures S6b-d).

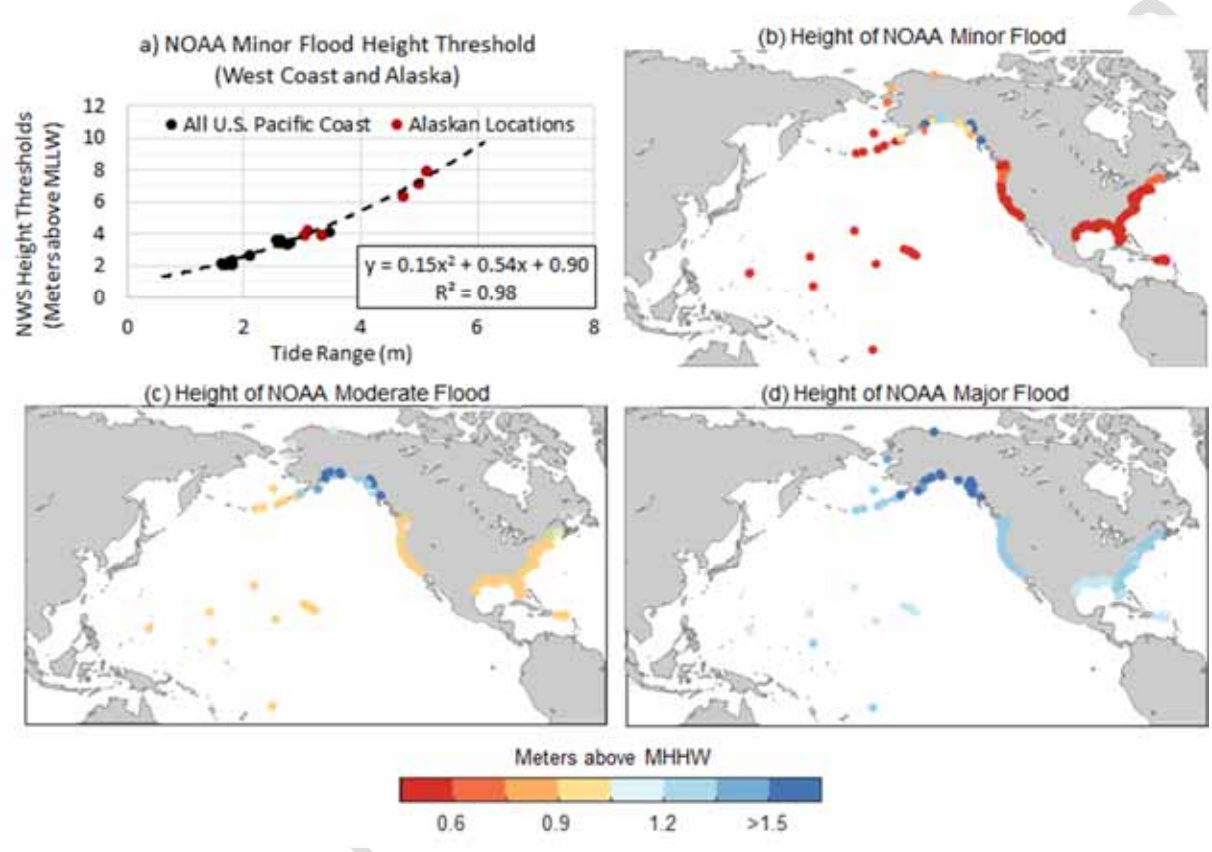

Figure A6: a) Quadratic regression of U.S. West Coast minor flood heights of NOAA's National Weather Service following methods of Sweet et al. (2020) to obtain a minor flood definition for Alaska's coastline. The NOAA flood heights for b) minor flooding, c) moderate flooding and d) major flooding are shown relative to MHHW.

References

Coles, S.G. (2001). An introduction to statistical modeling of extreme values. London, Springer. 208pp.

Coles, S., and Dixon, M. (1999). Likelihood-based inference for extreme value models. Extremes 2, 5–23. doi: 10.1023/A:1009905222644

Dalrymple, T. (1960). Flood Frequency Analysis. U.S. Geological Survey Water-Supply Paper 1543-A. Washington, D.C.: U.S. Government Printing Office.

Frau, R., Andreewsky, M., and Bernardara, P. (2018). The use of historical information for regional frequency analysis of extreme skew surge. Nat. Hazards Earth Syst. Sci. 18, 949–962. doi: 10.5194/nhess-18-949-2018

Hall, J.A., S. Gill, J. Obeysekera, W. Sweet, K. Knuuti, and J. Marburger (2016). Regional Sea Level Scenarios for Coastal Risk Management: Managing the Uncertainty of Future Sea Level Change and Extreme Water Levels for Department of Defense Coastal Sites Worldwide. U.S. Dept of Defense, Strategic Envir. Research and Development Program. 224 pp.

Hosking, J. R. M., and J. R. Wallis (1997). Regional Frequency Analysis: An Approach Based on L-Moments, Cambridge Univ. Press, Cambridge, U. K.

Merrifield, M. A., Genz, A. S., Kontoes, C. P., and Marra, J. J. (2013). Annual maximum water levels from tide gauges: contributing factors and geographic patterns. J. Geophys. Res. Oceans 118, 2535–2546. doi: 10.1002/jgrc.20173

NOAA (2020). National Weather Service Instruction 10-320. Surf Zone Forecast and Coastal/Lakeshore Hazard Services. http://www.nws.noaa.gov/directives/sym/pd01003020curr.pdf

NOAA (2003). Computational Techniques for Tidal Datums Handbook. NOAA Special Publication NOS CO-OPS 2. Silver Spring, MA: U.S. Department of Commerce.

Sweet, W.V., G. Dusek., J. Obeysekera, J. Marra (2018). Patterns and Projections of High Tide Flooding Along the U.S. Coastline Using a Common Impact Threshold. NOAA Tech. Rep. NOS CO-OPS 086. National Oceanic and Atmospheric Administration, National Ocean Service, Silver Spring, MD. 44p. https://tidesandcurrents.noaa.gov/publications/techrpt86_PaP_of_HTFlooding.pdf

Sweet, W. V., Genz, A. S., Obeysekera, J., & Marra, J. J. (2020). A Regional Frequency Analysis of Tide Gauges to Assess Pacific Coast Flood Risk. Frontiers in Marine Science, 7, 883.

Sweet, W. V., Dusek, G., Carbin, G., Marra, J. J., Marcy, D., and Simon, S. (2020). 2019 State of US High Tide Flooding With a 2020 Outlook. NOAA Tech. Rep. NOS CO-OPS., Vol. 92. Silver Spring, MD: National Oceanic and Atmospheric Administration, 17.

Zervas, C. (2013). NOAA Technical Report NOS Co-OPS 067: Extreme Water Levels of the United States 1893–2010. Silver Spring, MD: National Ocean Service.